SYNTHESIS, CHARACTERIZATION, RAMAN, AND SURFACE ENHANCED RAMAN STUDIES OF SEMICONDUCTOR QUANTUM DOTS

by

YI PAN

A dissertation submitted to the Graduate Faculty in Chemistry in partial fulfillment of the requirements for the degree of Doctor of Philosophy, The City University of New York

2012

This manuscript has been read and accepted for the
Graduate Faculty in Chemistry in satisfaction of the
dissertation requirement for the degree of Doctor of Philosophy

Prof. John R. Lombardi

Date

Chair of Examining Committee

Prof. Maria C. Tamargo

Date

Executive Officer

Prof. John R. Lombardi

Prof. Louis J. Massa

Prof. Maria C. Tamargo
Supervisory Committee

THE CITY UNIVERSITY OF NEW YORK

Abstract

Synthesis, Characterization, Raman, and Surface Enhanced Raman Studies of Semiconductor Quantum Dots

by

Yi Pan

Advisor: Professor John. R. Lombardi

The major contributions and discoveries of the dissertation include: (1) Homogeneous nucleation processes for the formation of nanocrystals can occur at low temperature and do not need to proceed at high temperature to overcome a high energy barrier. Monodisperse PbS quantum dots (QDs) obtained with nucleation and growth at 45°C support this finding. (2) Monodisperse single elemental Se QDs can be produced by simple solution crystallization from TDE (1-tetradecene) or ODE (1-octadecene). (3) TDE is a better non-coordinating solvent compare to ODE. STDE (S dissolved in TDE) and SeTDE (Se dissolved in TDE) are stable reagents with long storage time. They can be used as universal precursors for S-containing and Se-containing QDs. (4) QDs synthesis can be carried out at low temperature and relatively short reaction time using the simple, non-injection, one-pot synthetic method. (5) The one-pot method can be extended for the synthesis of QDs and graphene oxide nanocomposites and metal and graphene oxide nanocomposites. (6) $PbCl_2$-OLA (oleylamine) is a universal system for the synthesis of Pb-chaclogenides QDs. (7) Surface enhanced Raman spectroscopy (SERS) is used to probe both size and wave length dependent quantum confinement effects (QCEs) of PbS QDs. (8) Raman spectroscopy is a powerful tool to elucidate crystal structure of Se nanoclusters with size of 1-2 nm.

Semiconductor QDs have attracted considerable attention due to their potential for energy-efficient materials in optoelectronic and solar cell applications. When the radius of a QD is decreased to that of the exciton Bohr radius, the valence and conduction bands are known to split into narrower bands due to QCEs. QCEs are both size and wave length dependent. We have developed, synthesized and characterized a series of Pb-chaclogenide QDs, which all the sizes of the QDs are monodisperse and smaller than their respective exciton Bohr radius, to study the QCEs of these QDs.

SERS is used as a crucial tool to investigate these QCEs. The QCEs are due to any of the following three resonances or a combination among them: interband resonance, molecular state resonance, and charge-transfer resonance.

Acknowledgements

This scientific research was completed under the supervision of my mentor Professor John Lombardi at the City College of New York. I would like to thank him for providing me the opportunity to study on these fascinating topics. Without his guidance, advice, inspiration, support, and thoughtful discussions, the delighted and challenging journey of my PhD study would never be possible.

I would also like to extend my special thanks to both Professor Louis Massa and Professor Maria Tamargo for serving on my thesis committee. Without your expertise, encouragement, and the annual review of my research progresses, I would not reach this point.

I wish to thank Dr. Nan-Loh Yang and Dr. Shuiqin Zhou for enrolling me into the PhD program at the Graduate Center of the City University of New York.

I own thanks to Dr. Stephen O'Brien, Mr. Yadi Li, Dr. Liming Huang, Dr. Hongbo Liu, Mr. Yu Zao, and Mr. Zengyan Wei for helpful discussions throughout my research.

I would like to thank all my colleges and friends, especially:

Dr. Xiaoqi Fu, Dr. Marco Leona, and Dr. Pablo Londero for Raman support;

Dr. Hanying Bai, Mr. Bo Cai, and Mr. Zengyan Wei for high resolution transmission electron microscopy measurement;

Dr. Jorge Morales for transmission electron microscopy support;

Mr. Yadi Li for ^{1}HNMR and ^{13}CNMR measurement;

Mr. Le Peng for data process;

Dr. Swapnil Jadhav for differential scanning calorimetry measurement;

Dr. Lijia Yang for mass spectrometry measurement;

Dr. Alexey Bykov for XRD and UV-Vis-Near IR spectrophotometer support;

Dr. Tianjian Huang and Mr. Changhong Wan for their kind support.

I also gratefully to acknowledge the financial support from both National Science Foundation and U. S. Department of Justice that made my PhD research possible.

This is

dedicated to my family

My parents

Professor Weihan Pan and Bingxuan Hong

潘维瀚 教授 洪冰玄 女士

My wife

Cui Ye

叶翠 女士

My children

Brian Pan and Christina Pan

潘弘宇 潘婧瑜

Table of Contents

List of Tables

List of Figures

Chapter 1 Introduction

Quantum dots (QDs)[1-3] are promising energy-efficient materials for nanoelectronics, optoelectronics, molecular electronics and spintronics, nano-fabrication and nano-manufacturing, solar cell, and bioengineering applications.[4-9] Considerable efforts have been made in the synthesis of QDs,[10-12] while some experimental results[13-15] show that surface enhancement Raman scattering, which measure the quantum confinement effects (QCEs) of the QDs, occurred on the surface of semiconductor QDs although there are no theoretical predictions.

To better understand and evaluate the properties of energy-efficient QDs, methods to characterize QCEs needs to be further developed and investigated. In this dissertation, we focus on using surface enhanced Raman spectroscopy (SERS) to study the QCEs of the semiconductor QDs. SERS technique has a number of important advantages: sensitivity, selectivity, non-destructive detection, and feasibility for in-situ studies. Besides, SERS enables simple and straight forward determination of detailed information about adsorbed species, such as their molecular structure and orientation.

It has been almost two decades since Bawendi group[16] first introduced hot-injection colloidal synthetic method to obtain QDs. Nowadays, different hot-injection methods are still widely used to synthesize various kinds of QDs.[17-22] Researchers tend to add different kinds of reagents to acquire monodisperse size, different shape, and high quality QDs for various kinds of potential applications. This makes the synthesis and separation of QDs more complicated than before. In the meantime, it may also affect the stability of QDs due to the trace amount of reagents trapped inside the QDs. Also, some reagents used are toxic and expensive. Therefore,

simple, environmentally benign, cost-effective, and easy to be industrialized synthetic methods need to be developed, especially for the nucleation and growth of QDs at low temperature.

1.1 Objectives of the Dissertation

This dissertation addresses two important research areas in semiconductor QDs. One is the synthesis of monodisperse QDs and graphene oxide (GO) and QDs nanocomposites; the other is the measurement of their QCEs. We try to answer the following questions:

- Does QD formation really require high temperature?
- Can the current hot-injection method be simplified for Pb-chaclogenide QD synthesis using only one metal source and one capping ligand?
- Can a non-injection, one-pot synthetic method be developed for the synthesis of Pb-chaclogenide QDs, sulfur-containing QDs, and selenium-containing QDs?
- Is it possible to obtain single elemental Se nanoclusters or QDs via simply solution crystallization? How to characterize the Se nanoclusters synthesized?
- Can GO and QDs or GO and metal nanocomposites be synthesized via one-pot preparation?
- Can SERS be used to characterize strong QCEs of QDs with radius less than their exciton Bohr radius? If so, what causes the enhancement?
- Are QCDs size dependent or wave length dependent?

This dissertation presents several new discoveries in the fields of synthesis and characterization of semiconductor QDs to address the above-mentioned questions. Raman spectroscopy and SERS are used to determine their properties and QCEs. First, a new solvent for S or Se precursor, 1-tetradecene (TDE), is found and activated sulfide-containing S precursor

(STDE, S dissolved in TDE) solution or activated selenide-containing Se precursor (SeTDE, Se dissolved in TDE) solution is prepared. Second, a $PbCl_2$-OLA system including $PbCl_2$ as Pb precursor and oleylamine (OLA) as capping ligand is designed and developed for Pb-chaclogenide QD synthesis. Then, a novel, non-injection, one-pot temperature-based synthetic method to obtain monodisperse PbS QDs, PbSe QDs, MnSe QDs, ZnSe QDs, and GO and PbSe QDs nanocomposites with the $PbCl_2$-OLA system using STDE or SeTDE, is developed. It is extended to synthesize other GO and metal nanocomposites, for example, GO and Ag nanocomposites. At the same time, simple, cost-effective, hot-injection method with $PbCl_2$-OLA system to obtain monodisperse PbS, PbSe, and PbTe QDs is also achieved. Next, single elemental Se nanoclusters of 1-2 nm and Se QDs below 20 nm are obtained for the first time by dissolving Se powder in TDE or ODE or other liquid alkenes at elevated temperature followed by simple solution crystallization; their crystal structures are characterized by Raman spectroscopy. Last, the first SERS systematic study of PbS QDs with sizes less than its exciton Bohr radius and surface absorbed with 4-mercaptopyridine (4-Mpy) reveals that the QCEs of PbS QDs are both size dependent and wave length dependent where charge-transfer plays an important role for the enhancement.

1.2 Structure of the Dissertation

The dissertation consists of six chapters.

Chapter 1 describes the areas the dissertation focused on and the summary of the major achievements of the dissertation in these areas, followed by a brief introduction of each chapter.

Chapter 2 highlights the important discoveries of the dissertation and provides related background information. It also introduces the fundamental and experimental aspects of QD

formation, synthetic methods, characterization tools, Raman spectroscopy, and SERS to the extent of their applications in this research.

Chapter 3 presents the synthesis and characterization of several different energy-efficient QDs materials:

1. The synthesis and characterization of monodisperse binary semiconductor Pb-chaclogenide QDs via new, simple, non-injection, one-pot method and modified hot-injection method using $PbCL_2$-OLA system as the only source of metal precursor and capping ligand, including PbS QDs formed by nucleation and growth at 45°C.
2. Controlled synthesis and characterization of the single elemental Se semiconductor nanoclusters and QDs by solution crystallization.
3. Controlled synthesis of GO-QDs nanocomposites and other QDs.

Chapter 4 reveals that the QCEs of the PbS QDs with surface absorbed by 4-Mpy are both size dependent and wave length dependent. It demonstrates that charge-transfer can be used as effective probe to determine the efficiency of QCEs.

Chapter 5 proves that Raman spectroscopy is a powerful tool for the determination of the structure of Se nanoclusters. It also shows that Se nanoclusters can undergo a reversible crystal structure transformation under reduced laser power. The Se nanoclusters and QDs synthesized may have great potential for photo and thermal applications.

1.3 Chapter 1 Reference

(1) Brus, L. E. *The Journal of Chemical Physics* **1984**, *80*, 4403.

(2) Bawendi, M. G.; Steigerwald, M. L.; Brus, L. E. *Annual Review of Physical Chemistry* **1990**, *41*, 477.

(3) Alivisatos, A. P. *The Journal of Physical Chemistry* **1996**, *100*, 13226.

(4) Wang, L.-J.; Cao, G.; Tu, T.; Li, H.-O.; Zhou, C.; Hao, X.-J.; Su, Z.; Guo, G.-C.; Jiang, H.-W.; Guo, G.-P. *Appl Phys Lett* **2010**, *97*, 262113.

(5) Coe-Sullivan, S. *Nat Photon* **2009**, *3*, 315.

(6) Wolf, S. A.; Awschalom, D. D.; Buhrman, R. A.; Daughton, J. M.; von Molnár, S.; Roukes, M. L.; Chtchelkanova, A. Y.; Treger, D. M. *Science (New York, N.Y.)* **2001**, *294*, 1488.

(7) Nozik, A. J.; Beard, M. C.; Luther, J. M.; Law, M.; Ellingson, R. J.; Johnson, J. C. *Chem Rev* **2010**, *110*, 6873.

(8) Beard, M. C. *The Journal of Physical Chemistry Letters* **2011**, *2*, 1282.

(9) Hetsch, F.; Xu, X.; Wang, H.; Kershaw, S. V.; Rogach, A. L. *The Journal of Physical Chemistry Letters* **2011**, *2*, 1879.

(10) Donega, C. d. M. *Chemical Society Reviews* **2011**, *40*, 1512.

(11) Carbone, L.; Cozzoli, P. D. *Nano Today* **2010**, *5*, 449.

(12) Evans, C. M.; Evans, M. E.; Krauss, T. D. *J Am Chem Soc* **2010**, *132*, 10973.

(13) Sun, Z.; Zhao, B.; Lombardi, J. R. *Appl Phys Lett* **2007**, *91*, 221106.

(14) Richter, A. P.; Lombardi, J. R.; Zhao, B. *J Phys Chem C* **2010**, *114*, 1610.

(15) Fonoberov, V. A.; Balandin, A. A. *Appl Phys Lett* **2004**, *85*, 5971.

(16) Murray, C. B.; Norris, D. J.; Bawendi, M. G. *J Am Chem Soc* **1993**, *115*, 8706.

(17) De Mello Donegá, C.; Liljeroth, P.; Vanmaekelbergh, D. *Small* **2005**, *1*, 1152.

(18) Moreels, I.; Justo, Y.; De Geyter, B.; Haustraete, K.; Martins, J. C.; Hens, Z. *Acs Nano* **2011**, *5*, 2004.

(19) Murray, C. B.; Sun, S.; Gaschler, W.; Doyle, H.; Betley, T. A.; Kagan, C. R. *IBM J. Res. Dev.* **2001**, *45*.

(20) Li, H. B.; Chen, D.; Li, L. L.; Tang, F. Q.; Zhang, L.; Ren, J. *Crystengcomm* **2010**, *12*, 1127.

(21) Lu, W.; Fang, J.; Stokes, K. L.; Lin, J. *J Am Chem Soc* **2004**, *126*, 11798.

(22) Urban, J. J.; Talapin, D. V.; Shevchenko, E. V.; Murray, C. B. *J Am Chem Soc* **2006**, *128*

Chapter 2 Background and Experimental Techniques

The most important discoveries of this dissertation for the synthetic and Raman studies of quantum dots (QDs) are highlighted here. For the synthesis of QDs part, we find: (1) Homogeneous nucleation for the formation of nanocrystals can occur at low temperature and does not need high temperature to overcome a high energy barrier. We have obtained monodisperse PbS QDs at the nucleation and growth temperature of 45°C. (2) Monodisperse single elemental Se QDs can be produced by simple solution crystallization from TDE (1-tetradecene) or ODE (1-octadecene). (3) TDE is a better non-coordinating solvent compare to ODE. STDE (S dissolved in TDE) and SeTDE (Se dissolved in TDE) are stable reagents with long storage time. They can be used as universal precursors for S-containing and Se-containing QDs. (4) Monodisperse QDs synthesis can be carried out at low temperature and relatively short reaction time using the simple, non-injection, one-pot synthetic method. (5) The one-pot method can also be extended for the synthesis of QDs and graphene oxide (GO) nanocomposites and metal and GO nanocomposites. (6) $PbCl_2$-OLA (oleylamine) is a universal system for the synthesis of Pb-chaclogenide QDs.

For the Raman part: (1) Surface enhanced Raman spectroscopy (SERS) can be used to probe both size and wave length dependent quantum confinement effects (QCEs) of QDs. (2) Raman spectroscopy is a powerful tool to elucidate crystal structure of small single elemental Se nanoclusters of 1-2 nm, which cannot be characterized by X-ray diffractometer (XRD).

In addition, several fundamental theoretical backgrounds and experimental techniques are also introduced here to help better understand the discoveries.

2.1 Semiconductor Quantum Dots

Quantum dots[1-12] are semiconductor nanocrystals whose excitons (e^--h^+, electron-hole pair) are confined by potential barriers in all three spatial dimensions—zero dimensional points (0D) as Figure 2.1 indicated.

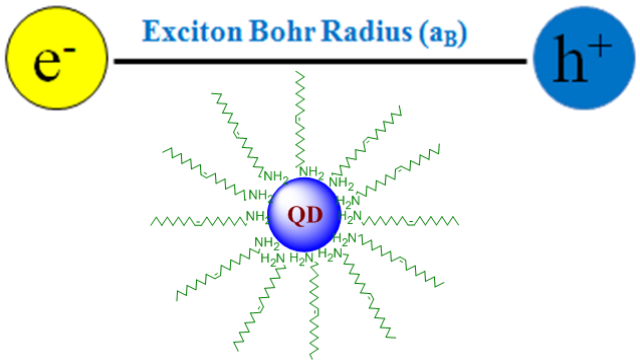

Figure 2.1 A 0D QD with size smaller than its exciton Bohr radius a_B.

The physical properties of QDs' lie in between those of bulk materials and those of discrete atoms or molecules. Similar to bulk semiconductors, [13-14] QDs are also characterized by a composition-dependent band gap energy (E_g), which is the minimum energy required to excite an electron from the ground state valence band into the vacant conduction band (Figure 2.2). When the energy of a photon absorbed in semiconductor QDs is greater than E_g, the excitation of an electron to the conduction band leaves an orbital hole in the valence band. The photogenerated e^--h^+ pairs created with excess energy above E_g (Figure 2.3) can be moved inside the semiconductor materials if a current generated by an electric field is present. The exciton's size within the bulk crystal is defined by the exciton Bohr radius (a_B) (from 0.5 nm to 45 nm) depending on the materials. If the size of a QD is smaller than a_B, it becomes spatially confined by potential barriers, which increase the QD band gap. Therefore, QDs show strong QCEs when their diameters are less than the Bohr radius of exciton in the bulk materials ($d < a_B$). These

QCEs (Figure 2.4) are due to discrete electronic transitions caused by various sizes and shapes of the QDs. In addition to the strong QCEs, weak QCEs occur when one of the dimensions of QDs is greater than a_B ($d \geq a_B$). The weak QCEs are functions of both size and shape of QDs; they include quantum rods or wires--1D confinement and quantum sheets or films--2D confinement. QCEs can be characterized by absorption spectra when electrons move to the conduction band and emission spectra when e^--h^+ recombination leads to photo-luminescence (PL). QCEs can also be measured by SERS[15-18] when certain molecules are absorbed on surface of QDs. The first exciton binding energy, the band gap of bulk material, the confinement energy, the Coulomb attraction, and the exciton effect are shown in Equation 1-3.[7, 19-23] The relations between band gap energy and size of QDs are shown in Equation 2. The exciton Bohr radius calculations are listed in Equation 4-7.[24-26]

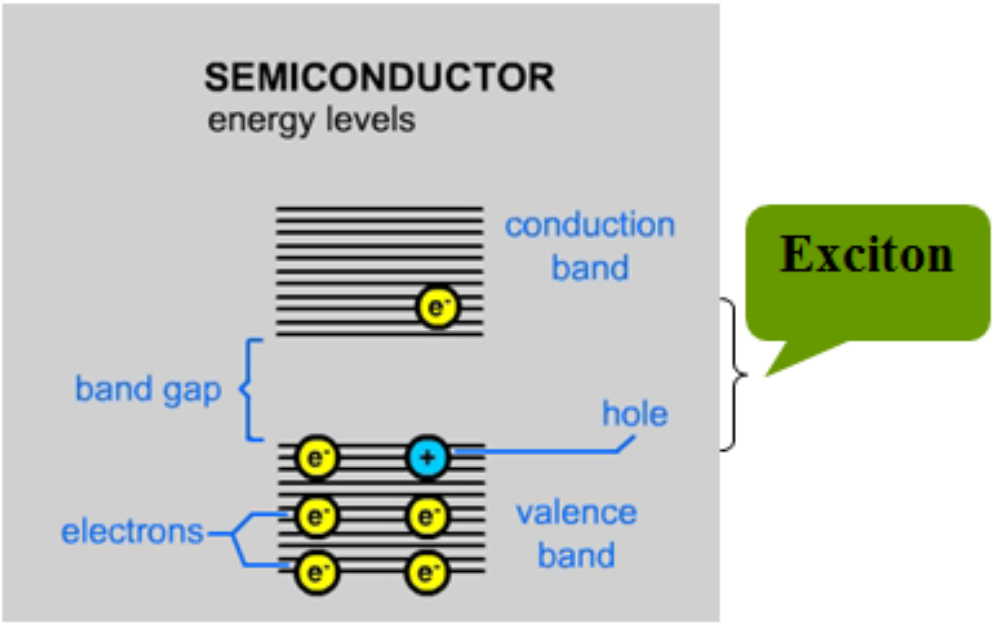

Figure 2.2 Exciton and band gap.

$$h\upsilon \leftrightarrow e^{-}(CB) + h^{+}(VB)$$

Figure 2.3 Electron-hole pair (exciton) generated by excess energy above E_g.

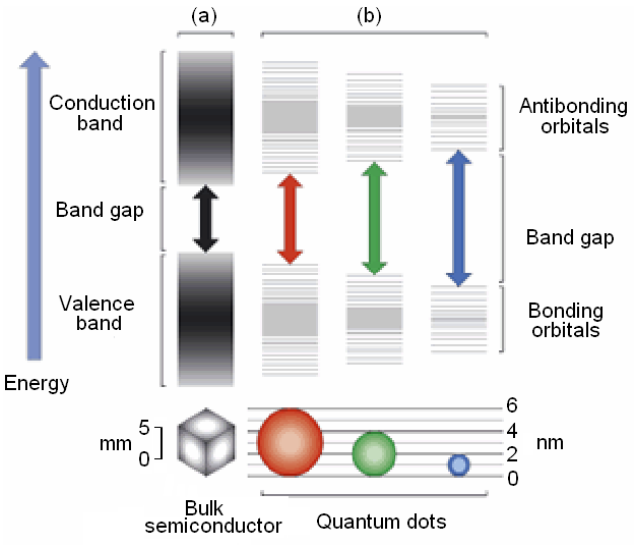

Figure 2.4 Quantum confinement effect (QCE): band gap energy and size of QDs. (a) bulk materials. (b) QDs. It shows the increasing band gap energy and intra-band spacing with QCE (from right to left). The QCE is the origin that allows the tuning of absorption and emission wavelengths over a range of wavelengths (Figure 2.5) as a function of size of QDs.

$$\boldsymbol{E_{ex} = E_g + \frac{\hbar^2\pi^2}{2\mu R^2} - \frac{1.786e^2}{\varepsilon R} - 0.248\frac{\mu e^4}{2\hbar^2\varepsilon^2}} \quad (1)$$

where:

- E_{ex} is the first exciton binding energy.
- E_g is the band gap energy of bulk materials.
- μ is the reduced mass.
- R is the radius.
- $\hbar$ is the reduced Planck's constant.

- e is the elementary charge.
- ε is the dielectric constant.

$$\boldsymbol{E_{QD} = E_g + \frac{\hbar^2 \pi^2}{2\mu R^2}} \quad (2)$$

$$\mu = \left(\frac{\mathbf{1}}{\boldsymbol{m_e^*}} + \frac{\mathbf{1}}{\boldsymbol{m_h^*}}\right)^{-\mathbf{1}} \quad (3)$$

where:

- E_{QD} is the energy band gap of QDs.
- m_e^* is the effective mass of electrons.
- m_h^* is the effective mass of holes.

Let us examine the right side of Equation 1. The second term represents the confinement energy, which is the origin of QCDs. The third term is the Coulomb attraction. The fourth term denotes the exciton effect.

$$\boldsymbol{a_B = \frac{\hbar^2 \varepsilon}{\mu m_0 e^2} = 5.30 \times 10^{-11} \frac{\varepsilon}{\mu}} \quad (4)$$

$$\boldsymbol{a_B = a_e + a_h} \quad (5)$$

$$\boldsymbol{a_e = 5.30 \times 10^{-11} \frac{\varepsilon}{m_e^*}} \quad (6)$$

$$\boldsymbol{a_h = 5.30 \times 10^{-11} \frac{\varepsilon}{m_h^*}} \quad (7)$$

where:

- a_B is the exciton Bohr radius in units of meter.

- a_e is radius of the electron in units of meter.
- a_h is radius of the hole in units of meter.
- m_0 is the mass of free electron.

Figure 2.5 shows optical properties of some QDs related to corresponding wave lengths (energies). The binary Pb-chaclogenide:[27-28] PbS, PbSe, PbTe QDs' absorption spectrum are in the range from 700 nm to 2500 nm. Extensive researches have been reported for these QDs due to their potential applications in optoelectronic, solar cell, sensor, and thermal electronic fields. Their QCEs are investigated by absorption spectra and PL spectra. However, there are no reports of using SERS to study QCEs of these Pb-chaclogenide QDs till now. We hypothesized that due to Pb-chaclogenides' large dielectric constants and their large exciton Bohr radii (Table 2.1)[29-31] among known semiconductor materials, their QCEs could be characterized by SERS if we can synthesize them and absorb certain molecules on their surfaces. To achieve our goal, we need to find simple methods to synthesize various sizes of monodisperse Pb-chaclogenide QDs. The colloidal synthesis of these QDs will be covered in section 2.5 of this chapter.

Table 2.1 Dielectric Constant, Band Gap Energy, and Exciton Bohr Radius of Pb-chaclogenides[29-31]

	Exciton Bohr Radius (a_B) (nm)	**Band Gap Energy (eV)**	**Dielectric Constant (ε)**
PbS	18	0.41	161
PbSe	46	0.278	280
PbTe	46	0.310	360

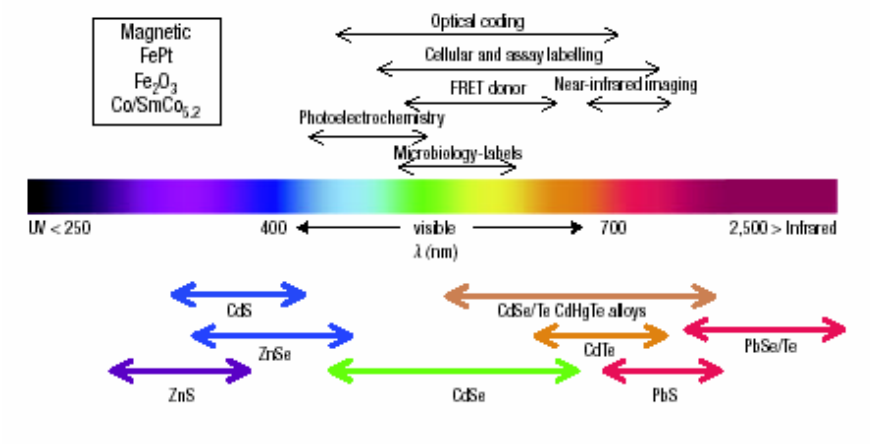

Figure 2.5 QDs and energy (wavelength).[31]

We also study the synthesis of single elemental Se QDs. During the synthesis of PbSe QDs, we found that we may obtain monodisperse Se nanoclusters if we have the proper solvents. That is, Se solutions used as PbSe QDs precursors can also be used to synthesize monodisperse Se nanoclusters and QDs. All of the QDs we investigated are direct band gap semiconductor materials, which are optically active materials. In a direct band gap semiconductor, the top of the valence band and the bottom of the conduction band (maximum energy) occurs at the same value of momentum, while in an indirect band gap semiconductor, the maximum energy of the valence band occurs at a different value of momentum as Figure 2.6 shown.

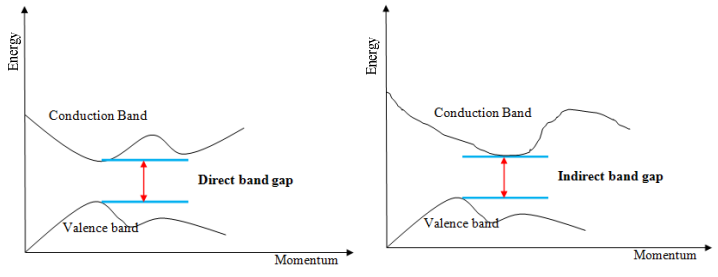

Figure 2.6 Direct and indirect band gap semiconductor materials.

2.2 Se nanoclusters and Se QDs

Selenium has several different structures[27, 33] in the bulk, including trigonal (t-Se, helical chain, indirect band gap material), monoclinic α and β (m-α-Se_8, m-β-Se_8, Se_8 rings, direct band gap material), rhombohedral (r-Se, Se_6 rings, direct band material), cubic α and β, and amorphous form (a-Se, disordered chains and rings, direct band material), making it an ideal candidate for QCE study as single elemental semiconductor Se QDs. The Bohr radius of t-Se is either 0.7 nm or 1.6 nm according to literature reports (Table 2.2). Bulk selenium has a wide range of applications[33-35] in glass, metallurgy, chemicals (pharmaceuticals, food supplements, anti-dandruff shampoos, lubricants and rubber compounding), pigments, electronics (photoreceptors laser printing, xerography, xeroradiography and electrostatic textile printing, semiconductors, solar cells and photoelectric cells), and agriculture (primarily additive to animal feed and fertilizers). Se QDs or nanoparticles can be used in optoelectronic, photonic, biological fields due to their unique size dependent electronic, optical, photoconductive properties and excellent bioavailability as well as high biological activity. Se QDs exhibit improved optoelectronic and photonic properties that could have considerable potential for applications[33, 36-37] in solar energy conversion, photocatalysis, photodetectors, photocopy machines, electrical rectifiers, photoluminescent sensors, and nonlinear optics if monodisperse and stable Se nanomaterials can be fabricated. Se QDs[38] are also very attractive as biological labels due to their small size, excellent biocompatibility, low toxicity, emission tunability, superphotostability, and longer PL decay times in comparison to dyes. In addition, Se has additional important health effects particularly in relation to the immune response and cancer prevention.

Few articles are reported for the synthesis of Se clusters and Se QDs with sizes below 20 nm[35, 39] though colloidal synthesis of single elemental Ge QDs[40-44] has received considerable

attentions due to its applications in semiconductor industry. Currently, Se QDs are either synthesized by redox reaction in aqueous solution or by embedding Se into inert nanoporous host such as zeolites to form Se zeolite nanocomposites.[45-46] The Se precursors we discovered for one-pot synthesis of PbSe QDs indeed make it possible to obtain monodisperse single elemental Se nanoclusters and Se QDs with sizes below 20 nm. The simple solution crystallization method we used for the synthesis of Se QDs may open a new route for the synthesis of single elemental QDs.

Table 2.2 Dielectric Constant, Band Gap Energy, and Exciton Bohr Radius of Se[24-26, 46-48]

	Exciton Bohr Radius (a_B) (nm)	**Band Gap Energy (eV)**	**Dielectric Constant (ε)**
t-Se	0.7 or 1.6	1.95	6.4
m-Se	2.13-2.31*	2.53	9.2

* It is estimated in chapter 3.

2.3 Semiconductor QDs and Graphene Oxide (GO) Nanocomposites

The semiconductor PbSe QDs and GO nanocomposites are 2D confined nanomaterials, which incorporate 0D QDs into a 2D graphene oxide sheets. These kinds of nanocomposites are hot-spots for material scientists.[49-51] They are energy-efficient materials that may have potential for fabricating solar cells. These materials can be produced just because the new non-injection, one-pot synthetic method for both S-containing and Se-containing binary QDs is available as section 2.5 of this chapter described.

2.4 GO and Ag Nanocomposites

The Ag QDs and GO nanocomposites[53-55] are also 2D confined nanomaterials, which incorporate 0D Ag QDs into a 2D graphene oxide sheets. Tremendous efforts have been made to develop these kinds of metal-graphene energy-efficient nanomaterials. We have obtained the nanocomposites during the development of the new non-injection, one-pot synthetic method for Se-containing binary QDs synthesis. It will be discussed in details in section 2.5 of this chapter.

2.5 Synthesis and Characterization

2.5.1 Synthesis

From the above discussions, we know that in order to study the QCEs of QDs, the most important thing is to obtain QDs with uniform size (size dispersion < 10%). Colloidal synthetic methods are widely used in obtaining micrometer scale colloids due to its scalability and the convenience of bench top synthesis. Colloidal synthetic methods of QDs were developed based on the classic work of LaMer and Dinegar in 1940-1950 on a three-stage colloid formation model (Figure 2.7), [56] which is, monomer accumulation (I), homogeneous nucleation (II), and diffusion controlled growth (III). A typical colloidal synthesis of QDs involves dissolving precursor compounds in solutions, much like traditional chemical processes. The synthesis generally includes a three-component system consisting of precursors, organic surfactants, and solvents. Experimentally, three steps are used to control the size distribution of QDs: [6] burst (homogeneous) nucleation (II in Figure 2.7), diffusion controlled growth (III in Figure 2.7), and Ostwald ripening.

It is commonly believed[57-58] that the burst nucleation is a homogeneous nucleation reaction according to LaMer crystal formation model. This reaction has a very high energy

barrier. An extra high super-saturation monomer level in the reaction solution has to be reached for the nucleation to proceed (stage I of LaMer model). Therefore, temperature is one of the crucial factors in determining optimal conditions for both the nucleation and growth of QDs. The temperature must be high enough to allow for the rearrangements of atoms or molecules involved during the synthetic process while being low enough to support QDs crystal growth. Another critical factor that must be strictly controlled during QDs growth is the monomer concentration. The growth of QDs can occur in two different processes, "focusing" and "defocusing". When concentrations of monomer are high, the critical size is relatively small, resulting in growth of nearly all particles. In this process, smaller particles grow faster than large ones (since larger crystals need more atoms to grow than small crystals) resulting in "focusing" of the size distribution to yield nearly monodisperse particles. When concentrations of monomer are lowered during growth, the critical size becomes larger than the average size existed, and the size distribution "defocusing". It leads to size broadening as a result of Ostwald ripening.

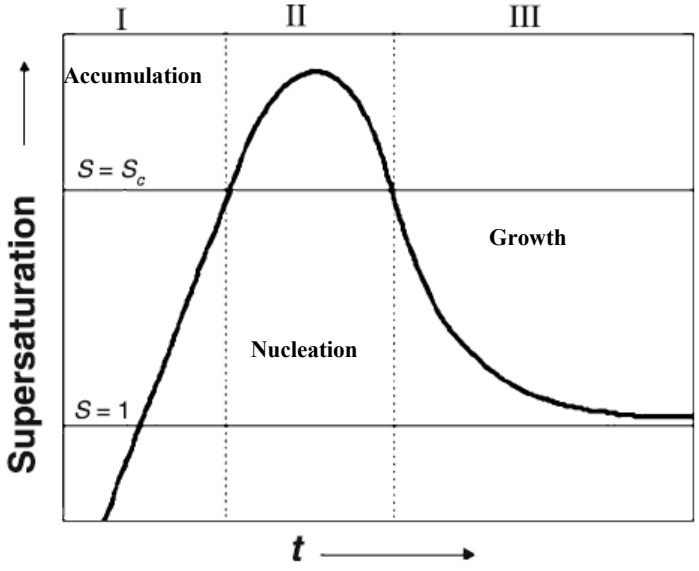

Figure 2.7 LaMer plot of the three-stage crystal formation.[54]

Two colloidal synthetic methods are used for QDs synthesis: hot-injection and non-injection (heat-up) approaches.[57-58] Hot-injection method was first reported by Bawendi's group[59] in 1993 for the synthesis of monodisperse cadmium chalcogenide QDs. The hot-injection method is a special case for the LaMer's three-stage crystal formation model (exclude stage I). The Heat-up method was revealed by Cao's group[60-61] in 2005 for the synthesis of CdSe and CdTe QDs. It matches all the three stages of LaMer model.

After we carefully reviewed and examined the synthesis of Pb-chaclogenide QDs, we realized that the current hot-injection method is not suitable for obtaining the PbS, PbSe, and PbTe QDs we desired for the investigation of QCEs in several aspects:

- Multiple sources of Pb precursor.
- Complicated metal-capping ligand system for PbS, PbSe, and PbTe QDs.
- Using oleic acid as capping ligand, which is too strong to be substituted.
- Using reagents which are not environmental friendly for the synthesis.
- Complicated synthesis for various sizes of Pb-chaclogenide QDs.
- Reaction time is too long.
- Reaction temperature is relatively high.

We need to find a simple Pb-capping ligand system to accommodate all the synthesis of PbS, PbSe, and PbTe QDs with monodisperse sizes below their exciton Bohr radius while optimizing the synthetic conditions. Such a system is the $PbCl_2$-OLA system. To achieve our goal of investigating QCEs of the binary Pb-chaclogenides, we need first to synthesize hydrophobic QDs with the $PbCl_2$-OLA system, then transfer the OLA capped QDs to hydrophilic QDs via ligand exchange[62] with 4-Mpy. We succeed in discovering the $PbCl_2$-OLA system by

reducing reactants used, adopting "green" reagents, lowering reaction temperature, shortening reaction time, synthesizing in open air environment, and simplifying the overall reaction process. Figure 2.8 illustrates the scheme of the hot-injection method developed by us for the synthesis of PbTe QDs with the $PbCl_2$-OLA model system. A typical synthetic procedure is described below. Two stock solutions of Te and Pb precursors were prepared separately. The Pb precursor was heated to an elevated temperature, and then the room temperature Te precursor was quickly injected in the Pb precursor solution. The reaction temperature dropped to its lowest point and the reaction was maintained at that temperature for PbTe QDs growth for various times. After reaction, the crudes were purified by cooling and centrifuge separation with both polar and non-polar solvents.

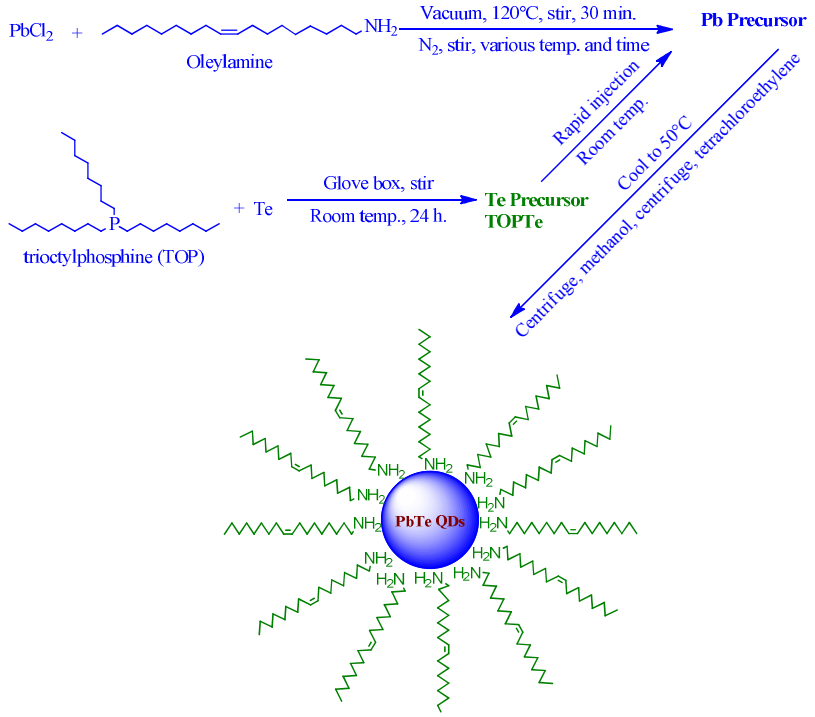

Figure 2.8 Hot-injection PbTe QDs synthetic scheme with $PbCl_2$-OLA system.

Figure 2.9 lists the main instruments used in the synthesis of PbTe QDs: glove box, oil-free vacuum pump, temperature controller, and Schlenk line vacuum manifold. Figure 2.10 elucidates the hot-injection method developed by us for the synthesis of PbSe QDs with $PbCl_2$-OLA model system. The synthesis uses environmentally benign ODE[63-64] as non-coordinating solvent and SeODE as Se precursor. The Se precursor is injected at elevated temperature instead of room temperature to further narrowing the size distribution of PbSe QDs. The SeODE precursor can also be used to obtain Se nanoclusters and Se QDs via solution crystallization.

Figure 2.9 Main instruments used in the synthesis of PbTe QDs: glove box, oil-free vacuum pump, temperature controller, and Schlenk line.

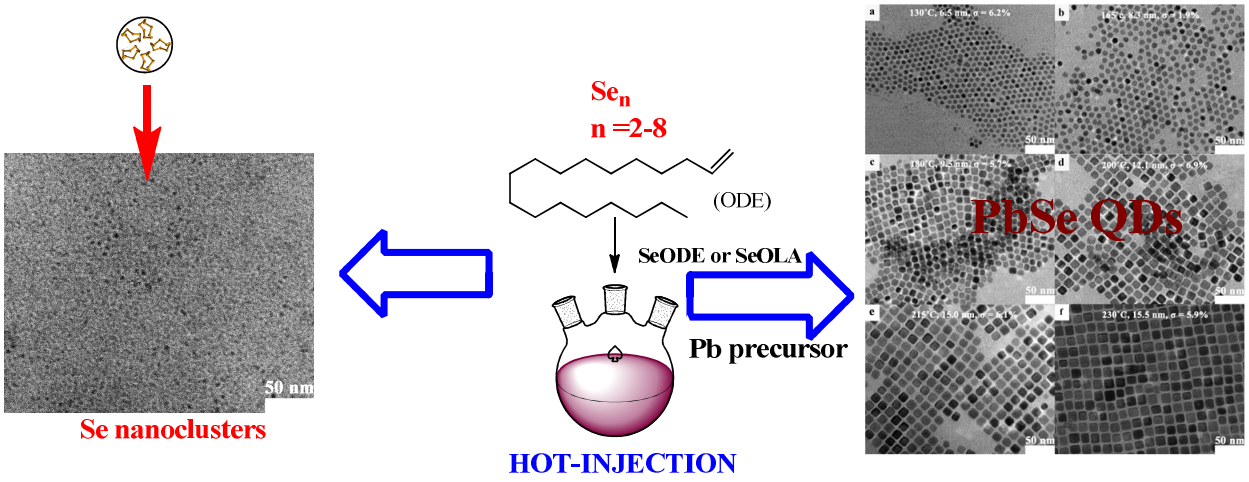

Figure 2.10 Hot-injection synthesis of PbSe QDs with $PbCl_2$-OLA system.

The non-injection heat-up method is simple, convenient, and efficient for large scale monodisperse QD synthesis or industrial tailored QD synthesis due to the less restrictive experimental requirements. Therefore, more reports of this method have been published within the last several years.[65-67] However, the current one-pot method still requires high reaction temperature and long reaction time due to the fact that non-metal precursors used are solids and need to be dissolved at elevated temperature to achieve the burst nucleation.

The perception that homogeneous nucleation process always requires high temperature hinders the development of QDs synthesis. The non-injection one-pot synthesis of PbS QDs with $PbCl_2$-OLA system developed by us lowers the nucleation and growth temperature by introducing activated components containing, homogeneous non-metal precursor solution. The synthetic route is shown in Figure 2.11. In contrast to the concept that the homogenous nucleation process needs high temperature to overcome the very high energy barrier, by using sulfide-containing STDE precursor or selenide-containing SeTDE precursor, we discovered that even at temperature of 45°C, monodisperse of PbS QDs with size of 2.1 nm can be synthesized within 5 min. while monodisperse PbSe QDs can also be obtained at 90°C. This is a crucial finding of the dissertation, which may dramatically change the way QDs are synthesized. The proposed PbS QDs formation mechanism of the one-pot synthesis in Equation 8-11 accounts for additional discovery of the dissertation.

Equation 8 shows that process of $PbCl_2$ and OLA form $PbCl_2$-OLA complex $(CH_3(CH_2)_7CH=CH(CH_2)_8(NH_3)^+)_2Pb(OH^-)_2Cl_2$, in the reaction mixture with the help of the trace water absorbed in OLA while heating, is a fast step. Equation 9 and 10 are slow steps: release of H_2S from either hydrogen polysulfides or the reaction of S_8 with TDE. The release of

H_2S is controlled kinetically by the reaction temperature (the heating ramp rate). The activated sulfides, which may control the nucleation process, in STDE were released at relatively low temperature. At high temperature, more H_2S was generated via the dehydrogenation of TDE by S_8 (Equation 10). Equation 11 is the overall reaction process.

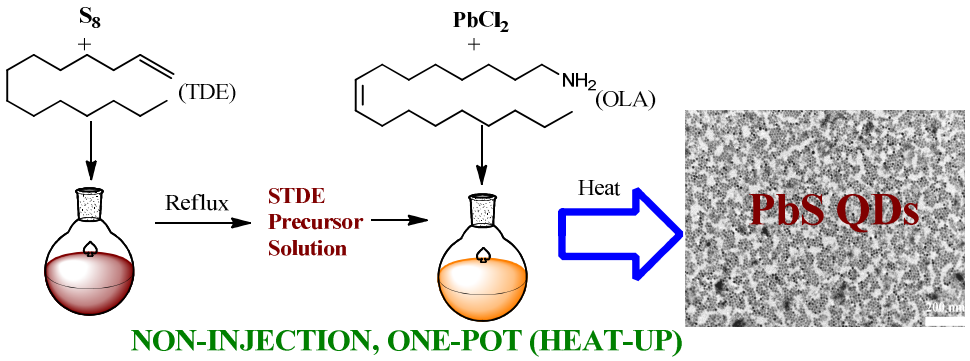

Figure 2.11 Non-injection, one-pot synthesis of PbS QDs with $PbCl_2$-OLA system.

$$PbCl_2 + 2\,CH_3(CH_2)_7CH{=}CH(CH_2)_8NH_2 \xrightarrow{2\,H_2O} (CH_3(CH_2)_7CH{=}CH\,(CH_2)_8(NH_3)^+)_2Pb(OH^-)_2Cl_2 \quad (8)$$

$$H\text{-}S_{(8x)}\text{-}S\text{-}H \longrightarrow x\,S_8 + H_2S \quad (9)$$

$x = 1, 2, 3...$

$$3\,S_8 + 8\,CH_3(CH_2)_{11}CH{=}CH_2 \longrightarrow 8\,CH_3(CH_2)_9(C_4H_3S) + 16\,H_2S \quad (10)$$

$$(CH_3(CH_2)_7CH{=}CH\,(CH_2)_8(NH_3)^+)_2Pb(OH^-)_2Cl_2 \xrightarrow[-2H_2O]{H_2S,\ OLA} PbS\ QDs + 2\,(NH_3^+(CH_2)_8CH{=}CH(CH_2)_7CH_3)Cl^- \quad (11)$$

The finding of TDE solvent is also an important discovery for the synthesis of S-containing and Se-containing QDs. Both S and Se have higher solubility in TDE compared to that of ODE. Further, TDE has low melting point of -13°C. All these tackle the low reactivity

and loss of reactivity problems of SeODE[57, 68-69] caused by using ODE as solvent. Figure 2.12 presents the application of the SeTDE based one-pot synthetic method for the synthesis of monodisperse GO and PbSe QDs nanocomposites (GO-PbSeQDs) with $PbCl_2$-OLA system. The one-pot method can further be used to obtain GO-Ag nanocomposites as Figure 2.13 indicated.

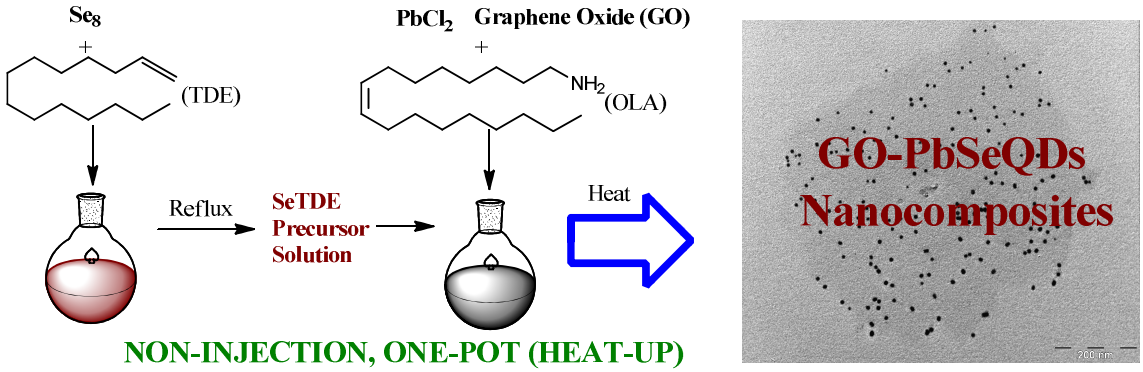

Figure 2.12 Application of the one-pot method in the synthesis of GO-PbSeQDs nanocomposites with $PbCl_2$-OLA system.

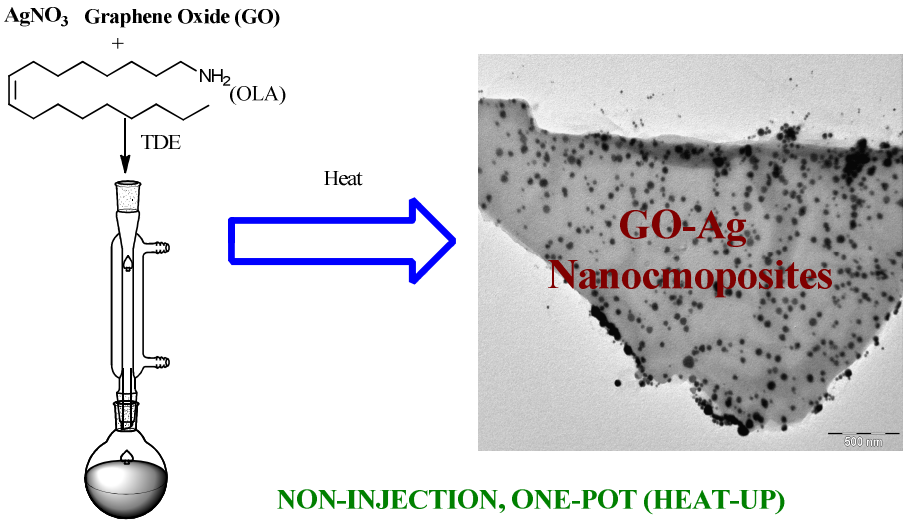

Figure 2.13 Application of the one-pot method in the synthesis of GO-Ag nanocomposites.

Perhaps, one of the most significant discoveries of this research is a method to synthesize various sizes of monodisperse, single elemental Se nanoclusters and Se QDs via solution crystallization[70] as shown in Figure 2.14. We find that TDE or ODE plays an important role in the synthesis of monodisperse Se QDs. They are actually weak capping ligands for Se. The interactions between the terminal double bonds of TDE or ODE and Se atoms in Se_8 may contribute to the size differences of Se QDs.

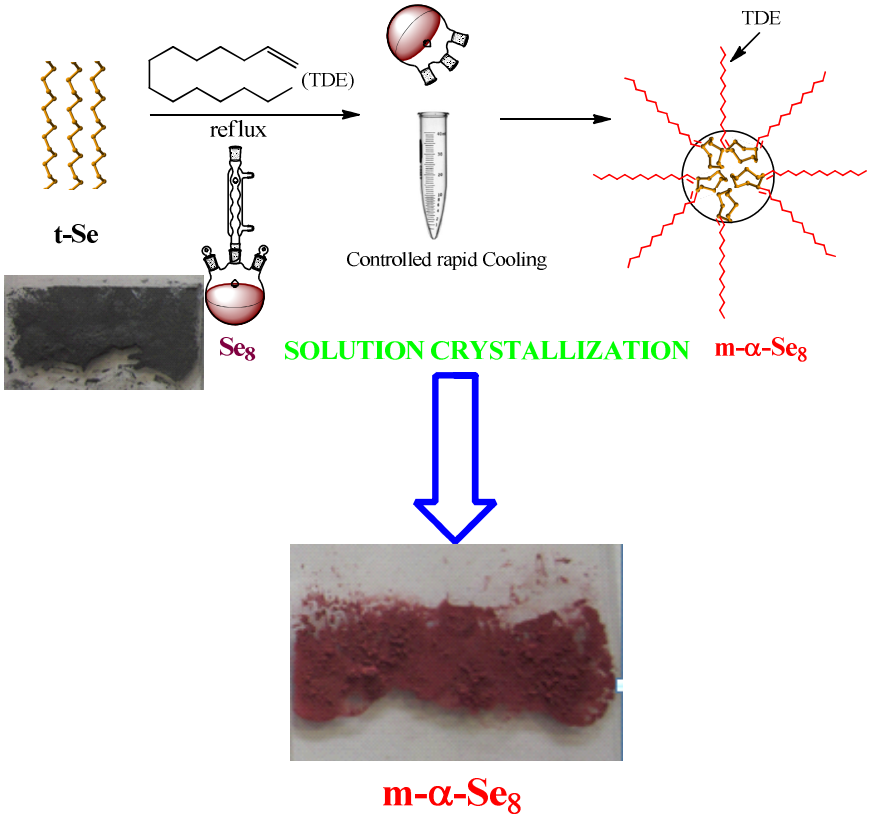

Figure 2.14 Monodisperse Se nanoclusters and Se QDs synthesized by solution crystallization.

After successfully synthesizing the binary PbS QDs, the hydrophobic OLA capped PbS QDs are converted to the hydrophilic 4-Mpy capped PbS QDs by ligand exchange as Figure-2.15 indicated. The 4-Mpy capped PbS QDs is then used for QCE study by SERS.

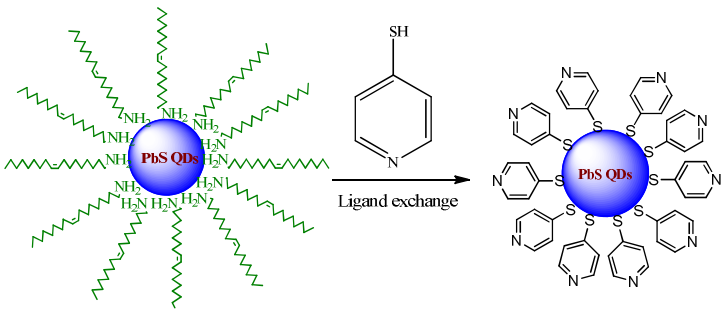

Figure 2.15 Ligand exchange of PbS QDs.

2.5.2 Characterization

Morphology of QDs

Understanding the morphology of QDs helps to better understand the physical and chemical structures of QDs. The size, size distribution, and shape of QDs synthesized are characterized using Transmission electron microscope (TEM), high resolution transmission electron microscope (HRTEM), and UV-Vis-Near IR spectrophotometer. TEM images of QDs were taken using a Zeiss EM 920 instrument operated at 80 kV. High resolution TEM images of QDs were taken using a JEOL, JEM-2100F instrument operated at 200 kV. The TEM samples were prepared by drop casting one drop of a dilute solution of QDs in tetrachloroethylene (TCE) or n-hexane on a 300 mesh carbon-coated, copper grid from Electron Microscope Sciences. The grid was dried by evaporating the solvent in air. The sizes and size distributions (relative standard deviation) of the QDs were measured from TEM images using iTEM 5.1 of Olympus Soft Imaging Solutions GmbH. A minimum of 120 QDs were counted on each image to obtain the average diameter of the QDs. The following sizing curves (Figure 2.16) and empirical equations[71] (Equation 12 is for PbS QDs[72] and Equation 13 is for PbSe QDs[73]) are also used to

estimate the sizes and band gap energies of the PbS, PbSe, and PbTe QDs. The UV-Vis-Near IR spectra were recorded by a Cary 500 UV-Vis-Near IR double beam spectrophotometer.

$$E_{ex\ (PbS)} = 0.41 + \frac{1}{0.0252d^2+0.283d} \tag{12}$$

$$E_{ex\ (PbSe)} = 0.278 + \frac{1}{0.016d^2+0.283d+0.45} \tag{13}$$

where, *d* is the diameter of the QDs.

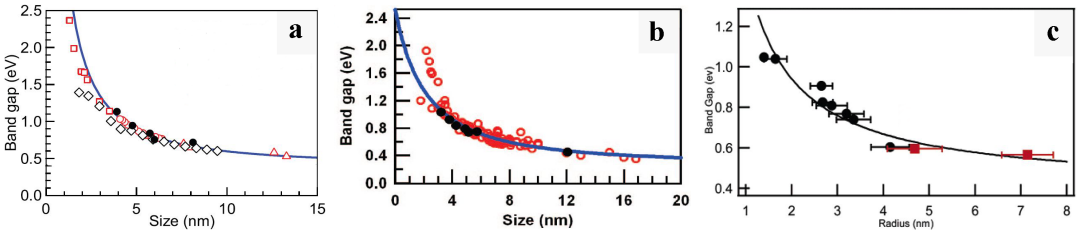

Figure 2.16 Band gap energy and size relationships of PbS, PbSe, and PbTe QDs. Figure 2.16 a-c are sizing curves of PbS[72] (size in diameter), PbSe[73] (size in diameter), and PbTe[74] (size in radius) respectively.

Composition of QDs

The composition of QDs is measured by energy-dispersive x-ray spectroscopy (EDS) for the qualitative and quantitative analysis of the elements in QDs. EDS measurements were performed using EDS attached to the JEM-2100F instrument. The composition of QDs is also characterized by powder x-ray diffraction (XRD) diffractometer.

Crystal Structure of QDs

The crystal structures of QDs are confirmed by the combined measurements using HRTEM, fast Fourier transformation of HRTEM (FFT), Raman spectroscopy, selected area x-ray diffraction (SAED), and XRD. The SAED was measured using JEM-2100F instrument. The Raman spectra were obtained using a Bruker Senterra Raman microscope with 785 nm excitation, a 1,200 l/mm holographic grating, a CCD detector, and power at the sample of 0.31 mW. A 50 X long working distance Olympus objective was also used. The XRD spectra were recorded on a PanXPert powder X-ray diffractometer with Cu Kα radiation (λ = 0.1542 nm). The sizes of QDs were also estimated from the full-width-half-maximum (FWHM) of the certain peaks of XRD using the Scherrer equation[75-76] (Equation 14).

$$d = \frac{B\lambda}{\beta \cos\theta} \tag{14}$$

where, *d* is the mean diameter of the QDs, B is a dimensionless shape factor of 0.9 (usually), λ is the X-ray wavelength (0.1542 nm), β (rad) is the FWHM of the reflection peak of 2θ, and θ is the diffraction angle.

Band Gap Energy and Optical Properties of QDs

The UV-Vis-Near IR spectra were recorded by a Cary 500 UV-Vis-Near IR double beam spectrophotometer. From the absorption data of the spectra, the extinction coefficient α can be calculated using Equation 15.[35, 77-78]

$$\alpha = B(h\nu - E_g)^n / h\nu \tag{15}$$

where, *h* is Planck's constant, hν is energy of photon, *B* is a constant related with semiconductor, *n* is an exponent which depends on the type of transition. The values of *n* of ½, and 2 correspond to indirect and direct transitions, respectively. The band gaps of QDs E_{QD} can be estimated using

Tauc plot $(\alpha h\nu)^2$ vs. $h\nu$. The radius of QD R can also be estimated from Equation 16 (derived from Equation 2):

$$R = \left(\frac{\hbar^2 \pi^2}{2\mu(E_{QD} - E_g)}\right)^{1/2} \quad (16)$$

Ligand Dynamics and Compounds Identification

Fourier transform infrared spectroscopy (FT-IR), Raman spectroscopy, ^{1}H and ^{13}C nuclear magnetic resonance spectroscopy (NMR), differential scanning calorimetry (DSC), mass spectrometry (MS), and gas chromatography and Mass Spectrometer (GC-MS) were used to monitor, analyze and identify reactants, products, and QDs synthesized. IR spectra were measured using Nicolet iS10 FT-IR Spectrometer from Thermo Scientific. Raman spectra (SERS) were obtained using a Bruker Senterra Raman microscope equipped with excitation wave length of 488 nm, 633 nm, and 785 nm. DSC curves were recorded with DSC-822 of Mettler Toledo. MS data was measured with 4000Q TRAP^{TM} LC/MS/MS System, GC-MS were recorded using Shimadzu GC-Chromatography GC-17A and Mass Spectrometer QP-5000. ^{1}HNMR and ^{13}CNMR spectra were measured with Varian Mercury-300 NMR Spectrometers.

2.6 Surface Enhanced Raman Spectroscopy (SERS)

Our group has reported two QCEs studies of size dependence of semiconductor QDs absorbed on thiol molecules by SERS recently. One is the ZnO QDs-4-Mpy and ZnO QDs-4-Mba (4-mercaptobenzoic acid) system,[79] the other is TiO_2 QDs-4-Mba system.[80] By scanning different sizes of ZnO QDs (18.2, 23.8, 25.2, 27.7, 30.6, and 32.8 nm) absorbed with either 4-Mpy or 4-Mba using excitation wave length of 514. 5 nm, ZnO QDs of size 27.7 nm generated the strongest QCEs. Similarly, probing TiO_2 QDs (6.8, 8.6, 10.9, 12.8, and 14.2 nm) absorbed

with 4-Mba using the same 514.5 nm excitation wave length, TiO_2 QDs size of 10.9 nm also produced the maximum QCEs. The latter enhancements are co-enhancement of 4-Mba molecular lines (modes) and the phonon modes of TiO_2 QDs. Charge-transfer was attributed to the enhancements. These studies are important for finding energy efficient solar cell materials. Since TiO_2 QDs are basic materials for solar cell manufacturing, SERS may be a fast and efficient method to select materials for solar cell application via measuring the charge-transfer rate of the materials. However, both the sizes of ZnO QDs and TiO_2 QDs we probed are much larger than their exciton Bohr radius (ZnO is 0.9 nm and TiO_2 has different values ranging from 0.8 nm to 2.2 nm). These materials may not generate the maximum QCEs due to their size constraints.

We expect smaller QDs with sizes less than their exciton Bohr radius to be better candidates for solar cell application and energy-efficient materials because these QDs will have much strong QCEs. We are also interested in the study of excitation wave length dependence of the QCEs to see at which wave length the QCEs of the same QDs have the maximum charge-transfer rate, which is also crucial for the development of solar cell materials. Two QD systems are available for SERS study:

1. A binary Pb-chaclogenide system with monodisperse PbS (2.1-16.5 nm), PbSe (3.6-15.5 nm), and PbTe (2.6 nm-14 nm), which all the sizes of QDs are less than their corresponding exciton Bohr radius.
2. A single elemental system with monodisperse monoclinic Se (1.6-12.0 nm), which the sizes of QDs are near the exciton Bohr radius.

We find both size and excitation wave length dependences of PbS QDs absorbed on 4-Mpy by SERS. Figure 2.17 demonstrates the QCEs of PbS QDs absorbed on 4-Mpy, which will be discussed in details in Chapter 4.

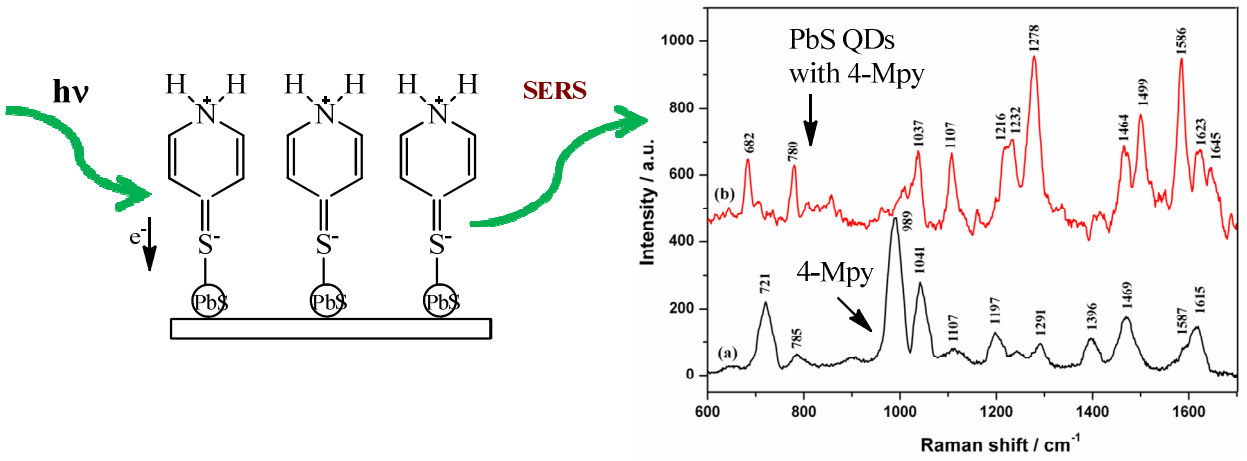

Figure 2.17 QCEs of PbS QDs absorbed on 4-Mpy.

Raman spectroscopy is really a powerful tool for structure characterization. Raman spectrum of Figure 2.18 reveals that the Se nanoclusters are m-α-Se_8 with HRETM data support. XRD failed to characterize the m-Se structure due to its measurement limit.

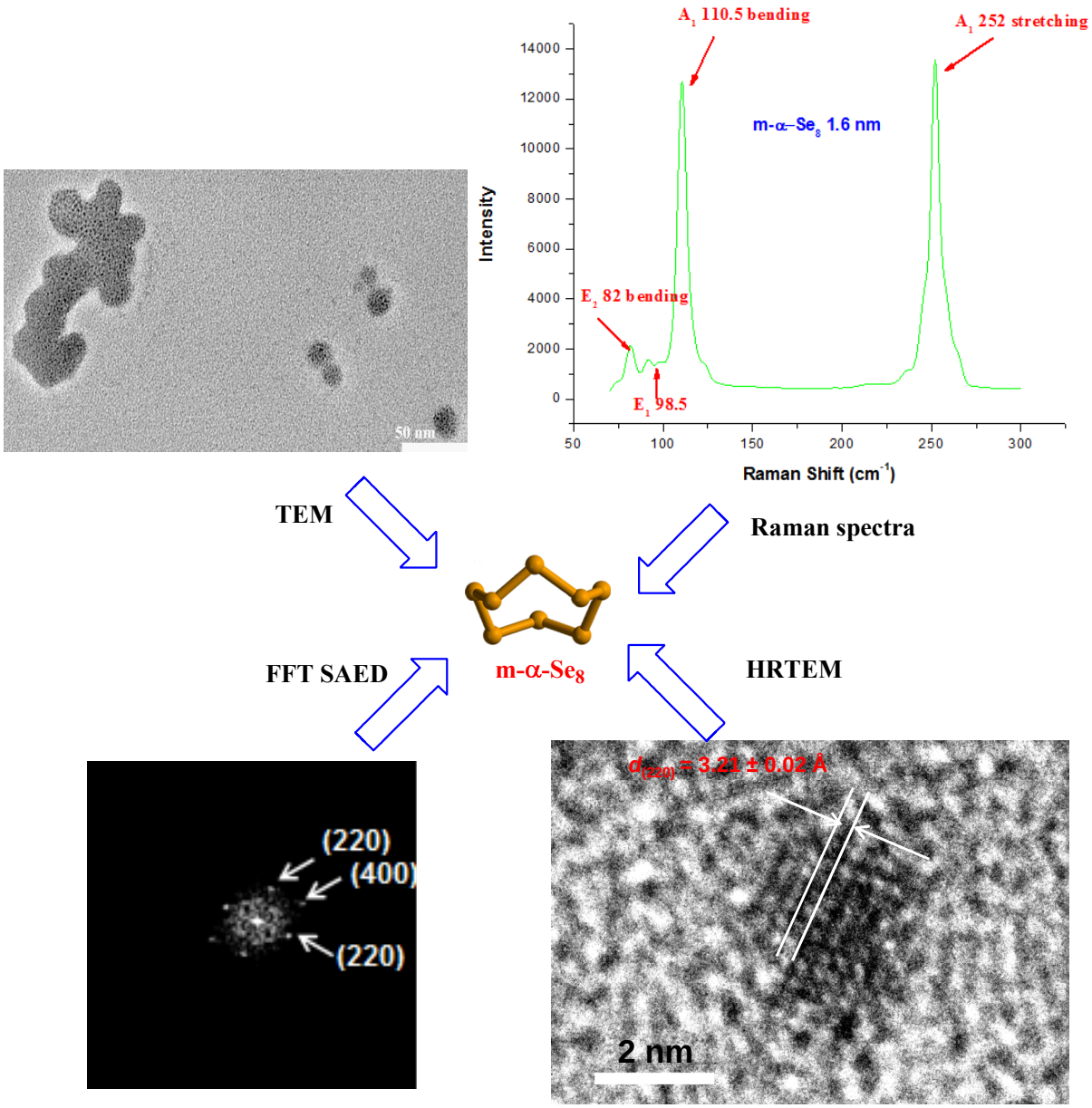

Figure 2.18 Crystal structure determinations of m-α-Se_8 using Raman spectra and HRTEM.

The following chapters report and discuss all the discoveries in details.

2.7 Chapter 2 Reference

(1) Alivisatos, A. P. *Science* **1996**, *271*, 933.

(2) Yoffe, A. D. *Advances in Physics* **2001**, *50*, 1.

(3) Donega, C. d. M. *Chemical Society Reviews* **2011**, *40*, 1512.

(4) Smith, A.; Nie, S. *Accounts Chem Res* **2010**, *43*, 190.

(5) Bera, D.; Qian, L.; Tseng, T.-K.; Holloway, P. H. *Materials* **2010**, *3*, 2260.

(6) Rogach, A. L. *Semiconductor nanocrystal quantum dots : synthesis, assembly, spectroscopy, and applications*; Springer: Wien ; New York, 2008.

(7) Sattler, K. D. *Handbook of nanophysics. Nanoparticles and quantum dots*; Taylor & Francis: Boca Raton, 2011.

(8) Sattler, K. D. *Handbook of nanophysics. Nanoelectronics and nanophotonics*; CRC Press/Taylor & Francis: Boca Raton, 2011.

(9) Sattler, K. D. *Handbook of nanophysics. Principles and methods*; Taylor & Francis: Boca Raton, Fla., 2011.

(10) Sattler, K. D. *Handbook of nanophysics. Nanotubes and nanowires*; Taylor & Francis: Boca Raton, Fla., 2011.

(11) Sattler, K. D. *Handbook of nanophysics. Functional nanomaterials*; Taylor & Francis: Boca Raton, 2011.

(12) Sattler, K. D. *Handbook of nanophysics. Clusters and fullerenes*; Taylor & Francis: Boca Raton, Fla., 2011.

(13) Yu, P. *Fundamentals of semiconductors : physics and materials properties*; 4th ed.; Springer: New York, 2010.

(14) Lamberti, C. *Characterization of semiconductor heterostructures and nanostructures*; 1st ed.; Elsevier: Amsterdam, Netherlands ; Boston Mass., 2008.

(15) Birke, R. L.; Znamenskiy, V.; Lombardi, J. R. *The Journal of Chemical Physics* **2010**, *132*, 214707.

(16) Richter, A. P.; Lombardi, J. R.; Zhao, B. *J Phys Chem C* **2010**, *114*, 1610.

(17) Ma, S.; Livingstone, R.; Zhao, B.; Lombardi, J. R. *The Journal of Physical Chemistry Letters* **2011**, *2*, 671.

(18) Livingstone, R.; Zhou, X.; Tamargo, M. C.; Lombardi, J. R.; Quagliano, L. G.; Jean-Mary, F. *The Journal of Physical Chemistry C* **2010**, *114*, 17460.

(19) Brus, L. E. *The Journal of Chemical Physics* **1984**, *80*, 4403.

(20) Kayanuma, Y. *Phys Rev B* **1988**, *38*, 9797.

(21) Wong, E. M.; Bonevich, J. E.; Searson, P. C. *The Journal of Physical Chemistry B* **1998**, *102*, 7770.

(22) Cherkasov, Y. A. *Russian Physics Journal* **1976**, *19*, 203.

(23) Dedigamuwa, Gayan S. (2010) *Fabrication and characterization of surfactant-free PbSe quantum dot films and PbSe-polymer hybrid structures*. (Doctoral Dissertation). Retrieved from Scholar Commons Citation.

(24) Huber, C. A.; Huber, T. E. *J Appl Phys* **1988**, *64*, 6588.

(25) Tutihasi, S.; Chen, I. *Solid State Commun* **1967**, *5*, 255.

(26) Tutihasi, S.; Chen, I. *Physical Review* **1967**, *158*, 623.

(27) Bouroushian, M. *Electrochemistry of metal chalcogenides*; 1st.ed. ed.; Springer: New York, 2009.

(28) Devillanova, Francesco A. Handbook of Chalcogen Chemistry: New Perspectives in Sulfur, Selenium and Tellurium. Cambridge: RSC Publishing, 2007.

(29) Lide, D. R. *CRC Handbook of Chemistry and Physics*; 77th ed.; Boca Raton, 1996.

(30) Wise, F. W. *Accounts Chem Res* **2000**, *33*, 773.

(31) Kothiyal, G. P.; Ghosh, B. *Prog Cryst Growth Ch* **1990**, *20*, 313.

(32) Medintz, I. L.; Uyeda, H. T.; Goldman, E. R.; Mattoussi, H. *Nat Mater* **2005**, *4*, 435.

(33) Popescu, A. Mihai *Non-Crystalline Chalcogenides*; Kluwer Academic Publishers: New York, 2002.

(34) Chen, Z.; Shen, Y.; Xie, A.; Zhu, J.; Wu, Z.; Huang, F. *Cryst Growth Des* **2009**, *9*, 1327.

(35) Mehta, S. K.; Chaudhary, S.; Kumar, S.; Bhasin, K. K.; Torigoe, K.; Sakai, H.; Abe, M. *Nanotechnology* **2008**, *19*.

(36) Zhang, Y.; Wang, J.; Zhang, L. *Langmuir* **2010**, *26*, 17617.

(37) Sarin, Love. (2010) *Nano-Selenium: Novel Formulations for Biological and Environmental Applications*. (Doctoral Dissertation). Retrieved from Internet.

(38) Singh, S. C.; Mishra, S. K.; Srivastava, R. K.; Gopal, R. *The Journal of Physical Chemistry C* **2010**, *114*, 17374.

(39) Johnson, J. A.; Saboungi, M.-L.; Thiyagarajan, P.; Csencsits, R.; Meisel, D. *The Journal of Physical Chemistry B* **1998**, *103*, 59.

(40) Lee, D. C.; Pietryga, J. M.; Robel, I.; Werder, D. J.; Schaller, R. D.; Klimov, V. I. *J Am Chem Soc* **2009**, *131*, 3436.

(41) Warner, J. H.; Tilley, R. D. *Nanotechnology* **2006**, *17*, 3745.

(42) Codoluto, S. C.; Baumgardner, W. J.; Hanrath, T. *Crystengcomm* **2010**, *12*, 2903.

(43) Taylor, B. R.; Kauzlarich, S. M.; Delgado, G. R.; Lee, H. W. H. *Chem Mater* **1999**, *11*, 2493.

(44) Prabakar, S.; Shiohara, A.; Hanada, S.; Fujioka, K.; Yamamoto, K.; Tilley, R. D. *Chem Mater* **2009**, *22*, 482.

(45) Gates, B.; Mayers, B.; Cattle, B.; Xia, Y. *Adv Funct Mater* **2002**, *12*, 219.

(46) Goldbach, A.; Saboungi, M.-L. *Accounts Chem Res* **2005**, *38*, 705.

(47) Stroyuk, A. L.; Raevskaya, A. E.; Kuchmiy, S. Y.; Dzhagan, V. M.; Zahn, D. R. T.; Schulze, S. *Colloids and Surfaces A: Physicochemical and Engineering Aspects* **2008**, *320*, 169.

(48) Caywood, John. (1969). *Optical and Electric Properties of a-Selenium*. (Doctoral Dissertation). Retrieved from Internet.

(49) Huang, X.; Yin, Z.; Wu, S.; Qi, X.; He, Q.; Zhang, Q.; Yan, Q.; Boey, F.; Zhang, H. *Small* **2011**, *7*, 1876.

(50) Stankovich, S.; Dikin, D. A.; Dommett, G. H. B.; Kohlhaas, K. M.; Zimney, E. J.; Stach, E. A.; Piner, R. D.; Nguyen, S. T.; Ruoff, R. S. *Nature* **2006**, *442*, 282.

(51) Prezhdo, O. V.; Kamat, P. V.; Schatz, G. C. *The Journal of Physical Chemistry C* **2011**, *115*, 3195.

(52) Gong, Ru J. *Graphene - Synthesis, Characterization, Properties and Applications*. Rijeka: InTech, 2011.

(53) Kamat, P. V. *The Journal of Physical Chemistry Letters* **2010**, *1*, 520.

(54) Kamat, P. V. *The Journal of Physical Chemistry Letters* **2011**, *2*, 242.

(55) Bai, S.; Shen, X. *RSC Advances* **2012**, *2*, 64.

(56) LaMer, V. K.; Dinegar, R. H. *J Am Chem Soc* **1950**, *72*, 4847.

(57) Kwon, S. G.; Hyeon, T. *Small* **2011**, *7*, 2685.

(58) de Mello Donegá, C.; Liljeroth, P.; Vanmaekelbergh, D. *Small* **2005**, *1*, 1152.

(59) Murray, C. B.; Norris, D. J.; Bawendi, M. G. *J Am Chem Soc* **1993**, *115*, 8706.

(60) Yang, Y. A.; Wu, H.; Williams, K. R.; Cao, Y. C. *Angewandte Chemie International Edition* **2005**, *44*, 6712.

(61) Cao, Y. C.; Wang, J. *J Am Chem Soc* **2004**, *126*, 14336.

(62) McDowell, M.; Wright, A. E.; Hammer, N. I. *Materials* **2010**, *3*, 614.

(63) Jasieniak, J.; Bullen, C.; van Embden, J.; Mulvaney, P. *The Journal of Physical Chemistry B* **2005**, *109*, 20665.

(64) Pan, Y.; Lombardi, J. In *Nanotech 2011--NanoTech Conference & Expo 2011*; NSTI: Boston, USA, 2011; Vol. 1, p 303.

(65) Li, N.; Zhang, X.; Chen, S.; Hou, X.; Liu, Y.; Zhai, X. *Materials Science and Engineering: B* **2011**, *176*, 688.

(66) Li, Z.; Ji, Y.; Xie, R.; Grisham, S. Y.; Peng, X. *J Am Chem Soc* **2011**, *133*, 17248.

(67) Ouyang, J.; Schuurmans, C.; Zhang, Y.; Nagelkerke, R.; Wu, X.; Kingston, D.; Wang, Z. Y.; Wilkinson, D.; Li, C.; Leek, D. M.; Tao, Y.; Yu, K. *ACS Appl Mater Interfaces* **2011**, *3*, 553.

(68) Lokteva, Irina. (2010) *Synthesis and Surface Characterization of Semiconductor Nanocrystals for Photovoltaic Application*. (Doctoral Dissertation). Retrieved from Internet.

(69) Bullen, C.; van Embden, J.; Jasieniak, J.; Cosgriff, J. E.; Mulder, R. J.; Rizzardo, E.; Gu, M.; Raston, C. L. *Chem Mater* **2010**, *22*, 4135.

(70) Leubner, I. H. *Precision crystallization : theory and practice of controlling crystal size*; CRC Press/Taylor & Francis: Boca Raton, 2010.

(71) Moreels, Iwan. (2009) *Colloidal Semiconductor Nanocrystals: From Synthesis to Photonic Applications*. (Doctoral Dissertation). Retrieved from Internet.

(72) Moreels, I.; Lambert, K.; Smeets, D.; De Muynck, D.; Nollet, T.; Martins, J. C.; Vanhaecke, F.; Vantomme, A.; Delerue, C.; Allan, G.; Hens, Z. *Acs Nano* **2009**, *3*, 3023.

(73) Moreels, I.; Lambert, K.; De Muynck, D.; Vanhaecke, F.; Poelman, D.; Martins, J. C.; Allan, G.; Hens, Z. *Chem Mater* **2007**, *19*, 6101.

(74) Urban, J. J.; Talapin, D. V.; Shevchenko, E. V.; Murray, C. B. *J Am Chem Soc* **2006**, *128*, 3248.

(75) Patterson, A. L. *Physical Review* **1939**, *56*, 978.

(76) Holzwarth, U.; Gibson, N. *Nat Nanotechnol* **2011**, *6*, 534.

(77) Manifacier, J. C.; De Murcia, M.; Fillard, J. P.; Vicario, E. *Thin Solid Films* **1977**, *41*, 127.

(78) Mills, G.; Li, Z.; Meisel, D. *The Journal of Physical Chemistry* **1988**, *92*, 822.

(79) Sun, Z.; Zhao, B.; Lombardi, J. R. *Appl Phys Lett* **2007**, *91*, 221106.

(80) Wang, D.; Zhao, H.; Wu, N.; El Khakani, M. A.; Ma, D. *The Journal of Physical Chemistry Letters* **2010**, *1*, 1030.

Chapter 3 Semiconductor QDs Synthesis and Characterization

This chapter covers the synthesis and characterization of a series of monodisperse, binary QDs, single elemental Se QDs, and QD and graphene oxide (GO) nanocomposites. Topics including:

1. A new universal $PbCl_2$-OLA (oleylamine) based system developed for PbS, PbSe, PbTe, and other Se-containing QDs as well as nanocomposites formed by PbSe QDs and (GO).

2. A novel, non-injection, one-pot, temperature based synthetic method for PbS, PbSe QDs, and nanocomposites formed by PbSe QDs and GO with 1.

3. A new solvent 1-tetradecene (TDE) for S to generate activated sulfide-containing STDE solution used as universal S precursor for S-containing QD synthesis.

4. Se solution from Se dissolved and reacted with TDE (SeTDE) as universal Se precursor for Se-containing QD synthesis.

5. A new, simple, solution precipitation method for obtaining single elemental Se QDs using SeTDE from 4 and SeODE (Se dissolved and reacted with ODE).

6. Modified hot-injection methods for PbSe with different Pb sources, capping reagents, Pb and Se feed mole ratios, and two Se precursors (SeOLA and SeODE) for PbSe QD synthesis with 1.

7. Modified hot-injection methods for PbTe QD synthesis with 1 using different Pb sources and PbTe QDs stability tests.

They are discussed in the following five sections of this chapter.

3.1 Controlled Synthesis of PbS QDs

A new activated sulfide-containing solution was discovered by dissolving sulfur in TDE at elevated temperatures. The components of the activated sulfides in the STDE solution are hydrogen polysulfides and 2-decylthiophene. Using this high concentration S precursor, a novel, simple, non-injection, one-pot, temperature-based synthetic method was developed to obtain size controlled monodisperse PbS semiconductor QDs in short time at low nucleation temperature. It reveals that nucleation process of the nanoscaled QD formation is not necessary always a high temperature process as widely acknowledged. A general PbS QDs formation mechanism is also proposed.

3.1.1 Introduction

For many years, considerable research has been carried out to find synthetic protocols using one-pot, green synthetic methods that can be tailored to industrial production to obtain size and morphology controlled, high quality monodisperse chalcogen-containing semiconductor QDs.[1-3] Recently, environmentally benign solutions of sulfur, such as S powder dissolved in oleylamine OLA[4-6] or ODE[7] have been used as the S precursor for hot-injection methods to synthesis monodisperse chalcogen-containing QDs.

It was not until recently that Yu's group reported a low temperature, non-injection,[8-10] one-pot synthesis of PbS QDs using bis(trimethylsilyl)sulfide ($(TMS)_2S$), thioacetamide (TAA),

and elemental sulfur as S precursors at growth temperature of 30-120°C.[11] Simply combining all the reactants, PbS QDs were synthesized at relative low temperatures. This represented a significant improvement and trend for the synthesis of PbS QDs. Not only was the reaction process simplified, the reaction temperature lowered, and the cost reduced, but they also revealed that hot-injection can be further substituted by one-pot synthesis via varying the reaction temperature. Mokari's group used lead bisdiethyldithiocarbamate as single source of both Pb and S precursor with the non-injection approach to obtain PbS nanowires at high temperatures.[12] Peng's group also adopted alkylthiols as S precursor source with the non-injection method to produce PbS QDs at high temperatures.[13] Si's group synthesized PbS QDs using injection method to obtain PbS QDs with aqueous media at room temperature.[14]

However, all of the above mentioned non-injection methods use toxic thiol-containing reagents which are very sensitive to water. They are also not simple—use of several reagents in the reaction processes. Some of them have to be carried out at temperature over 200°C with long reaction time. In addition, except the room temperature injection approach, there is limited information of the size, size distribution of the QDs synthesized though absorption spectra are available. Further, the size of the PbS QDs synthesized at room temperature ranged from 7 nm to 18 nm with a broad size distribution of 10%-20% because it is very difficult to control the release of H_2S in aqueous solution. Moreover, there has been very few discussion of PbS QDs formation mechanism[15-17] in the literature, especially for the chemical reactions involved.

Actually, all of the previous synthetic approaches intended to solve a key problem: how to generate and release the reactive species H_2S in a controlled manner so that nucleation and growth can be achieved at low temperature with relatively short time?

To achieve the goal of establishing simple, environmentally benign, size controlled and industry tailored synthetic protocol and solve the low temperature nucleation problem, additional developments are needed, especially for the S precursor to be controlled to release reactive species H_2S during reaction.

Previously, we developed a temperature-based, hot-injection synthetic procedure through which size controlled monodisperse PbSe QDs was synthesized by just controlling temperatures to accommodate the nucleation and growth processes.[18] The rationale behind our hot-injection method was by mixing two homogenous precursor solutions (instead of mixing with Se solids) at an elevated temperature (nucleation process), size controlled monodisperse QDs were prepared after nucleation and a short time growth at a lower temperature. The existing environmentally benign S precursor solution for hot-injection synthesis made by ODE (S powder dissolved in ODE around 90°C) was a heterogeneous solution when cooled to room temperature due to sulfur's low solubility in ODE. This is not suitable for the non-injection, one-pot synthesis we designed, which mixing two homogeneous precursor solutions at room temperature. Therefore, the discovery of novel homogeneous S precursors was crucial for the new non-injection, one-pot synthesis of size controlled monodisperse QDs.

We also confirmed that if high concentration S stock solutions containing activated components of sulfides were available at room temperature, we can further simplify the reaction protocol to eliminate the hot-injection step by adding the homogeneous S precursor in the starting reactant mixture to proceed with one-pot synthesis. Thus, most of the above-mentioned problems can be solved by the proposed environmentally friendly, cost effective, and simple one-pot synthetic method. This would be helpful to achieve the goal of setting up the size controlled

and industry tailored synthetic method by streamlining the process of producing hydrogen sulfide, reducing the reaction time, carrying out the reaction at low temperature, and facilitating industrial batch productions. We proposed that the stable, sulfide-containing high concentration S stock solutions can be the universal S precursor for the synthesis of sulfur-containing QDs.

In this section, we report the following discoveries: (1) A new, activated sulfide-containing high concentration S stock solution, S powder dissolved in TDE at elevated temperatures, is evaluated systematically. The activated components and the reactivity study of STDE compare with SODE and SOLA (S powder dissolved in OLA). (2) Design and develop a $PbCl_2$-OLA model system to demonstrate that size controlled monodisperse PbS QDs below its exciton Bohr radius can be obtained in a dramatically reduced reaction time with our non-injection, one-pot synthetic method. To the best of our knowledge, there are no reports of these kinds of synthesis until now. (3) A new PbS QDs formation mechanism.

The formation of PbS QDs is shown in Figure 3.1.

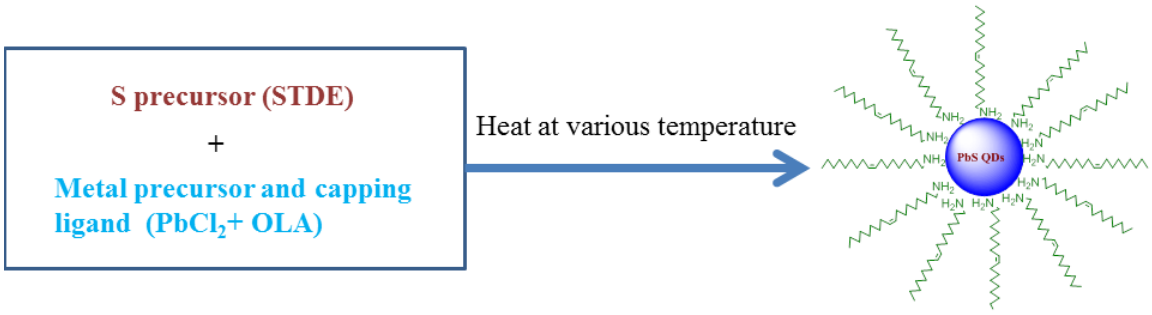

Figure 3.1 Non-injection, one-pot synthesis of PbS QDs.

3.1.2 Experimental

Chemicals

$PbCl_2$ (99-100%) was from J.T. Baker. Sulfur (S, 99.5-100.5%, powder) was from Fisher

Chemical. Methanol (absolute reagent, 99.8%, A.C.S.) was purchased from Spectrum Chemical. Tetrachloroethylene (TCE, 99%, extra pure), oleylamine (OLA, 80-90%), 1-octadecene (ODE, 90%), 1-tetradecene (TDE, 94%), and chloroform-d ($CDCl_3$, D-enrichment > 99.75%) were purchased from ACROS Organic. Lead acetate paper was from Thermo Fisher Scientific, Inc. All chemicals were used as received without further purification.

SODE, SOLA, and STDE Precursor Preparation and Reactivity Test

0.8 M, 10 mL S precursor stock solution SODE was prepared by dissolving 0.256 g of S powder in 10.0 mL ODE at 200-260°C or reflux. Then it was cooled to room temperature for storage. Only at elevated temperature as high as over 200°C, the SODE solution can be homogeneous when cooled to room temperature.

0.8 M, 10 mL S precursor stock solution SOLA was prepared by dissolving 0.256 g of S powder in 10.0 mL OLA at 50-60°C. Then it was cooled to room temperature for storage. It was used as S precursor for the modified hot-injection, solvent-free synthesis of PbS QDs. The reactants only include three compounds: $PbCl_2$, OLA, and S.

0.8 M, 20 mL S precursor stock solution STDE was prepared by dissolving 0.513 g of S powder in 20.0 mL TDE at 200-250°C or reflux. Then it was cooled down to room temperature for storage. The maximum concentration of STDE can reach at more than 4 M without any precipitation at room temperature.

Several drops of the 0.8 M STDE, 0.8 M SODE, and 0.8 M SOLA were place on the lead acetate papers respectively to check the activated components' reactivity. The color of lead acetate papers did not change for a long time if water is not added. When water was added to

each lead acetate papers, only the color of SOLA's test paper changed from white to black within 15 s (Table 3.1).

Both SOLA solution generated some precipitates when cooled to room temperature due to the melting point of OLA is close to room temperature. SODE and STDE remained as a clear solution.

Table 3.1 SODE, SOLA, and STDE Reactivity Test

	Color Change		
Lead acetate paper	SODE	SOLA	STDE
Without water	-	-	-
With water	-	Black in 15 s	-

^{1}HNMR and ^{13}CNMR spectra of STDE were recorded for STDE solution component analysis. The STDE sample was also passed through a column of GC-MS for separation and additional component analysis.

Non-injection, one-pot synthesis of PbS QDs using STDE with $PbCl_2$-OLA system

In a typical example of synthesis of the 7.0 nm spherical PbS QDs (a-3), 0.110 g (0.40 mmol) $PbCl_2$, 3.39 g (10.14 mmol, 4.19 mL) OLA, and 1.0 mL 0.8 M STDE solution was introduced into a three-neck round-bottom flask at room temperature. The mixture was magnetically stirred and heated to 30℃ under vacuum for 15 min. Then, the vacuum was removed and the temperature of the mixture was further raised to 130℃ with a heating rate at about 13.5˚C/min. The temperature of the mixture was maintained at that level for 5 min. Then,

the crude solution was cooled immediately in a water bath. The crude was centrifuged and washed with methanol. Next, 5 mL of TCE was added into the crude to extract PbS QDs. After centrifuging, the as-synthesized PbS QDs were stored in TCE.

This non-injection, temperature-based synthetic method was used to obtain various sizes of PbS QDs by running various batches of the synthesis under the same conditions: the same amounts of chemical reagents were used, Pb to OLA feed mole ratio of 1:26, Pb to S feed mole ratio of 1:2, the growth time of 5 min., but at a variety of reaction temperatures (45℃ to 220℃). The synthetic conditions and results of PbS QDs sample a-1 to a-7 are listed in Table 3.2.

Table 3.2 Non-injection, One-pot Synthesis of PbS QDs with STDE

Sample #	**a-1**	**a-2**	**a-3**	**a-4**	**a-5**	**a-6**	**a-7**	**a-8***
Pb to S Feed Mole Ratio	1:2	1:2	1:2	1:2	1:2	1:2	1:2	1:2
OLA to Pb Mole Ratio	26:1	26:1	26:1	26:1	26:1	26:1	26:1	32:1
Heating rate (°C/min.)	3.0	14.2	13.5	16.5	16.3	18.5	19.3	-
Growth time (min.)	5	5	5	5	5	5	5	5
Growth Temperature (°C)	45	90	130	160	185	200	220	55
Sample Size (nm)	**2.1**	**4.0**	**7.0**	**8.2**	**8.9**	**14.8**	**16.5**	**10-20**
σ	8.6%	6.9%	6.9%	7.1%	6.8%	7.3%	7.0%	-

* S precursor is SOLA instead of STDE. Reaction time is 5 min. at corresponding growth temperature.

Non-injection, one-pot synthesis of PbS QDs using SOLA with $PbCl_2$-OLA system

PbS QDs sample a-8 (Table 3.2) was synthesized using a non-injection, solvent-free synthetic method by adding 0.110 g (0.40 mmol) $PbCl_2$, 3.39 g (10.14 mmol, 4.19 mL) OLA and 1.0 mL 0.8 M SOLA into a three-neck round-bottom flask at room temperature. The mixture was magnetically stirred and heated to 30℃ under vacuum for 15 min. Then, the vacuum was

removed and the temperature of the mixture was further raised to 55℃. The temperature of the mixture was maintained at that level for 5 min. Then, the crude solution was cooled immediately in a water bath. The crude was centrifuged and washed with methanol.

Sample characterization

The size, shape, crystal structure and composition of PbS QDs were characterized by transmission electron microscope (TEM), high resolution transmission electron microscope (HRTEM), selected area x-ray diffraction (SAED), and energy-dispersive x-ray spectroscopy (EDS). Component analysis was performed by GC-MS, ^{1}HNMR, and ^{13}CNMR.

TEM images of PbS QDs were taken by a Zeiss EM 920 instrument operated at 80 kV. High resolution TEM images of PbS QDs were taken using a JEOL, JEM-2100F instrument operated at 200 kV. The TEM samples were prepared by drop casting one drop of a dilute solution of PbS QDs in TCE on a 300 mesh carbon-coated, copper grid from Electron Microscope Sciences. The grid was dried by evaporating the solvent in air. The sizes and size distributions (relative standard deviation) of the PbS QDs were measured from TEM images using iTEM 5.1 of Olympus Soft Imaging Solutions GmbH. A minimum of 120 QDs were counted on each image to obtain the average diameter of the PbS QDs. SAED patterns were obtained using JEM-2100F. The EDS spectra were recorded using EDS attached to JEM-2100F. GC-MS were recorded using Shimadzu GC-Chromatography GC-17A and Mass Spectrometer QP-5000. ^{1}HNMR and ^{13}CNMR spectra were measured with Varian Mercury-300 NMR Spectrometers.

3.1.3 Results and Discussion

SODE, SOLA, and STDE Precursor Preparation and Reactivity Test

Table 3.1 lists the test results of reactivity of SODE, SOLA, and STDE measured by lead acetate paper. The results indicate that both SODE and STDE do not release any activated components of H_2S or polysulfides with either water presented or not at room temperature. They may be good candidates for the non-injection method because the release of the activated components can be controlled by temperature. SOLA is a relatively active reagent since it can react with Pb at room temperature with trace water. For the SOLA solution, the activated components are alkylammonium polysulfides as reported by Ozin group.[19] We found that S_8 can fully dissolve in OLA to form 0.8 M SOLA upon heating to 50-60˚C. Judging from the test results of using the same 0.8 M of SODE, SOLA, and STDE, the reactivity of the S precursor solutions may be in the order of SODE < STDE < SOLA. However, SOLA generate some precipitates during storage at room temperature. We choose either STDE or SODE as the S precursor for the non-injection, one-pot synthesis of PbS QDs. They can also be used as the universal S precursor for S-containing QD synthesis.

Non-injection, one-pot synthesis of PbS QDs using STDE with $PbCl_2$-OLA system

The synthetic conditions and the results are listed in Table 3.2. Both HRTEM image (Figure 3.2b) and SAED diffraction pattern (Figure 3.2a top right inset) of sample a-3 of 7.0 nm confirm that the nanoparticles are single crystals. The lattice fringe of PbS is measured at 3.0 ± 0.1 Å, which is in consistent with the (200) lattice planes for bulk PbS (JCPDS No. 770244, 2.967 Å). The TEM images of the PbS QDs synthesized using STDE as precursor (a-1 to a-7) are shown in Figure 3.3. The size ranged from 2.1 nm to 16.5 nm, below the 18 nm exciton Bohr radius of bulk S. The size distribution is from σ = 6.8%-8.6%, which is narrowly distributed. The shape of the PbS QDs is either spherical or cubic. Compared to Table 4.1 of the hot-

injection synthetic results of PbS QDs, which has a size distribution from 9.8% to 11.8%, the non-injection synthetic method demonstrates the following advantages:

1. Wider size range: from 2.1 nm to 16.5 nm instead of 5.0 nm to 10.2 nm.
2. Narrower size distribution: from 6.8% to 8.6% instead of 9.8% to 11.8%.
3. Lower reaction and growth temperatures: as low as 45°C, instead of 210°C.
4. Reduced reaction time to 5 min., instead of from 5 min. to 120 min.
5. Reactions are carried out in open air environment, instead of under nitrogen protection.
6. The QDs have both spherical and cubic shapes instead of only spherical shape.

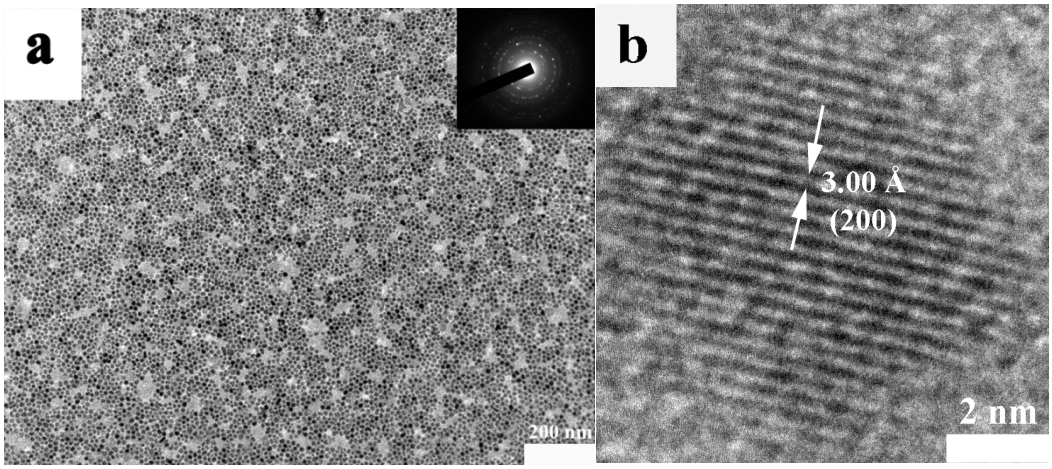

Figure 3.2 TEM and HRTEM images and SADE of PbS QDs sample a-3 with size of 7.0 nm synthesized using the non-injection, one-pot method. The lattice fringe of the PbS QDs is measured at 3.00 ± 0.1 Å.

The XRD of PbS QDs is listed in Figure 4.1 of chapter 4. It reveals that the crystal structure of PbS QDs synthesized is the same as bulk PbS. The composition of PbS QDs was

verified by EDS (Figure 3.4 and Figure 3.5). TEM, HRTEM, SAED, and EDS data confirmed the size, shape, size distribution, and crystal structure of the QDs synthesized are PbS.

The synthetic curve obtained (Figure 3.6) is a useful guideline for the synthesis of various sizes of PbS QDs using the similar synthesis conditions.

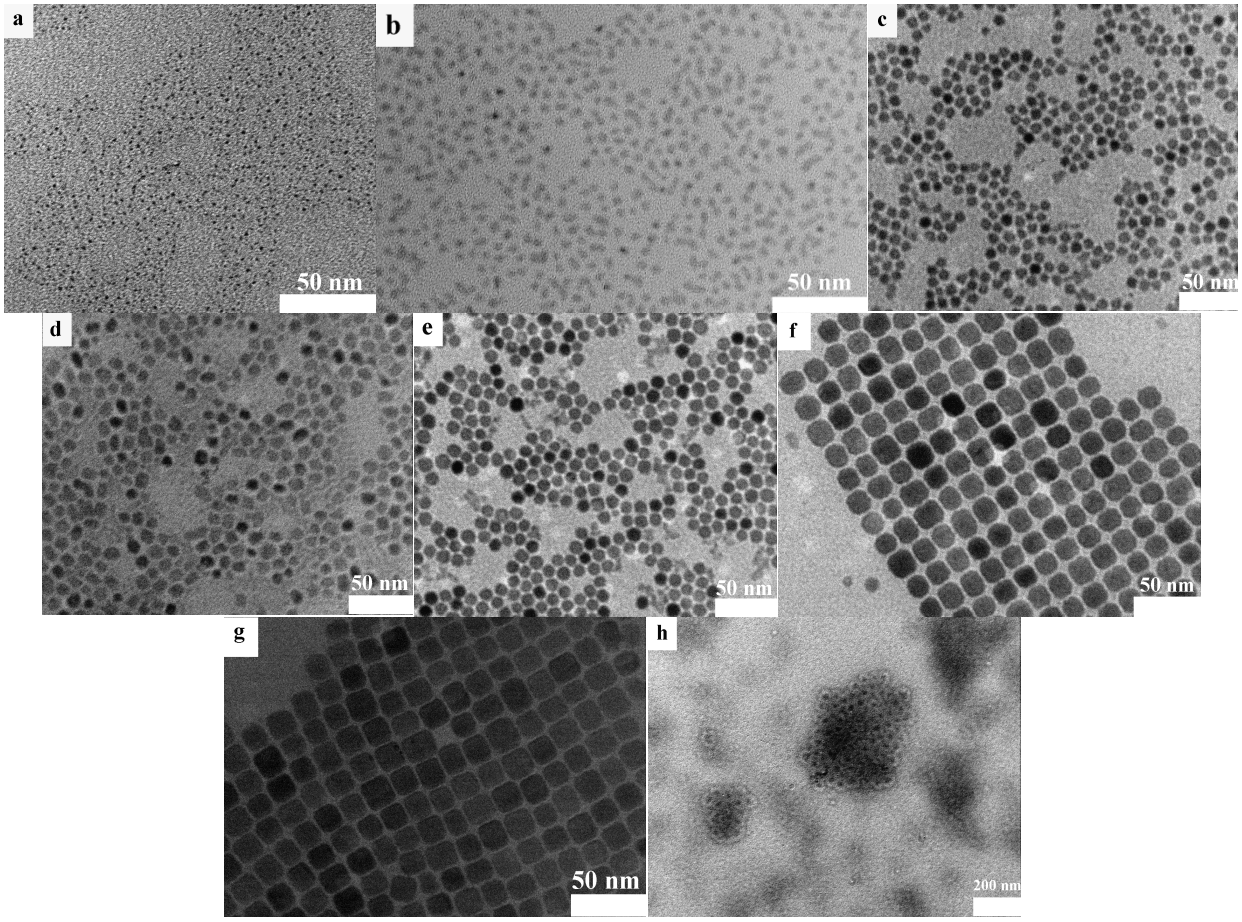

Figure 3.3 TEM images of PbS QDs synthesized using non-injection, one-pot method. Figure 3.3a to Figure 3.3g corresponding to PbS QDs sample a-1 of 2.1 nm with size distribution σ = 8.2%, a-2 of 4.0 nm with σ = 6.9%, a-3 of 7.0 nm with σ = 6.9%, a-4 of 8.2 nm with σ = 7.0%, a-5 of 8.9 nm with σ = 6.8%, %, a-6 of 14.0 nm with σ = 7.3%, a-7 of 16.5 nm with σ = 7.0% respectively. Their reaction temperatures are 45°C, 90°C, 130°C, 160°C, 185°C, 200°C, and

220°C respectively. Figure 3.3h is the preliminary result of sample a-8 prepared by a non-injection, solvent-free method using SOLA at 45°C. Its size is from 10 nm to 20 nm with a relatively broad distribution.

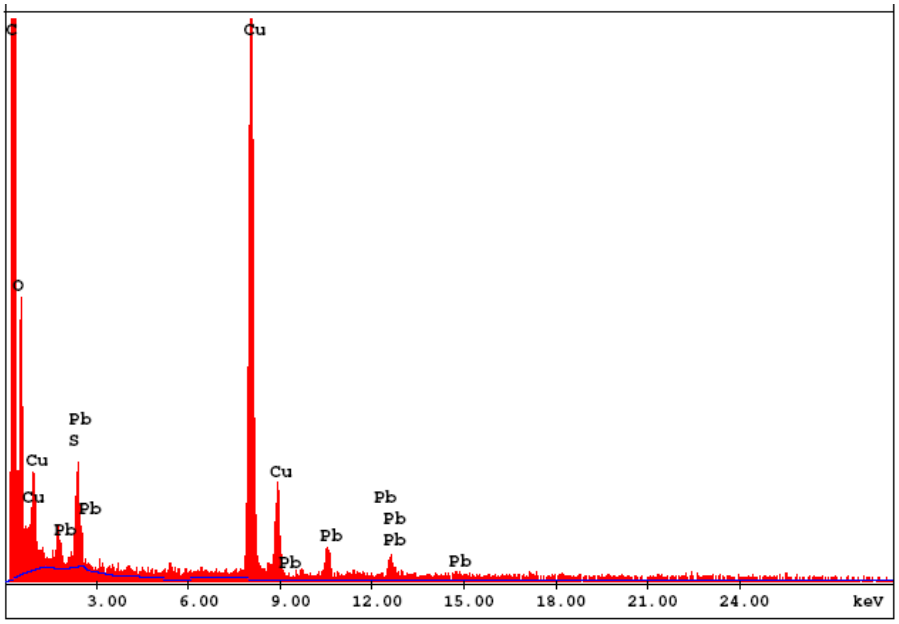

Figure 3.4 EDS result of PbS QDs sample a-2 of 4.0 nm.

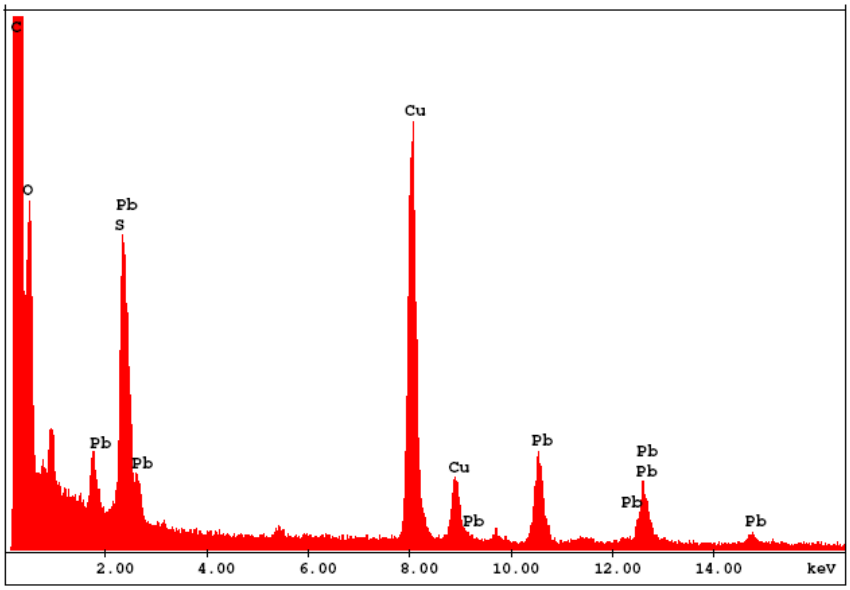

Figure 3.5 EDS result of PbS QDs sample a-3 of 7.0 nm.

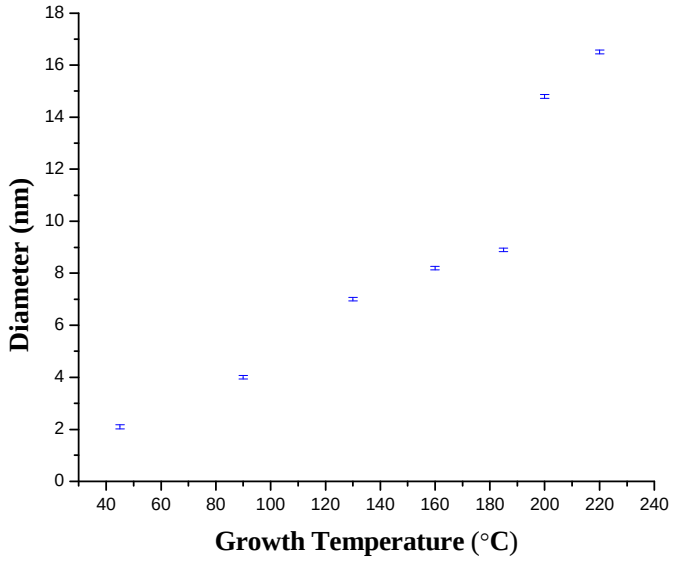

Figure 3.6 The temperature-based synthetic curve of PbS QDs. When other conditions remain constant and the reaction growth time is at 5 min., narrowly distributed PbS QDs were synthesized with various reaction temperatures.

Non-injection, one-pot synthesis of PbS QDs using SOLA with $PbCl_2$-OLA system

Figure 3.3h indicates that the non-injection, solvent-free synthesis of PbS QDs is possible using only Pb source, capping ligand OLA, and SOLA. Further optimization of the reaction conditions is necessary to obtain monodisperse PbS QDs.

Reaction mechanism

We propose a reaction mechanism for the PbS QDs formation. $PbCl_2$ and OLA form $PbCl_2$-OLA complex: $(CH_3(CH_2)_7CH=CH(CH_2)_8(NH_3)^+)_2Pb(OH^-)_2Cl_2$ in the reaction mixture with the help of the trace water absorbed in OLA while heating (Equation 1). It is a fast step. Indeed, the recently observed $(CH_3(CH_2)_7CH=CH(CH_2)_8(NH_3)^+)_2PbCl_4^{2-}$ complex in a similar

reaction system by Koutselas group[20] provides experimental support for this hypothesis. Equation 2 and 3 are slow steps: release of H_2S from either hydrogen polysulfides or the reaction of S_8 with TDE. The release of H_2S is controlled kinetically by the reaction temperature (the heating ramp rate). The activated sulfides, which may control the nucleation process, in STDE were released at relative low temperature. At high temperature, more H_2S were generated via the dehydrogenation of TDE by S_8 (Equation 3). The hydrogen polysulfides formation in liquid sulfur proposed by Wiewiorowski group,[21] the post-reaction thiophene observed by Peng's group,[8] and the 2-decylthiophene detected in STDE solution by our group (GC-MS, ^{1}HNMR: δ = 7.09 ppm [dd], δ = 6.90 ppm [dd], δ = 6.78 ppm [m], and ^{13}CNMR results, Figure 3.7 to Figure 3.9) provide evidences for the postulate. Equation 4 is a fast step of the formation of PbS QDs between Pb metal complex, H_2S, and the capping ligand OLA (the nucleation process), followed by the growth process of the PbS QDs. This is a very fast process due to the high value of solubility product constant of PbS. It is a process that involves both chemical reaction and nucleation.

$$PbCl_2 + 2\,CH_3(CH_2)_7CH{=}CH(CH_2)_8NH_2 \xrightarrow{2\,H_2O} (CH_3(CH_2)_7CH{=}CH\,(CH_2)_8(NH_3)^+)_2Pb(OH^-)_2Cl_2 \quad (1)$$

$$H\text{-}S_{(8x)}\text{-}S\text{-}H \longrightarrow x\,S_8 + H_2S \quad (2)$$

x =1, 2, 3...

$$3\,S_8 + 8\,CH_3(CH_2)_{11}CH{=}CH_2 \longrightarrow 8\,CH_3(CH_2)_9(C_4H_3S) + 16\,H_2S \quad (3)$$

$$(CH_3(CH_2)_7CH{=}CH\,(CH_2)_8(NH_3)^+)_2Pb(OH^-)_2Cl_2 \xrightarrow[-2H_2O]{H_2S,\ OLA} PbS\ QDs + 2\,(NH_3^+(CH_2)_8CH{=}CH(CH_2)_7CH_3)Cl^- \quad (4)$$

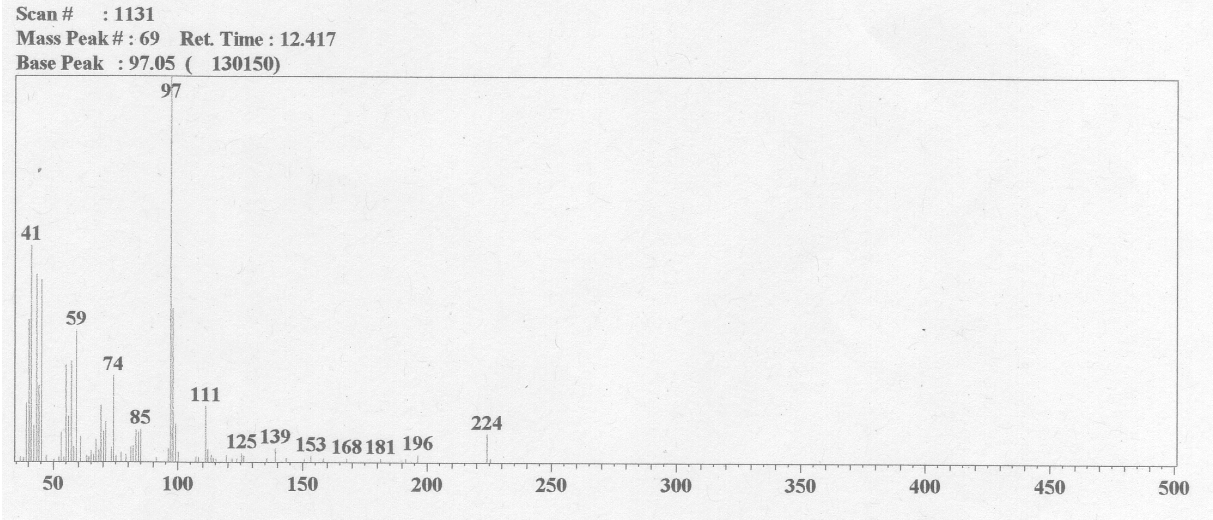

Figure 3.7 GC-MS results of STDE solution. The peak at *m/z* = 224 is the molecular peak of 2-decylthiophene.

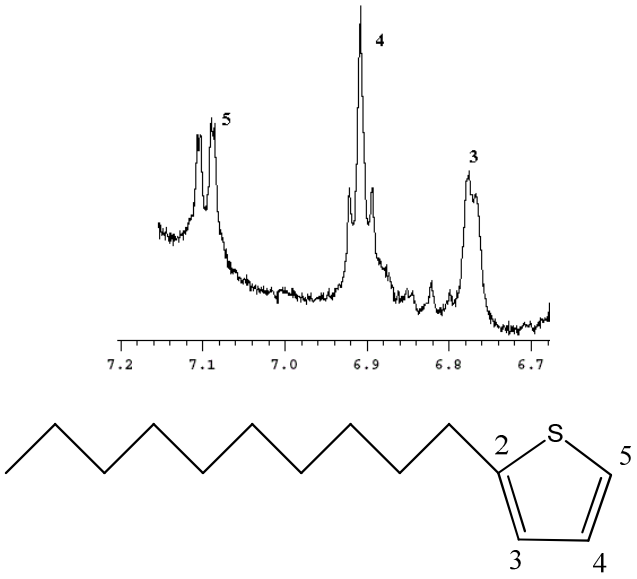

Figure 3.8 ^{1}HNMR result of STDE solution. Top: ^{1}HNMR. 2-decylthiophene: δ = 7.09 ppm (proton at 3 position); δ = 6.90 ppm (proton at 4 position); δ = 6.78 ppm (proton at 5 position). Bottom: structure of 2-decylthiophene.

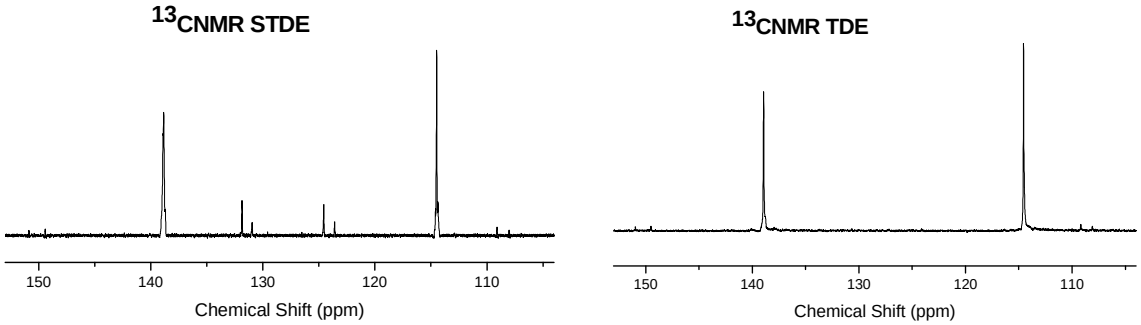

Figure 3.9 ^{13}CNMR results of STDE solution. Left: STDE solution. 2-decylthiophene: δ = 131.97 ppm (carbon at 2 position); δ = 130.96 ppm (carbon at 3 position); δ = 124.58 ppm (carbon at 4 position); δ = 123.60 ppm (carbon at 5 position). Right: 94% TDE.

There are two kinds of S stock solutions: one is the S solution currently used by some researchers--S powder dissolves in ODE below 159˚C.[22-23] Upon cooling the light yellow solution to room temperature, S crystals formed. The other is the S solution made by dissolving S in TDE with reflux. The color of this S solution is deep brown. At around 170˚C, the S_8 in the TDE solution reacts with the double bond of the TDE to generate small amount of thiophene (2-decylthiophene) (Equation 3) and release H_2S (the gas released turned lead acetate paper to black). Then H_2S react with S_8 to form hydrogen polysulfides (the reverse reaction of Equation 2), which is the activated components of sulfides. Therefore, in the STDE solution, S_8, thiophenes, hydrogen polysulfides, and TDE co-exist. The interaction among these species make the S_8 remain soluble and stable in STDE solution even at room temperature at a concentration higher than 4 M. This STDE solution is the S precursor we developed and used in the one-pot synthesis.

The formation of PbS QDs sample a-1 of 2.1 nm at 45˚C revealed a very important finding that nucleation can occur at a lower temperature. It demonstrated that the nucleation process does not need to overcome a high energy barrier. This would have a significant impact on the synthesis of nanomaterials if the one-pot S-containing QDs synthesis could be carried out below 100˚C. The energy provided at 45˚C is only about 2.64 kJ/mol K. A thermodynamic calculation is necessary to estimate the activation energy based on the proposed mechanism to guide the experiments. Solvent-free, hot-injection methods have been used in the synthesis of PbS for at least five years. However,[5-6, 24] to our limited knowledge, this is the first report of a non-injection, one-pot synthesis of PbS QDs with SOLA. In any case, our results suggest that solvent-free, one-pot synthesis of PbS QDs using only Pb precursor ($PbCl_2$+ OLA) and SOLA are possible. This is crucial for the understanding of the formation of S-containing QDs since the reaction is further streamlined with only three reagents. We realize that several questions still need to be addressed systematically to optimize the synthetic conditions, for example, the heating rate effects on the nucleation process. Can nucleation temperature be lowered by optimizing the interactions among reactant species? How are thiophenes generated in the S precursor? Does the concentration of the S precursor have any influence on the formation of QDs?

3.1.4 Conclusion

In conclusion, a new solvent TDE for S was discovered, followed by the development of a procedure to obtain the activated sulfide-containing STDE precursor. The STDE precursors can lower the nucleation temperature via a newly designed non-injection, one-pot thermal synthetic method to synthesis size controlled monodisperse PbS QDs. A reaction mechanism is proposed and discussed for the formation of PbS QDs. We envision that the TDE, the activated sulfide-

containing S precursors, one-pot thermal synthetic method, and the proposed reaction mechanism will be applicable to many practical applications and further be extended to the field of S-containing QDs synthesis. Table 3.3 summarized PbS QDs synthesized by both hot-injection and non-injection methods.

Table 3.3 PbS QDs Synthesized by Hot-injection and Non-injection Methods

Sample #	Average size (nm)	Size distribution (%)	Synthetic Method
PbS QD-1	2.1	8.6	Non-injection
PbS QD-2	4.0	6.9	Non-injection
PbS QD-3	5.0	10.0	Solvent-free, hot-injection
PbS QD-4	6.1	9.8	Solvent-free, hot-injection
PbS QD-5	7.0	6.9	Non-injection
PbS QD-6	7.3	11.0	Solvent-free, hot-injection
PbS QD-7	8.2	7.1	Non-injection
PbS QD-8	8.9	6.8	Non-injection
PbS QD-9	10.2	11.8	Solvent-free, hot-injection
PbS QD-10	14.8	7.3	Non-injection
PbS QD-11	16.5	7.0	Non-injection

3.2 Controlled Synthesis of PbSe QDs

We developed one new non-injection, one-pot method and two modified hot-injection methods to synthesize PbSe QDs with the universal $PbCl_2$-OLA system using three Se precursors: SeODE, SeOLA, and SeTDE (Se powder dissolved in these solvents, similar as SODE, SOLA, and STDE):

1. Non-injection, one-pot method using SeTDE as Se precursor.

2. Solvent-free, hot-injection method using SeOLA as Se precursor.

3. Hot-injection method using SeODE as Se precursor.

All syntheses are simple, environmentally benign, and phosphine-free. They can be carried out under open air. It achieves simplicity without compromising the quality of the PbSe QDs synthesized. Herein, temperature-based synthetic procedure was used to control the size and shape of the PbSe QDs while time-based synthetic procedure was also discussed.

With SeTDE precursor, four different sizes of PbSe QDs and one PbSe nanorods: 5.5 nm with σ = 5.6%, 8.4 nm with σ = 5.0%, 9.2 nm with σ = 5.6%, and 11.1 nm with σ = 4.9%, and rod with size of (5-10 nm x 40-80 nm), were synthesized via the non-injection method. The shape of the PbSe QDs was either spherical (< ~9-10 nm) or cubic (> ~9-10 nm) or rod.

With SeOLA precursor, two synthetic approaches: time-based and temperature-based synthesis of PbSe QDs by the solvent-free, hot-injection method, were investigated. The size of the PbSe QDs ranged from 3.6 nm to 15.0 nm with relative standard deviation of ~2.8-8.1%. The shape of the PbSe QDs was either spherical or cubic.

With SeODE precursor, four synthetic combinations with $PbCl_2$ or lead stearate as Pb source, OLA or oleic acid (OA) as the capping ligand were tested. The size of the PbSe QDs ranged from 6.5 nm to 15.5 nm with relative standard deviation of ~1.9-6.9%. The shape of the PbSe QDs was also either spherical or cubic. The optimal synthetic conditions were found for both synthetic combinations: OLA with $PbCl_2$ and OA with lead stearate.

3.2.1 Introduction

Semiconductor PbSe QDs have attracted considerable attention due to their strong quantum confinement properties. The quantum confinement to its nanostructures stems from its unique properties of small band gap (0.27 eV at 300K),[25] large exciton Bohr radius of 46 nm,[26] and large static dielectric constant of 280.[27]

Since Murray's group[28] reported the first colloidal synthesis of PbSe QDs in 2001, several modified synthetic methods have been reported.[29-32] PbSe QDs are usually synthesized by rapidly injecting of TOPSe precursor—Se powder dissolved in tri-n-octylphosphine (TOP) or in tri-n-butylphosphine (TBP) solution, into a heated solution of Pb precursor, typically lead acetate or lead oleate in a non-coordinating solvent ODE solution. OA was used as the capping ligand. TOP or TBP were used either as capping ligand or as assistant to OA. Either diphenylphosphine (DPP) or 1, 2-hexadecanediol (HDD) was used to increase the yield and quality of the PbSe QDs. The main problems of the above synthetic methods are complicated reaction conditions with multiple reagents. TOP and TBP are very toxic, air sensitive and expensive reagents. They need special handling. Although, Tang's group reported phosphine-free synthesis using SeODE as the Se precursor recently,[33] they still had to use OLA to "assist" the capping ligand OA to obtain narrowly distributed PbSe QDs.

Herein, we have developed a non-injection, one-pot synthetic method, a solvent-free hot-injection method, and a modified hot-injection method to solve these problems.

We select stable phosphine-free solutions[34] to replace both TOPSe and TBPSe as Se precursor. We use three phosphine-free Se stock solutions. They are SeODE, SeOLA, and SeTDE. Among them, SeTDE and SeOLA reported here is probably the first time used as Se

precursors for the synthesis of PbSe QDs, while SeODE is widely used as Se precursor. Raston's group found that the SeODE precursor was about as twice reactive as that of TOPSe. All three Se precursors are easy to prepare, inexpensive, and air-stable. Several key factors to determine the optimal experimental conditions are also examined. They include choosing precursors, capping ligands, synthetic systems, and synthetic methods. They also involve the study of temperature, time, concentrations of the reaction species, and ratios of the reaction species effects on the synthesis of monodisperse PbSe QDs.

With SeTDE, we investigated precursor ratio effect on the size and shape of PbSe QDs. With SeOLA, we tested time-based and temperature-based synthetic protocols, using either reaction temperature or reaction time to effectively control the size and shape of PbSe QDs. With SeODE, we examined it more thoroughly using a systematic approach. First, we use low cost reagents: $PbCl_2$ or lead stearate as Pb metal source. Then, we choose only one capping ligand, either OLA or OA to simplify the reaction processes. Next, the reactions were carried out without inert gas protection in open air. The synthesis results are reproducible with relatively high yield. Thus, nearly monodisperse PbSe QDs capped with only OLA or only OA were synthesized without any assistant reagents. The morphology of the PbSe QDs was controlled by changing variables such as injection temperature, growth temperature, and growth time. Both Pb to OLA or OA and Pb to Se feed mole ratios have been examined to obtain the optimal synthetic conditions. We choose to inject Se precursor at elevated temperature instead of injecting it at room temperature as for the synthesis of PbTe QDs (section 3.3 of this chapter) to successfully narrowing the size distribution of the PbSe QDs synthesized. Further, the resulting PbSe QDs synthesized by the open air method were compared with PbSe QDs obtained by the reference experiments at the same reaction conditions except carrying out under the inert nitrogen

protection environment. We found that there are no size, size distribution, and quality differences of PbSe QDs between syntheses with protection and without protection.

The new synthetic methods use little reaction equipment, less reagents and reduce cost via simplified reaction and post reaction processes. The synthetic method greatly changed the way in which PbSe QDs were synthesized. It achieves simplicity without compromising the quality of the PbSe QD synthesized.

3.2.2 Experimental

Chemicals

$PbCl_2$ (99-100%) was from J.T. Baker Chemical Company. Lead stearate (90-100%) was purchased from MP Biomedicals, LLC. Oleic acid (OA, tech, 90%) was from Alfa Aesar. Methanol (absolute reagent, 99.8%, A.C.S.) was purchased from Spectrum Chemical. Tetrachloroethylene (TCE, 99%, extra pure), selenium (Se, 99.5%, powder, 200 mesh), oleylamine (OLA, 80-90%), 1-octadecene (ODE, 90%), acetone (99.9%), 1-tetradecene (TDE, 94%), chloroform-d ($CDCl_3$, D-enrichment > 99.75%), and n-hexane (99+%) were purchased from ACROS Organic. Lead acetate paper was from Thermo Fisher Scientific, Inc. All chemicals were used as received without further purification.

SeODE, SeOLA, and SeTDE Precursor Preparation and Reactivity Test

The three Se precursor solutions were prepared as Table 3.4 indicated. 0.37 M SeOLA precursor stock solution was prepared by dissolving 0.878 g of Se powder in 24.30 g OLA at 260-290°C. It was used as Se precursor for solvent-free, hot-injection synthesis of PbSe QDs. The reactants only include three compounds: $PbCl_2$, OLA, and Se. 0.6 M SeTDE precursor stock solution was prepared by dissolving 0.305 g of Se powder in 15.0 g TDE under reflux.

Then it was cooled to room temperature for storage. 0.2 M SeODE precursor stock solution was prepared by dissolving 0.300 g of Se powder in 15.0 g ODE at 260-280°C. Then it was cooled to room temperature for storage.

Several drops of the 0.2 M SeODE, 0.37 M SeOLA, and 0.6 M SeTDE were place on the lead acetate papers respectively to check the activated components' reactivity. The color of lead acetate papers did not change with or without water added (Table 3.5).

We found that both SeODE and SeOLA generated some precipitates when cooled to room temperature due to the melting point of either ODE or OLA is close to room temperature. SeTDE remained as a clear solution.

^{1}HNMR, ^{13}CNMR, and MS spectra of SeTDE were recorded for solution component analysis. The SeTDE sample was also passed through a column of GC-MS for separation and additional component analysis.

Table 3.4 SeODE, SeOLA, and SeTDE Stock Solutions

	SeODE (0.2 M)	**SeOLA (0.37 M)**	**SeTDE (0.6 M)**
Se (g)	0.300	0.878	0.305
ODE (g)	15.0	-	-
OLA (g)	-	24.30	-
TDE (g)	-	-	15.0

Table 3.5 SeODE, SeOLA, and SeTDE Reactivity Test

	Color Change		
Lead acetate paper	SeODE	SeOLA	SeTDE
Without water	-	-	-
With water	-	-	-

Non-injection, one-pot synthesis of PbSe QDs using SeTDE with $PbCl_2$-OLA system

In a typical example of synthesis of the 8.4 nm spherical PbSe QDs (b-2), 0.094 g (0.34 mmol) $PbCl_2$, 3.365 g (10.07 mmol, 4.15 mL) OLA, and 0.85 mL 0.6 M SeTDE solution was introduced into a three-neck round-bottom flask at room temperature. The mixture was magnetically stirred and heated to 60℃ under vacuum for 15 min. Then, the vacuum was removed and the temperature of the mixture was further raised to 160℃ with a heating rate at about 20.1˚C/min. The temperature of the mixture was maintained at that level for 5 min. Then, the crude solution was cooled immediately in a water bath. The crude was centrifuged and washed with methanol. Next, 5 mL of TCE was added into the crude to extract PbSe QDs. After centrifuging, the as-synthesized PbSe QDs were stored in TCE.

The non-injection, temperature-based synthetic method can be used to obtain various sizes of PbSe QDs by running various batches of the synthesis under the same conditions similar to Section 3.1.2 of PbS QDs synthesis. Here the feed ratio of Pb to Se was altered to check its effects on the size of PbSe QDs. In contrast to the synthesis of PbS QDs, when the reaction was carried out at 130°C, PbSe nanorods were obtained. The synthetic conditions and results are listed in Table 3.6.

Table 3.6 Non-injection, One-pot Synthesis of PbSe QDs with SeTDE

Sample #	b-1	b-2	b-3	b-4	b-5
Pb to Se Feed Mole Ratio	1:2	1:1.5	1:2	1:3	1:2
OLA to Pb Mole Ratio	30:1	30:1	31:1	50:1	30:1
Heating rate (°C/min.)	21.0	20.1	20.1	20.1	8.8
Growth time (min.)	5	5	5	5	5
Growth Temperature (°C)	140	160	160	160	130
Sample Size (nm)	**5.5**	**8.4**	**9.2**	**11.1**	**5-10 x 40-80**
σ	5.6%	5.0%	5.9%	4.9%	-

Solvent-free, hot-injection synthesis of PbSe QDs using SeOLA with $PbCl_2$-OLA system

Temperature-based synthesis of PbSe QDs

In a typical example of synthesis of the 7.6 nm spherical PbSe QDs (c-1), 0.139 g (0.50 mmol) $PbCl_2$ and 5.000 g (18.69 mmol, 6.17 mL) OLA were introduced into a three-neck round-bottom flask at room temperature. The mixture was magnetically stirred and heated to 120℃ under vacuum for 15 min. Then, the temperature of the Pb precursor solution was further raised to 140˚C. 4 mL (1.48 mmol) 0.37 M SeOLA precursor (the feed mole ratio of Pb to Se was 1:3) at 128 ˚C was quickly injected into the Pb precursor solution. The temperature of the reaction mixture dropped to 130˚C and was maintained at that level for 5 min. Then, the crude solution was cooled immediately in a water bath to about 50-60˚C. The crude was centrifuged. 5 mL of methanol was added, and the crude was centrifuged again and the supernatant was removed. 5 mL of TCE was added into the crude to extract PbSe QDs. The solution was centrifuged. After centrifuging the resulting mixture solution, the as-synthesized PbSe QDs were stored in TCE. The PbSe QDs solution was converted to solid PbSe QDs using vacuum pump to remove TCE for further measurement.

The solvent-free, hot-injection temperature-based synthetic method was used to obtain various sizes of PbSe QDs by carrying various batches of the synthesis under the same conditions: the same amounts of chemical reagents were used, Pb to OLA feed mole ratio of 1:38, Pb to Se feed mole ratio of 1:3, the growth time of 5 min., but at a variety of reaction temperature. The reaction conditions and results are listed in Table 3.7.

Table 3.7 Solvent-free, Temperature-based Synthesis of PbSe QDs with SeOLA

Sample #	**c-1**	**c-2**	**c-3**	**c-4**
Pb to Se Feed Mole Ratio	1:3	1:3	1:3	1:3
OLA to Pb Mole Ratio	38:1	38:1	38:1	38:1
Vacuum Heating (min., °C)	15, 120	15, 210	15, 120	15, 120
SeOLA temperature (°C)	128	156	152	160
Injection temperature (°C)	140	180	220	240
Growth Temperature (°C)	130	165	200	215
Growth Time (min.)	5	5	5	5
Sample Size (nm)	**7.6**	**10.3**	**11.8**	**13.9**
σ	5.6%	5.0%	5.9%	4.9%

Time-based synthesis of PbSe QDs

In a typical example of synthesis of the 5.4 nm spherical PbSe QDs (d-1), 0.139 g (0.50 mmol) $PbCl_2$ and 5.000 g (18.69 mmol, 6.17 mL) OLA were introduced into a three-neck round-bottom flask at room temperature. The mixture was magnetically stirred and heated to 120℃ under vacuum for 15 min. Then, the temperature of the Pb precursor solution was further raised to 140˚C. 4 mL (1.48 mmol) of 0.37 M SeOLA precursor (the feed mole ratio of Pb to Se was 1:3) at room temperature was quickly injected into the Pb precursor solution. The temperature of the reaction mixture dropped to 130˚C and was maintained at that level for 0.5 min. Then, the crude solution was cooled immediately in a water bath to about 50-60˚C. The crude was

centrifuged. 5 mL of methanol was added, and the crude was centrifuged again and the supernatant was removed. 5 mL of TCE was added into the crude to extract PbSe QDs. The solution was centrifuged. After centrifuging the resulting mixture solution, the as-synthesized PbSe QDs were stored in TCE. The PbSe QDs solution was converted to solid PbSe QDs using vacuum pump to remove TCE for further measurement.

The solvent-free, hot-injection time-based synthetic method was used to obtain various sizes of PbSe QDs by carrying various batches of the synthesis under the same conditions: the same amounts of chemical reagents were used, Pb to OLA feed mole ratio of 1:38, Pb to Se feed mole ratio of 1:3, the growth temperature of 130˚C, but at a variety of reaction time. The reaction conditions and results are listed in Table 3.8.

Table 3.8 Solvent-free, Time-based Synthesis of PbSe QDs with SeOLA

Sample #	**d-1**	**d-2**	**d-3**	**d-4**	**d-5**
Pb to Se Feed Mole Ratio	1:3	1:3	1:3	1:3	1:2
OLA to Pb Mole Ratio	38:1	38:1	38:1	38:1	38:1
Vacuum Heating (min., °C)	15, 120	15, 210	15, 120	15, 120	15, 120
SeOLA temperature (°C)	20	20	20	20	20
Injection temperature (°C)	140	140	140	140	140
Growth Temperature (°C)	130	130	130	130	130
Growth Time (min.)	0.5	1	5	10	20
Sample Size (nm)	**5.4**	**5.6**	**7.6**	**7.9**	**10.0**
σ	7.4%	8.0%	8.6%	7.1%	8.0%

Hot-injection synthesis of PbSe QDs using SeODE with $PbCl_2$-OLA system

Synthesis and separation of PbSe QDs

The synthesis of PbSe QDs was performed in a three-neck round-bottom flask with a

condenser, connected with a Schlenk line, a temperature controller and a vacuum pump. The Pb precursor was prepared by adding OLA into a three-neck, round-bottom flask loaded with $PbCl_2$. The feed mole ratio of Pb to OLA was varied from 1:30 to 1:38. The Pb concentration was from 0.05 to 0.069 M. The mixture was then stirred vigorously while being pre-heated under vacuum at 120˚C for about 15 to 30 min. Then, it was heated to the targeted injection temperature. The Se precursor solution was heated to an elevated temperature. A portion of the heated Se stock solution (corresponding to various Pb to Se feed mole ratio) was injected into the Pb precursor rapidly. After the injection, the temperature of the mixture dropped to its lowest point swiftly, the reaction was maintained at that temperature for QD growth for various times. After the reaction, the crude solution was cooled immediately in a water bath to about 50-60˚C. The crude was centrifuged. A proper amount of methanol was added. The crude was centrifuged again to remove OLA and other starting materials by dumping the supernatant. Finally, about an equal amount of TCE or n-hexane which is equivalent to the volume of the reaction solution was added into the crude to extract PbSe QDs. The crude was centrifuged again to precipitate solid impurities and starting materials. After centrifuging the resulting mixture solution, the as-synthesized PbSe QDs were stored in the extracting solvent. The PbSe QDs can further be converted to solid PbSe QDs to calculate the actual yield or for further measurement by using vacuum pump to remove the solvent.

When either OA is used as the capping ligand or lead stearate is used as the Pb source, the operational procedure is similar to the synthetic and separation procedure described above.

Open air, temperature-based synthesis of PbSe QDs with OLA as capping ligand

In a typical example of synthesis of the cubic 15.0 nm PbSe QDs (e-5), Pb precursor was

prepared by introducing 0.093 g (0.33 mmol) $PbCl_2$ and 3.35 g (10.17 mmol, 4.14 mL) OLA to a three-neck round-bottom flask. The mixture was magnetically stirred and heated to 120℃ under vacuum for 15 min. Then, the temperature of the Pb precursor solution was further raised to 235℃. 2.5 mL (0.50 mmol) of 0.2 M SeODE precursor (the feed mole ratio of Pb to Se was 1:1.5) from 0.2 M SeODE stock solution maintained at 160˚C was quickly injected into the Pb precursor solution. The temperature of the reaction mixture dropped to 215℃ and was maintained at that level for 5 min. Then, the crude solution was cooled immediately in a water bath to about 50-60˚C. The crude was centrifuged. 5 mL of methanol was added, and the crude was centrifuged again and the supernatant was removed. 5 mL of TCE was added into the crude to extract PbSe QDs. The solution was centrifuged. After centrifuging the resulting mixture solution, the as-synthesized PbSe QDs were stored in TCE.

Table 3.9 Hot-injection, Temperature-based Synthesis of PbSe QDs

Sample #	**e-1**	**e-2**	**e-3**	**e-4**	**e-5**	**e-6**	**e-7***
Pb to Se Feed Mole Ratio	1/1.5	1/1.5	1/1.5	1/1.5	1/1.5	1/1.5	1/1.5
OLA to Pb Mole Ratio	31	31	31	31	31	31	31
SeODE Temperature (°C)	128	130	140	160	160	160	160
Injection Temperature (°C)	140	180	200	220	235	245	235
Growth Temperature (°C)	130	165	180	200	215	230	215
Sample Size (nm)	**6.5**	**8.3**	**9.5**	**12.1**	**15.0**	**15.5**	**15.0**
σ	6.2%	1.9%	5.7%	6.9%	6.1%	5.9%	4.9%

* Under nitrogen protection

The temperature-based synthetic method was used to obtain various sizes of PbSe QDs by running various batches of the synthesis under the same conditions: the same amounts of

chemical reagents were used, Pb to OLA feed mole ratio of 1:31, Pb to Se feed mole ratio of 1:1.5, the growth time of 5 min., but at a variety of reaction temperatures. The synthetic conditions and results are listed in Table 3.9. The actual yield is around 20%-70%.

Reference synthesis of PbSe QDs under nitrogen protection

All other conditions for the reference synthesis of PbSe QDs (e-7) under nitrogen are the same as the open air, temperature-based synthesis of PbSe QDs with OLA as capping ligand (e-5), except using standard Schlenk line techniques with dry nitrogen.

Synthesis of PbSe QDs using lead stearate as Pb source OLA as capping ligand

The synthesis and separation steps are similar to the typical synthesis of the cubic 15.0 nm PbSe QDs. Pb precursor was prepared using 0.259 g (0.33 mmol) of lead stearate, 1.50 g of OLA (5.61 mmol, 1.85 mL), and 1.85 g (2.34 mL) ODE (OLA to Pb feed mole ratio was 17:1). The Pb precursor was heated to 180˚C followed by the injection of 2.50 mL of 0.2 M SeODE stock solution maintained at 130˚C (the feed mole ratio of Pb to Se was 1:1.5). The growth temperature was 160˚C, and the growth time was 5 min. The reaction mixture was washed with methanol and extracted with TCE.

Synthesis of PbSe QDs using $PbCl_2$ as Pb source OA as capping ligand

Pb precursor was prepared using 0.094 g (0.34 mmol) of $PbCl_2$, 1.72 g (5.48 mmol, 1.92 mL) OA, and 1.69 g (2.14 mL) ODE (OA to Pb feed mole ratio was 16:1). The Pb precursor was heated to 160˚C followed by the injection of 2.50 mL of 0.2 M SeODE stock solution maintained at 120˚C (the feed mole ratio of Pb to Se was 1:1.5). The growth temperature was 146˚C, and the growth time was 5 min. The reaction mixture was washed with acetone and extracted with TCE.

Synthesis of PbSe QDs using lead stearate as Pb source OA as capping ligand

Pb precursor was prepared using 0.189 g (0.33 mmol) of lead stearate, 1.89 g (6.02 mmol, 2.11 mL) OA, and 1.64 g (2.08 mL) ODE (OA to Pb feed mole ratio was 18:1). The Pb precursor was heated to 180˚C followed by the injection of 2.50 mL of 0.2 M SeODE stock solution maintained at 130˚C (the feed mole ratio of Pb to Se was 1:1.5). The growth temperature was 171˚C, and the growth time was 5 min. The reaction mixture was washed with acetone and extracted with n-hexane.

Sample characterization

TEM, HRTEM, SAED, EDS, and powder x-ray diffraction (XRD) diffractometer were used to characterize the size, shape, crystal structure and composition of PbSe QDs. Component analysis was performed by GC-MS, MS, ^{1}HNMR, and ^{13}CNMR.

3.2.3 Results and Discussion

SeODE, SeOLA, and SeTDE Precursor Preparation and Reactivity Test

The reactivity test results in Table 3.5 reveal that the reactivity of Se precursors are less than that of S precursors because none of them reacts with Pb salt even when water is presented. The solubility of Se in ODE, OLA, and TDE is also lower than that of S. The maximum concentration of Se in ODE, OLA, and TDE is 0.2 M, 0.37 M, and 0.6 M respectively (Table 3.4). This indicates that there are some kinds of activated components of selenides in those Se precursors, but they are not as active as those of sulfides. The reactivity of SeTDE should be higher than that of SeODE because Se has higher solubility in TDE and TDE has shorter chain than ODE. Therefore, there are strong solvent and solute (Se_8) interactions in SeTDE solution, resulting increased solubility. The SeOLA solution may contain alkyl selenides. Its reactivity is

also higher than that of SeODE. However, additional experiments are needed to compare the reactivity of SeOLA and SeTDE.

The ^{1}HNMR and ^{13}CNMR spectra show that the species in SeTDE (Figure 3.10 to Figure 3.11) is quite different than in STDE. In STDE solution, large amount of TDE is mainly unchanged and remain in the solution as solvent, together with some small amount of thiophenes, S_8 and hydrogen polysulfides. However, by comparing the ^{1}HNMR spectra of TDE solvent and 0.6 M SeTDE solution, we find that the typical chemical shifts of protons at the terminal carbon-carbon double bond of TDE at 5.8 ppm disappeared in SeTDE; instead signal of 5.07 ppm is observed. ^{13}CNMR spectra also confirm that the position of the carbon-carbon double bond is shifted. The signals of 114.5 ppm and 138.9 ppm of the terminal carbon-carbon double bond of TDE are also missing in SeTDE, showing signals of 124 ppm and 131 ppm instead, indicating formation of different carbon-carbon double bond in SeTDE. This is in accordance with literature reports of ODE and SeODE[7, 34-36]. The strong signal at 1.68 ppm of SeTDE is probably represent the hydrogen atoms shown in Figure 3.12 or protons adjacent to Se atom of alkyl selenides and polyselenides.

The positive ion EI mass spectra analytical results are shown in Figure 3.13. Due to the purity of the TDE reagents is only 94%, some twelve (DDE, dodec-1-ene), fifteen (PDE, pentadec-1-ene), and eighteen carbon (ODE) solvents co-exist in TDE. The signals of charged species are attributed to Se (*m/z* = 80); C_5H_9 (pentene) + Se (*m/z* = 149); DDE (*m/z* = 167); PDE (*m/z* = 209); C_6H_{11} (hex-1-ene) + 2Se (*m/z* = 242); TDE + Se (*m/z* = 279); TDE_2 (*m/z* = 291); ODE + 2Se (*m/z* = 413); TDE + PDE + ^{78}Se (*m/z* = 487); TDE + PDE + ^{80}Se (*m/z* = 489); TDE + PDE + ^{82}Se (*m/z* = 491); TDE_2 + Se (*m/z* = 551); TDE_3 (*m/z* = 590); TDE_3 + 2 ^{78}Se (*m/z* =

748.5); TDE_3 + 2 ^{80}Se (*m/z* = 751.5). The only factor that cannot be explained is the intensity of the molecular peak involved with isotope ^{82}Se. It is the strongest among the three Se isotopes. According to natural abundance, ^{82}Se should have the least peak intensity, while ^{80}Se should have the strongest peak intensity.

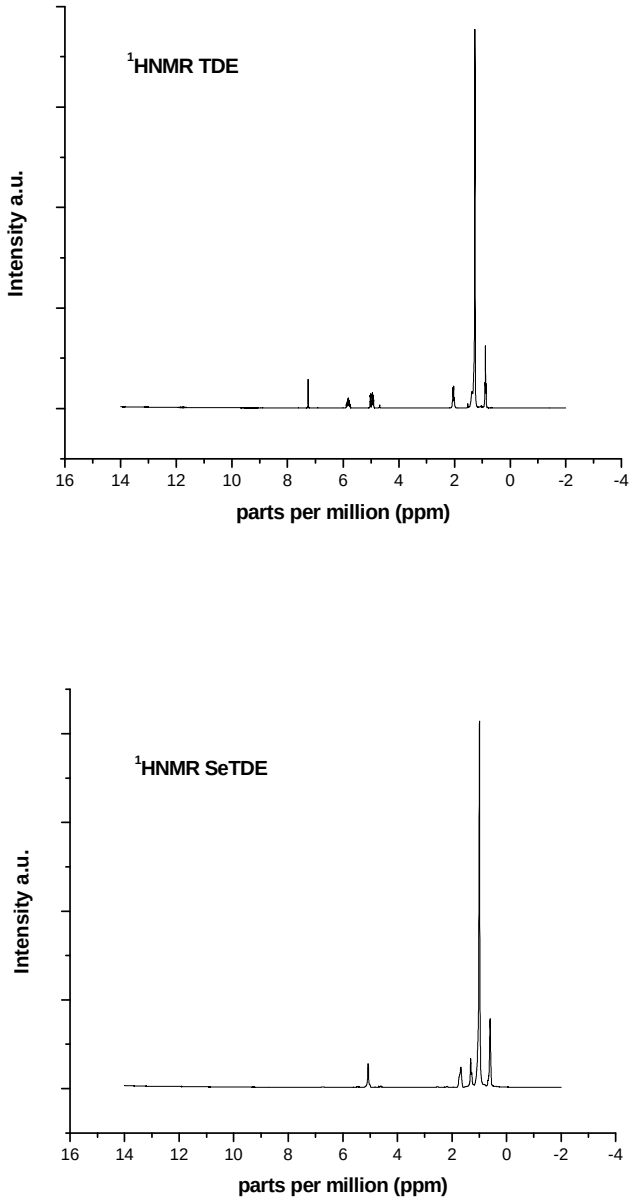

Figure 3.10 ^{1}HNMR spectra of TDE and SeTDE. The signal of 5.8 ppm at the terminal carbon-

carbon double bond of TDE disappeared in SeTDE, instead signal of 5.07 ppm is observed.

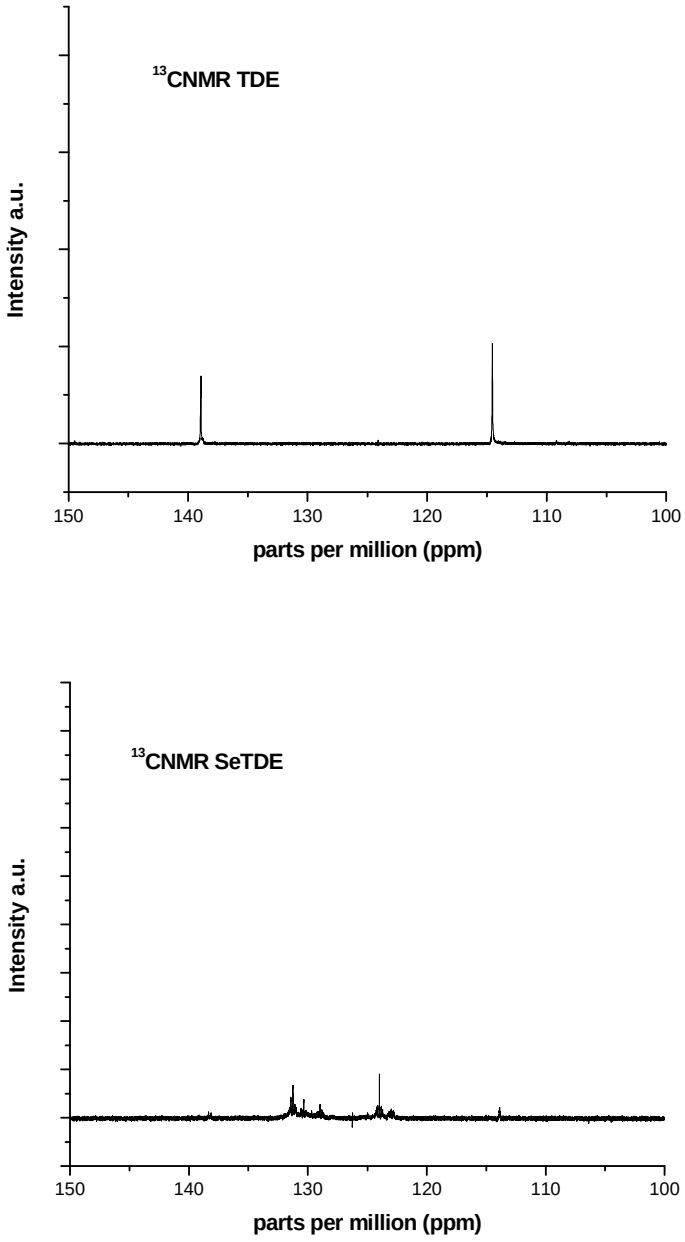

Figure 3.11 ^{13}CNMR spectra of TDE and SeTDE. The signals of 114.5 ppm and 138.9 ppm of the terminal carbon-carbon double bond of TDE also shifted in SeTDE, showing signals of 124 ppm and 131 ppm instead, indicating formation of different carbon-carbon double bond in

SeTDE.

SeTDE solution has complicated components. Unlike STDE, there is no selenophene in the solution because no chemical shifts are observed at round 7.00 ppm, which is the characteristic peak of protons at the selenohene ring. GC-MS result also proved that no selenophenes were presented in SeTDE solution. Se exists in Se_8 form in the TDE solution (Raman spectra in Section 3.4 will prove that). Se also forms single Se-C bond with SP^2carbon atom of carbon-carbon double bond or SP^3 carbon atom as selenides or polyselenides. The selenides are more stable than sulfides formed in STDE solution. Therefore, SeTDE, SeODE, and SeOLA do not react with Pb salt at room temperature even water is presented. This makes the controlled release of H_2Se from SeTDE at higher temperatures possible.

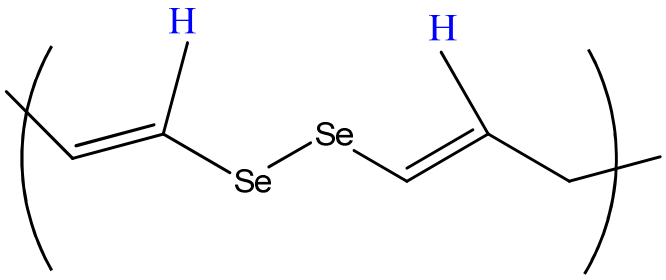

Figure 3.12 Proposed protons (blue) with chemical shift of 1.68 ppm.

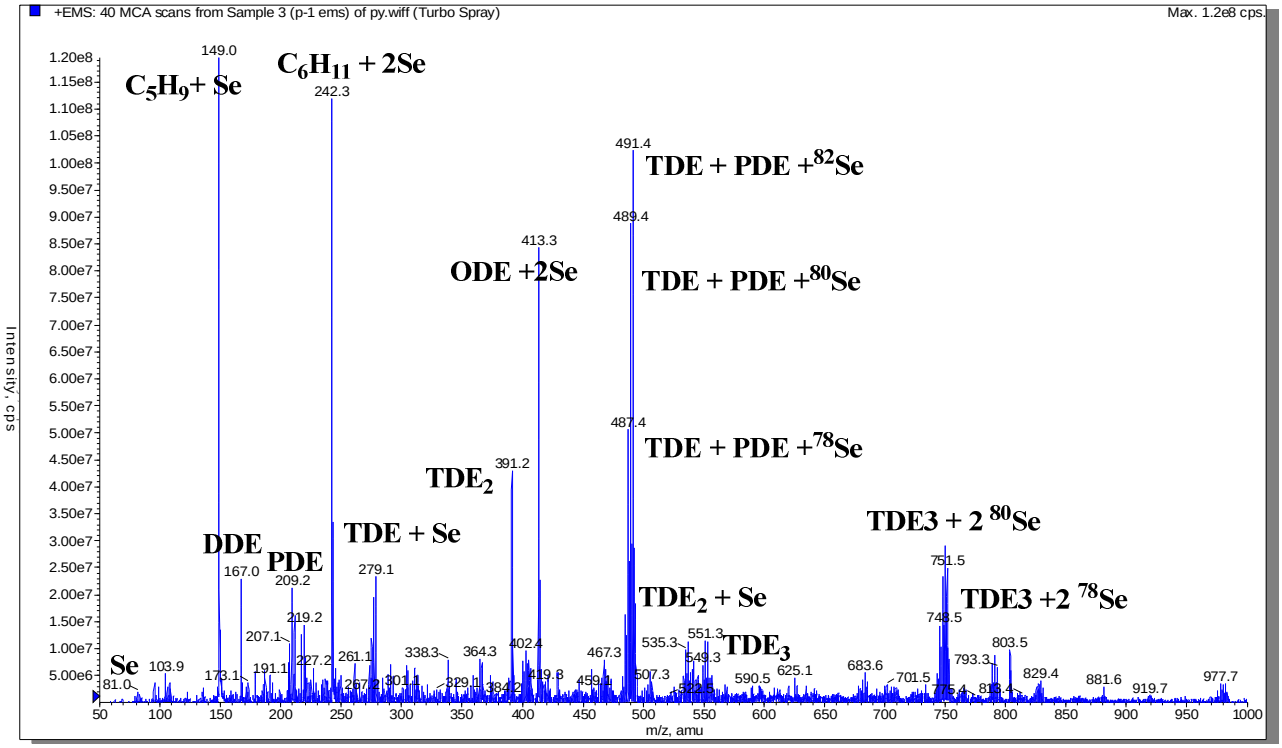

Figure 3.13 MS spectra of SeTDE solution.

Non-injection, one-pot synthesis of PbSe QDs using SeTDE with $PbCl_2$-OLA system

The TEM images of PbSe QDs synthesized are shown in Figure 3.14. When the Pb to Se feed mole ration is decreased from 1/1.5 to 1/3, the size of the PbSe QDs increased from 5.5 nm to 11.1 nm. This is the precursor ratio effect on the size of the QD formed. It demonstrated that different sizes of PbSe QDs can be obtained by changing the precursor ratios in the non-injection, one-pot method. The PbSe nanorods synthesized confirmed that the growth of PbSe is anisotropic at 130°C or below. Similar to the PbS QDs synthesis, the non-injection, one-pot synthetic method can produce a series size and shape of monodisperse PbSe QDs using SeTDE as precursors with $PbCl_2$-OLA system at relative low temperatures and short reaction time.

SeODE precursor is not suitable for the non-injection method due to its low concentration. However, it is still a good Se source for the hot-injection method. For the

SeOLA precursor, it is possible to develop a solvent-free, one-pot synthesis of PbSe QDs, just like the solvent-free, one-pot synthesis of PbS QDs because the preliminary test results revealed that point. The formation of PbSe nanorods (Figure 3.15) at 130°C also proves that nucleation can occur at low temperature. Our test results also demonstrated that even at 90°C, PbSe QDs can be formed, but they are mixture of QD and nanorods.

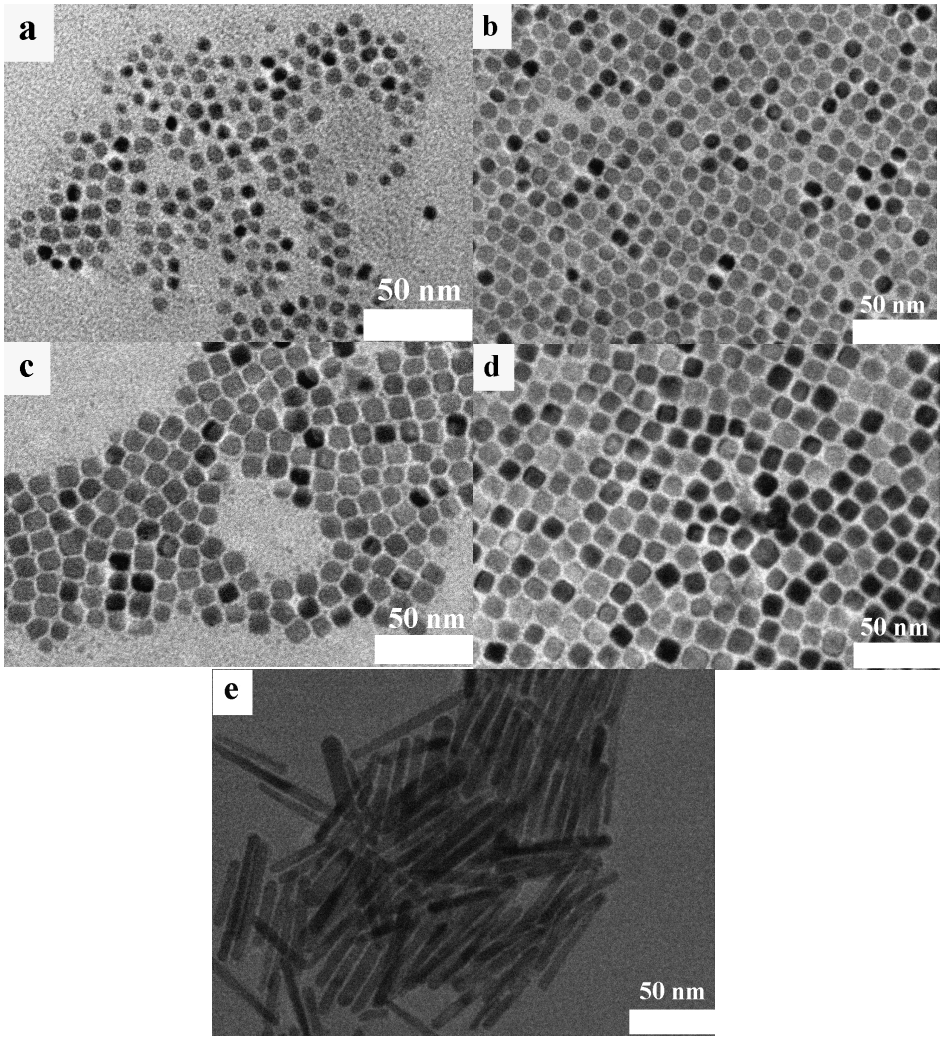

Figure 3.14 TEM images of PbSe QDs synthesized by non-injection, one-pot method using SeTDE as Se precursor. Figure 3.14a to Figure 3.14d corresponding to PbSe QDs sample b-1 of 5.5 nm with size distribution σ = 5.6%, b-2 of 8.4 nm with σ = 5.0%, b-3 of 9.2 nm with σ =

5.9%, b-4 of 11.1 nm with σ = 4.9%, b-5 of rod with size of 5-10 nm x 40-80 nm. Their reaction temperatures are 140°C, 160°C, 160°C, and 160°C respectively. Their reaction times are all 5 min. Figure 3.14e shows the PbSe nanorods synthesized at 130°C.

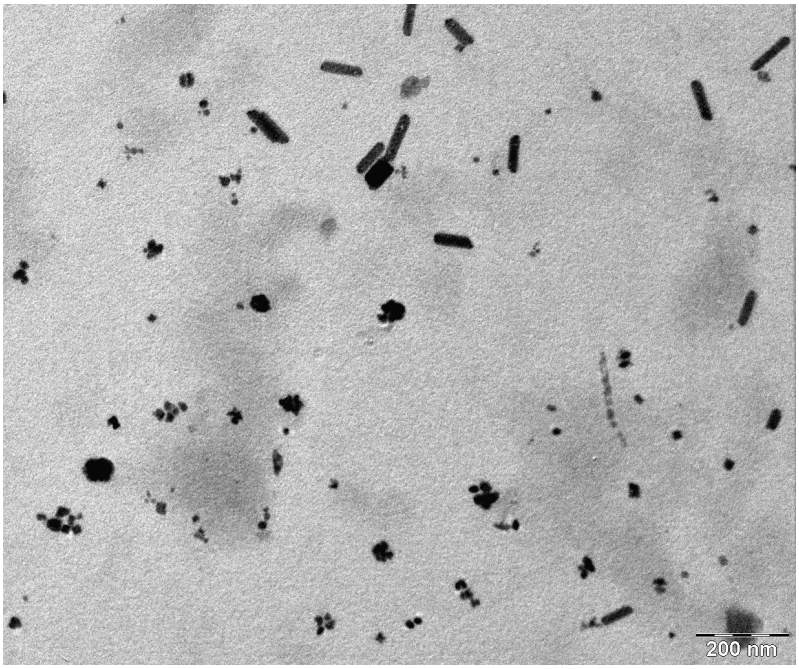

Figure 3.15 TEM images of PbSe QDs and nanorods formed at 90°C.

Solvent-free, hot-injection synthesis of PbSe QDs using SeOLA with $PbCl_2$-OLA system

The TEM images of PbSe QDs obtained via solvent-free, temperature-based and time-based synthetic methods are shown in Figure 3.16-Figure 3.17. Figure 3.18 and Figure 3.19 are the temperature-based diameter vs. temperature and time-base diameter vs. time synthetic curves, which can be used as guideline for the PbSe QDs synthesis. The time-based synthetic method is good for industrial production at low temperatures once all the reaction related parameters are optimized. The temperature-base synthetic method is suitable for academic research to obtain various size QDs in a short time. In this research, we focus on the temperature-based method.

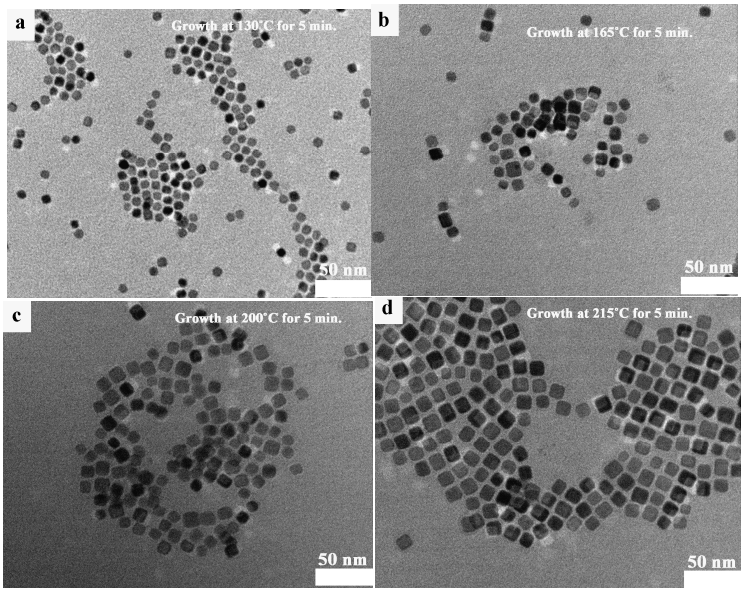

Figure 3.16 Temperature controlled synthesis of PbSe QDs. Figure 3.16a to Figure 3.16d corresponding to PbSe QDs sample c-1 of 7.6 nm with size distribution σ = 6.0%, c-2 of 10.3 nm with size distribution σ = 7.4%, c-3 of 11.8 nm with size distribution σ = 7.5%, and c-4 of 13.9 nm with size distribution σ = 8.6% respcetively.

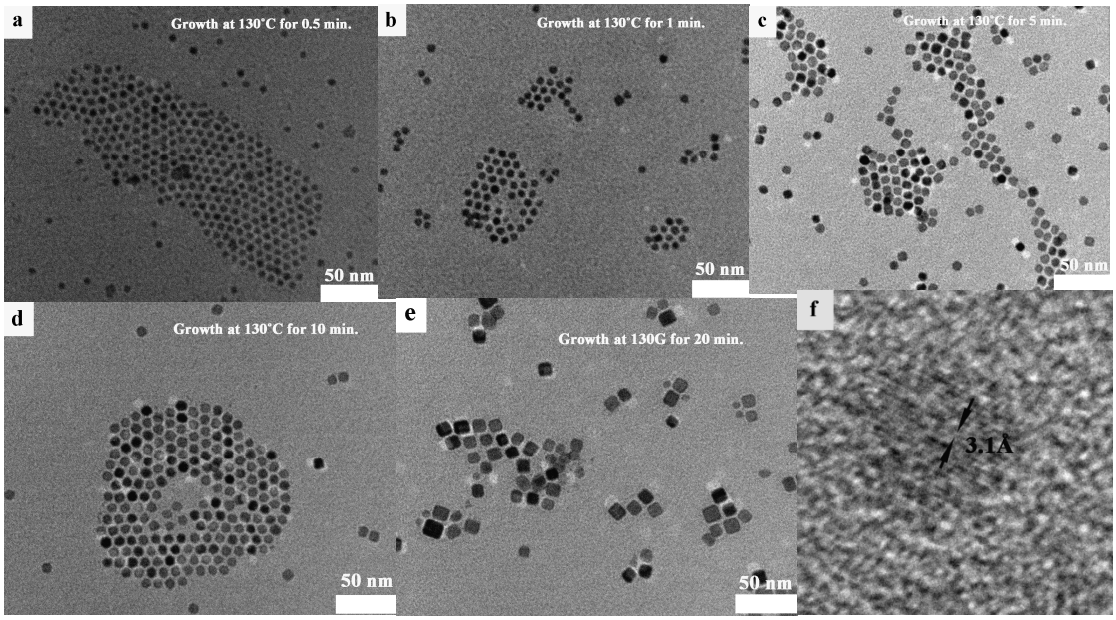

Figure 3.17 Time controlled synthesis of PbSe QDs. Figure 3.17a to Figure 3.17e corresponding to PbSe QDs sample d-1 of 5.4 nm with size distribution σ = 7.4%, d-2 of 5.9 nm with size distribution

σ = 8.0%, d-3 of 7.6 nm with size distribution σ = 8.6%, d-4 of 7.9 nm with size distribution σ = 7.1%, and d-5 of 10.0 nm with size distribution σ = 8.0% respectively. Figure 3.17f is the HRTEM image of sample d-1. It is 3.1 ± 0.1 Å, which matches the bulk PbSe data of ICDD, PDF Card 01-071-4753.

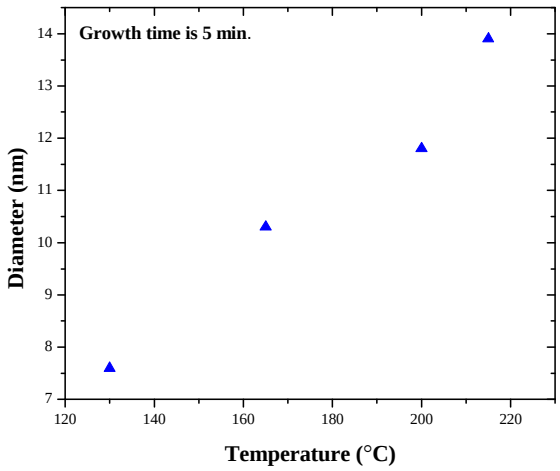

Figure 3.18 The temperature-based synthetic curve of PbSe QDs.

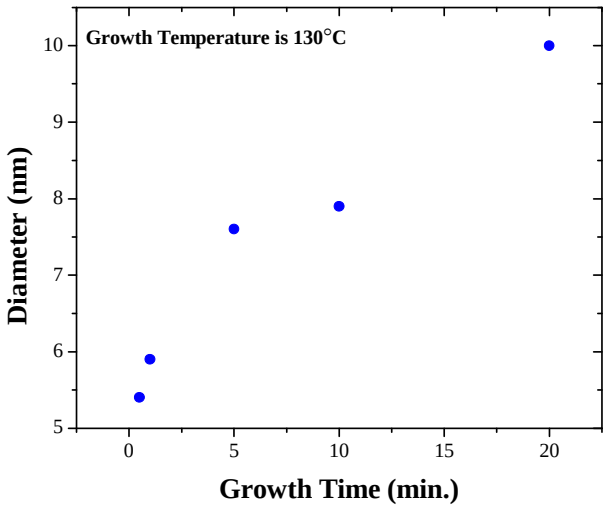

Figure 3.19 The time-based synthetic curve of PbSe QDs.

Hot-injection synthesis of PbSe QDs using SeODE with $PbCl_2$-OLA system

Synthesis and separation of PbSe QDs

Based on the synthetic results of the solvent-free, hot-injection method using SeOLA with $PbCl_2$-OLA system, a systematic investigation of the four synthetic combinations among two Pb sources ($PbCl_2$ and lead stearate) and two capping ligands (OLA and OA) using SeODE as Se precursor has been carried out. The experimental results revealed that the first two combinations below are in the optimal synthetic condition ranges, especially for the first combination between OLA and $PbCl_2$ (the universal $PbCl_2$-OLA system):

1. OLA and $PbCl_2$.
2. OA and lead stearate.
3. OA and $PbCl_2$.
4. OLA and lead stearate.

The other two synthetic combinations may be optimized by changing reaction conditions, such as, concentration of Se precursor, Pb to Se feed mole ratio, and OLA or OA to Pb feed mole ratio. The TEM images of PbSe QDs of sample e-1 to e-6 via the open air, temperature-based synthesis with $PbCl_2$-OLA system are shown in Figure 3.20. Table 3.9 includes the list of synthetic conditions, sizes and size distributions of PbSe QDs synthesized.

The sizes of the PbSe QDs were from 6.5 nm to 15.5 nm with a narrow distribution of relative standard deviations ~1.9-6.9%. From TEM image of Fig. 3.20c, we observed that the shape of the PbSe QDs began to transit from spherical to cubic around size of 9 to 10 nm. Comparing the results of PbSe QDs synthesized with and without nitrogen protection, we found that the element analysis results from EDS (Figure 3.21) of both sample e-5 and sample e-7 were

identical: both had Pb and Se elements with similar ratio; the TEM images also show that the two PbSe QDs samples have similar shape, size and size distribution (Figure 3.22). It is well known that PbSe QDs are sensitive in air due to desorption of OA-bonded Pb atoms.[37] However, in this study, we use OLA to substitute for OA as the capping ligand to prepare PbSe QDs. Although the synthetic results indicated that there was no significant quality difference between PbSe QDs obtained in air and under inert condition, the stability of PbSe QDs synthesized need to be further investigated. Nevertheless the ability to synthesize PbSe QCs in open air greatly simplified the overall process and makes the synthetic process more convenient.

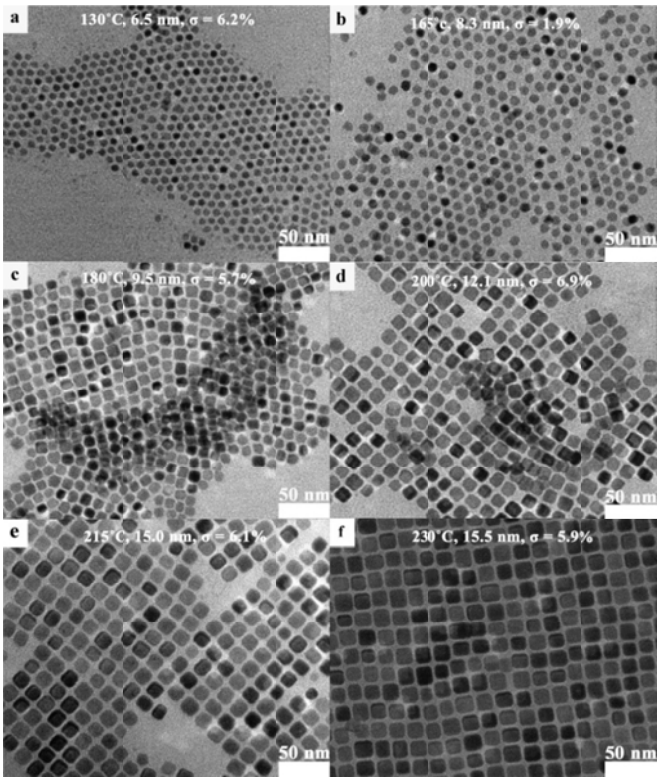

Figure 3.20 PbSe QDs synthesized by hot-injection method using SeODE as Se precursor. Fig.3.20a to Figure 3.20f corresponding to PbSe QDs samples e-1 to e-6. Their growth temperatures, sizes and relative size distributions are also shown there.

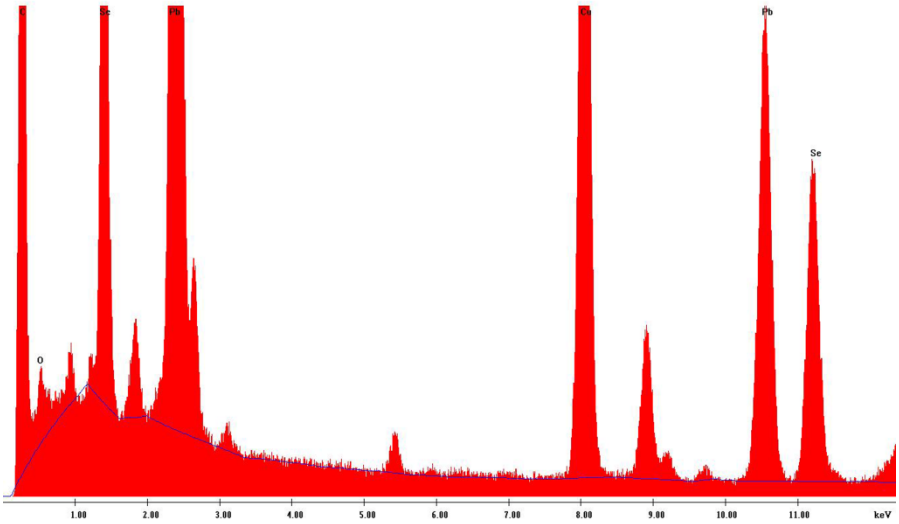

Figure 3.21 EDS Result of PbSe QDs sample e-5.

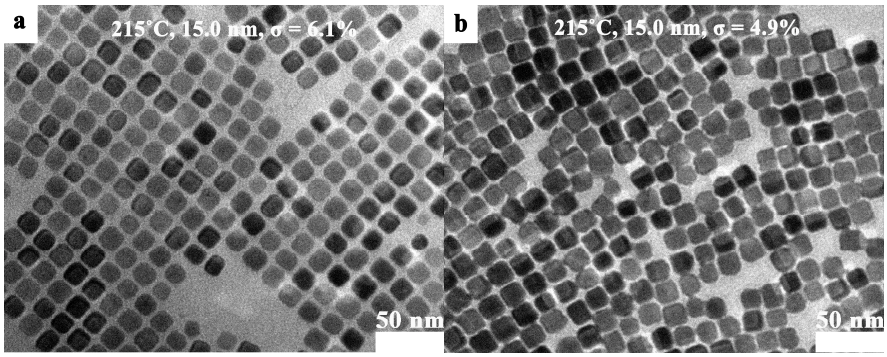

Figure 3.22 TEM images of PbSe QDs synthesized without (sample e-5, Figure 3.22a) and with nitrogen protection (sample e-7, Figure 3.22b).

Open air, temperature-based synthesis of PbSe QDs with OLA as capping ligand

The open air, temperature-based synthetic procedures developed using only reaction temperature to control the size of PbSe QDs are powerful and practical tools for the size controlled monodisperse nanoparticle synthesis. The synthetic curve obtained in Figure 3.23 is a

useful guideline for the synthesis of various sizes of PbSe QDs using the similar synthetic conditions. For example, to obtain PbSe QDs size of 10 nm, we can set the growth temperature at 190˚C and growth time for 5 min. To obtain PbSe QDs size smaller than 10 nm, one way is to keep the growth temperature unchanged while simply to reduce growth time to 3 min. or 1 min. or 0.5 min.; the other is to keep the reaction time unchanged at 5 min. and to reduce the growth temperatures below 190˚C.

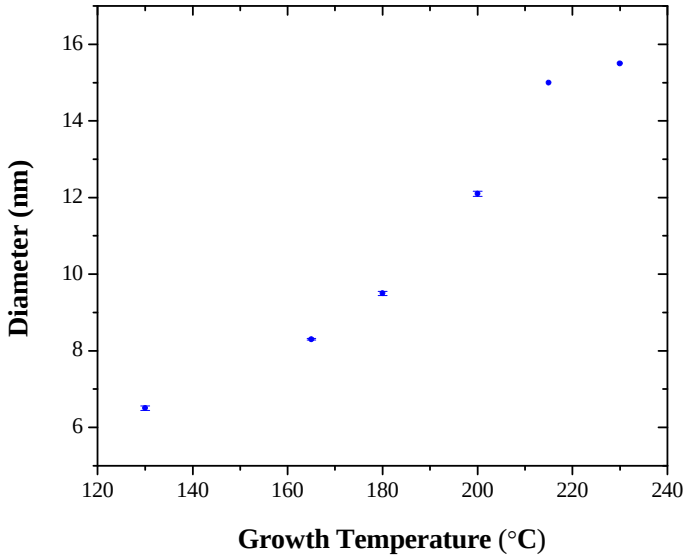

Figure 3.23 The temperature-based synthetic curve of PbSe QDs with SeODE. When other conditions remain constant and the growth time is at 5 min., narrowly distributed PbSe QDs were synthesized with various injection and growth temperatures.

Figure 3.24 shows the HRTEM image of PbSe QDs sample e-5. The lattice fringe of sample e-5 obtained from the HRTEM measurement is 3.1 ± 0.1 Å, which matches the standard card data of 3.07 Å (ICDD, PDF Card 01-071-4753). The XRD and SAED data of sample e-5 are shown in Figure 3.25.

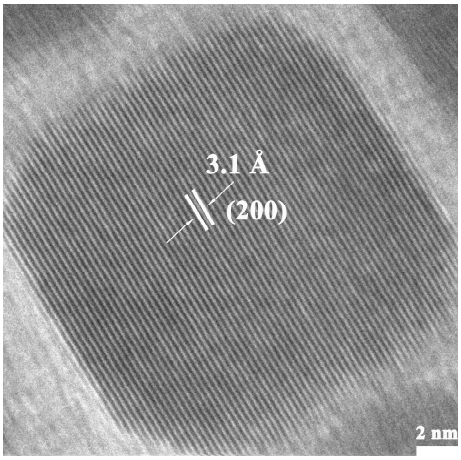

Figure 3.24 HRTEM image of PbSe QDs sample e-5 of 15.0 nm with lattice fringe of 3.1 ± 0.1 Å.

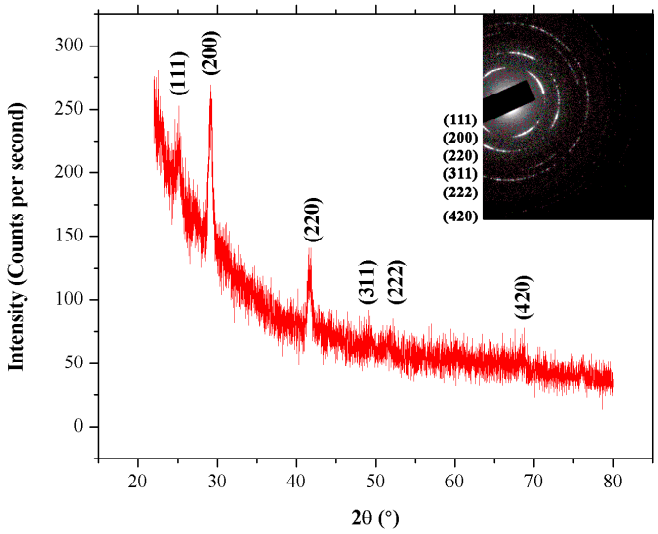

Figure 3.25 The XRD curve and SAED patterns of PbSe QDs sample e-5. The size of e-5 calculated from the full-width-half-maximum (FWHM) of the (200) peak of XRD using the Scherrer equation (Equation 14 of chapter 2) was 15.0 nm. Inset in the top right shows electron diffractogram linked with the main diffraction rings of sample e-5.

The SAED patterns at the top right insets of Figure 3.25 and the HRTEM image of Figure

3.24 confirmed the high crystallinity of PbSe QDs sample e-5. Sample e-5 has an fcc structure with the *Fm3m* space group (ICDD, PDF Card 01-071-4753). XRD pattern of the resulting PbSe QDs illustrated the values of the major peaks located in the range from 20° to 80° (2θ) corresponding to the characteristic diffraction of PbSe, verifying that only PbSe was present. The crystalline sizes were calculated by using the Scherrer equation for the line broadening of the (200) peak. It was 15.0 nm, which is also consistent with the HRTEM observation of sample e-5 (15.0 nm). The EDS results of sample e-5 (Figure 3.21) reveal that the PbSe QDs consist of Pb and Se elements. The XRD, TEM, HRTEM, SAED, and EDS data prove that sample e-5 is cubic PbSe QDs of 15.0 nm with a size distribution of 6.1%.

Synthesis of PbSe QDs using lead stearate as Pb source OLA as capping ligand

Figure 3.26 shows the TEM results of PbSe QDs synthesized with Pb to Se feed mole ratio of 1:1.5. The PbSe QDs sample obtained were unevenly distributed with sizes ranging from 5 nm to 15 nm. The experimental and separation conditions need to be changed to obtain the monodisperse PbSe QDs. The necessary changes including: (1) use acetone to replace methanol as the post-reaction washing agent; (2) adjust the Pb to Se feed mole ratio; (3) use n-hexane instead of TCE to extract the PbSe QDs.

Synthesis of PbSe NCs using $PbCl_2$ as Pb source OA as capping ligand

Figure 3.27 shows one of the TEM results of PbSe QDs synthesized with Pb to Se feed mole ratio of 1:1.5. The PbSe QDs sample obtained were unevenly distributed with sizes ranging from 10 nm to 20 nm and shapes varying from cubic to triangular, rectangular or other irregular shapes. This is probably due to lack of sufficient “monomers” to form well-developed PbSe NCs. Obviously, more trials of synthesizing PbSe QDs using $PbCl_2$ and OA are needed to obtain

the optimal synthetic conditions. A possible adjustment is to try the synthesis with different Pb to Se feed mole ratio while keeping other synthetic condition unchanged. However, the maximum concentration of SeODE is only 0.2 M. It is a hurdle for the optimization of the synthetic conditions. Perhaps, SeTDE is the right choice to obtain monodisperse PbSe QDs with $PbCl_2$ as Pb source and OA as capping ligand due to SeTDE's high concentration up to 0.6 M.

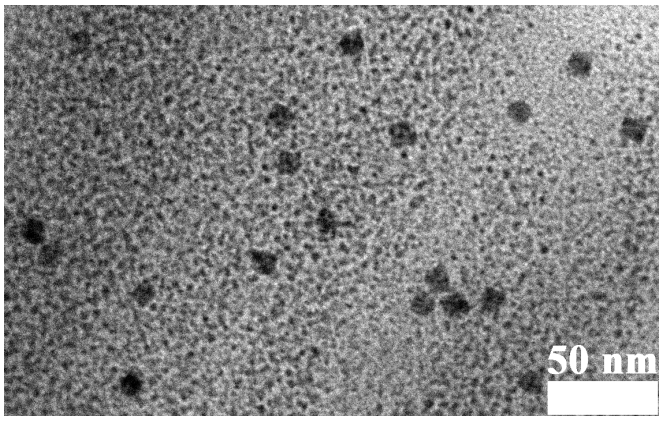

Figure 3.26 Unevenly distributed PbSe QDs synthesized using lead stearate as Pb source OLA as capping ligand.

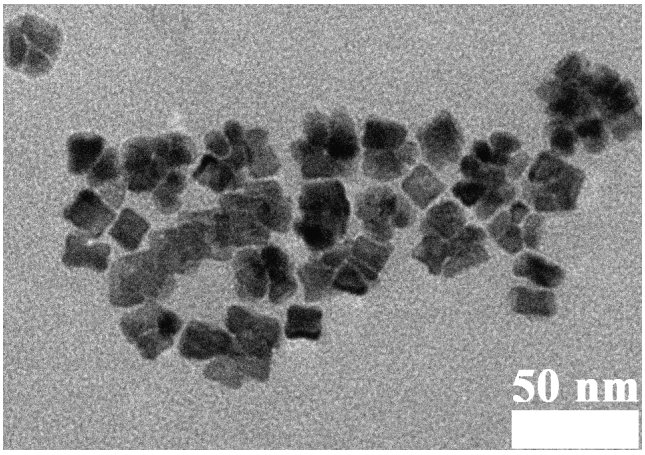

Figure 3.27 Unevenly distributed PbSe QDs synthesized using $PbCl_2$ as Pb source OA as capping ligand.

Synthesis of PbSe QDs using lead stearate as Pb source OA as capping ligand

The synthetic combination of lead stearate and OA has resulted in the successful synthesis of PbSe QDs with size of 12.0 nm and σ = 4.6%. Figure 3.28 is the TEM image of the PbSe QDs synthesized using this method.

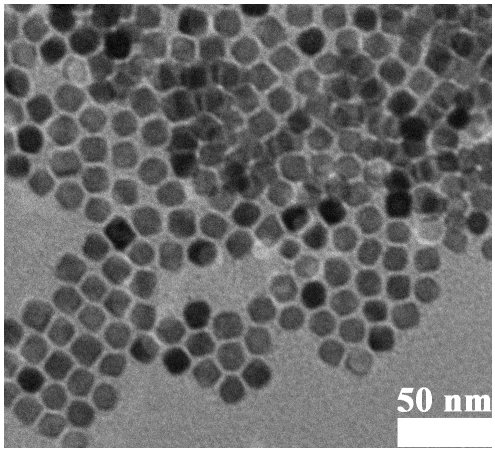

Figure 3.28 Monodisperse PbSe QDs of 12.0 nm with σ = 4.6% synthesized using lead stearate as Pb source and OA as capping ligand.

The formation mechanism of PbSe QDs is similar to that of PbS QDs (Equation 1 to 4 of this chapter). $PbCl_2$ and OLA form $PbCl_2$-OLA complex; TDE or ODE or OLA is oxidized by Se_8 to form alkyl selenides and alkyl polyselenides; the activated selenides (by heat) release H_2Se; then $PbCl_2$-OLA react with H_2Se and OLA to generate PbSe QDs.[38]

3.2.4 Conclusion

We have developed a new non-injection, one-pot method using SeTDE, a solvent-free, hot-injection method using SOLA, and a modified hot-injection methods using SeODE, to synthesize a series of monodisperse, different shapes and sizes of PbSe QDs with the universal

$PbCl_2$-OLA system. A partial list of the synthetic results is shown in Table 3.10. We also found that the formation mechanism of PbSe QDs is similar to that of PbS. QDs

With SeTDE, we used the non-injection, one-pot method to investigate precursor ratio effect on the size and shape of PbSe QDs. We found that SeTDE is the Se precursor for the synthesis of Se-containing QD either with non-injection or hot-injection method.

With SeOLA, we tested time-based and temperature-based synthetic protocols with the solvent-free, hot-injection method, using either reaction temperature or reaction time to effectively control the size and shape of PbSe QDs. It is also possible to develop, solvent-free, non-injection method use SeOLA.

The new, open air, environmentally benign, phosphine-free, hot-injection method with SeODE to synthesize monodisperse and size selective PbSe QDs was systematically investigated. We achieve simplicity without compromising the quality of the PbSe QD. Four synthetic combinations with $PbCl_2$ or lead stearate as Pb source, OLA or OA as the capping ligand were tested using our group's temperature-based synthetic procedures to control the size and shape of the PbSe QDs. By using the optimal synthetic conditions for combinations of $PbCl_2$ with OLA and lead stearate with OA, PbSe QDs from 6.5 nm to 15.5 nm with relative standard deviation of ~1.9-6.9% were successfully synthesized. The nanocrystals were either spherical (< ~9-10 nm) or cubic (> ~9-10 nm). The temperature-based synthetic procedures developed with SeOLA precursor proved to be powerful and practical tools for the size controlled synthesis of monodisperse nanoparticles. The synthetic method uses little reaction equipment, less reagents and reduces cost via simplified reaction and post-reaction processes.

Table 3.10 PbSe QDs Synthesized by Solvent-free, Hot-injection, Hot-injection and Non-injection Methods.

Sample #	Average size (nm)	Size distribution (%)	Synthetic Method
PbSe QD-1	3.6	6.9	Solvent-free, hot-injection
PbSe QD-2	4.5	5.9	Solvent-free, hot-injection
PbSe QD-3	5.5	5.6	Non-injection
PbSe QD-4	6.5	6.2	Hot-injection
PbSe QD-5	7.5	6.1	Solvent-free, hot-injection
PbSe QD-6	8.4	5.0	Non-injection
PbSe QD-7	9.5	5.7	Hot-injection
PbSe QD-8	10.5	5.0	Hot-injection
PbSe QD-9	11.1	4.9	Non-injection
PbSe QD-10	12.1	6.9	Hot-injection
PbSe QD-11	13.5	5.3	Hot-injection
PbSe QD-12	13.9	6.0	Solvent-free, hot-injection
PbSe QD-14	14.7	6.8	Hot-injection
PbSe QD-15	15.0	4.9	Hot-injection
PbSe QD-16	15.5	5.9	Hot-injection
PbSe QD-17	5-10 x 40-80 (rod)	-	Hot-injection

3.3 Controlled Synthesis of PbTe QDs

We report a new, simple method to synthesize a series of monodisperse hydrophobic PbTe QDs followed by a stability study of the as-synthesized QDs in air. We provide evidence that small air-stable PbTe QDs may be synthesized using this method. $PbCl_2$-OLA was again used as the model system. Te powder dissolved in TOP was used as Te precursor. OLA was

used as the capping ligand. The size and shape of the PbTe QDs were controlled by changing variables such as injection temperature, growth temperature, and growth time. Both Pb to OLA and Pb to Te feed mole ratios have been examined to obtain the optimal synthetic conditions. The PbTe QDs can be changed from hydrophobic to hydrophilic through ligand exchange using 4-mercaptopyridine (4-Mpy) to replace OLA as capping ligand. The colloidal PbTe QDs were characterized by transmission electron microscope, high resolution transmission electron microscope, selected area x-ray diffraction, energy-dispersive x-ray spectroscopy, UV-Vis-Near IR spectrophotometer, and powder x-ray diffraction. The sizes of the PbTe QDs synthesized ranged from 2.6 nm to 14.0 nm with a standard deviation of ~5.6-9.1%. The shape of the PbTe QDs was either spherical (< ~9-10 nm) or cubic (> ~9-10 nm).

3.3.1 Introduction

Semiconductor QDs have been widely investigated, due to their quantum confinement properties,[39-41] phonon confinement features,[42-43] and potential for electronic and optoelectronics applications,[44] thermoelectric applications,[45-46] and solar cells.[47-50]

PbTe QDs have attracted much attention with respect to its small band gap (0.32 eV at 300K),[25] largest exciton Bohr radius 46 nm[26, 51] among known crystalline semiconductor QDs, and large static dielectric constant of 360.[27]

A typical PbTe QDs synthesis uses lead acetate trihydrate as Pb precursor, TOPTe as Te precursor, TOP and OA as capping ligand, and phenyl ether as non-coordinating solvent, was first reported by Fang's group in 2004.[52] Since then, several groups[51, 53-58] reported synthesis of high quality monodisperse PbTe QDs ranging from 2.6 nm to 50 nm with various shapes. Most of the syntheses use OA as ligand and lead acetate trihydrate or PbO as Pb precursor in some

high boiling point non-coordinating solvents, such as ODE or phenyl ether. Only few studies involved using basic, solid, long chain primary amine as capping ligand or $PbCl_2$ as starting materials for Pb precursor.[56-57] Moreover, the PbTe QDs obtained either have a relatively large size distribution or need a long reaction time at high temperature. To the best of our knowledge, there are no reports of using liquid primary amine--OLA as the capping ligand and $PbCl_2$-OLA system for the synthesis of PbTe QDs.

In this study, we report a modified, simple, hot-injection method to synthesize monodisperse hydrophobic PbTe QDs using liquid OLA as capping ligand and $PbCl_2$-OLA as Pb precursor in relatively short reaction times without any non-coordinating solvent. We have obtained nearly monodisperse PbTe QDs ranging from 2.6 nm to 14 nm. The shape of the PbTe QDs was either spherical or cubic. We performed a systematic study on the temperature controlled synthesis of PbTe QDs, ligand exchange of PbTe QDs from hydrophobic to hydrophilic, and the stability of as-synthesized PbTe QDs in ambient environment. The synthetic approach has the following advantages: (1) Use of OLA as both capping ligand and solvent to eliminate unnecessary reagents and reaction process. This offers a convenient and alternative way to further investigate the fundamental synthetic mechanism and formation process of PbTe QDs. (2) The hydrophobic PbTe QDs synthesized can easily be changed to various kinds of ligand[59] capped PbTe QDs due to OLA's surface ligand dynamics that makes OLA a good leaving ligand.[6] This makes it possible to obtain bio-conjugated PbTe QDs which otherwise cannot be directly synthesized. (3) Some small PbTe QDs synthesized are air-stable either in tetrachloroethylene (TCE) solution or as thin film. (4) Temperature-based synthetic procedures were developed to use only reaction temperature to control the size of nanoparticles. (5) The synthetic results are reproducible with relatively high yield. The synthesis may be a

potential candidate for industrial scale production due to fewer reagents usage and reduced cost via simplified reaction and post reaction processes.

3.3.2 Experimental

Chemicals

$PbCl_2$ (99-100%) was from J.T. Baker Chemical Company. Lead stearate (90-100%) was purchased from MP Biomedicals, LLC. 4-mercaptopyridine (4-Mpy, 97%) was from Sigma-Aldrich. Tri-n-octylphosphine (TOP, tech, 97%) was purchased from Alfa Aesar. Methanol (absolute reagent, 99.8%, A.C.S.) was purchased from Spectrum Chemical. Tetrachloroethylene (TCE, 99%, extra pure), tellurium (Te, 99.80%, powder, 200 mesh), oleylamine (OLA, 80-90%), 1-octadecene (ODE, 90%), and n-hexane (99+%) were purchased from ACROS Organic. All chemicals were used as received without further purification.

Synthesis and separation of PbTe QDs

Te precursor stock solution (TOPTe) of 0.5 M was prepared by dissolving Te powder in TOP in a glove box and stirred overnight at room temperature. The synthesis of PbTe QDs was performed in a three-neck round-bottom flask with a condenser, connected with a Schlenk line, a temperature controller and a vacuum pump. The Pb precursor was prepared by adding OLA into a three-neck, round-bottom flask loaded with $PbCl_2$. The feed mole ratio of Pb to OLA was varied from 1:30 to 1:38. The Pb concentration was from 0.05 to 0.069 M. The mixture was then stirred vigorously while being pre-heated under vacuum at 120˚C for about 30 min. Then, it was heated to the targeted injection temperature under nitrogen. A portion of the Te stock solution (corresponding to various Pb to Te feed mole ratio) stored at room temperature was injected into the Pb precursor rapidly. After the injection, the temperature of the mixture dropped to its lowest

point swiftly, the reaction was maintained at that temperature for QDs growth for various times. After reaction, the crude solution was cooled immediately in a water bath to about 50-60˚C. The crude was centrifuged. A proper amount of methanol was added. The crude was centrifuged again to remove OLA and other starting materials by dumping the supernatant. Finally, about an equal amount of TCE or n-hexane which is equivalent to the volume of reaction solution was added into the crude to extract PbTe QDs. The crude was centrifuged again to precipitate solid impurities and starting materials. After centrifuging the resulting mixture solution, the as-synthesized PbTe QDs were stored in the extracting solvent. The PbTe QDs can further be converted to solid PbTe QDs to calculate the actual yield or for further measurement by using vacuum pump to remove the solvent.

Temperature-based synthesis of PbTe QDs

A typical synthesis of cubic 14.0 nm PbTe QDs (f-6) is described below. 0.5 M TOPTe stock solution was prepared by dissolving 0.56 g (8.5 mmol) of Te powder in 17 mL TOP in a glove box and stirred overnight. Pb precursor was prepared by introducing 0.093 g (0.33 mmol) $PbCl_2$ and 3.36 g (10.17 mmol, 4.15 mL) OLA (the feed mole ratio of Pb to OLA is 1:30) to a three-neck round-bottom flask. The mixture was magnetically stirred and heated to 120˚C under vacuum for 30 min. The Pb precursor was kept under nitrogen at that temperature for another 5-10 min. Then, the temperature of the Pb precursor solution was further raised to 250˚C. 0.7 mL (0.35 mmol) Te precursor (the feed mole ratio of Pb to Te was 1:1) from 0.5 M TOPTe stock solution was quickly injected into the Pb precursor solution. The temperature of the reaction mixture dropped to 225˚C and was maintained at that level for 5 min. Then, the crude solution was cooled immediately in a water bath to about 50-60˚C. The crude was centrifuged. 5 mL of methanol was added, and the crude was centrifuged again and the supernatant was removed. 5

mL of TCE was added into the crude to extract PbTe QDs. The solution was centrifuged. After centrifuging the resulting mixture solution, the as-synthesized PbTe QDs were stored in TCE. The PbTe QDs solution was converted to solid PbTe QDs using vacuum pump to remove TCE for further measurement.

The temperature-based synthetic method was used to obtain various sizes of PbTe QDs by carrying various batches of the synthesis under the same conditions: the same amounts of chemical reagents were used, Pb to OLA feed mole ratio of 1:30, Pb to Te feed mole ratio of 1:1.5, the growth time of 5 min., but at a variety of reaction temperature. The reaction conditions and results are listed in Table 3.11.

Table 3.11 Reaction Conditions and Results of Temperature-based Synthesis of PbTe QDs

Sample #	Size (nm)	Injection Temp. (˚C)	Growth Temp. (˚C)	Pb to Te Feed Mole Ratio	Pb to Te Mole Ratio by EDS	Relative Standard Deviation	Yield (%) based on the theoretical yield of PbTe
f-2	3.3	140	125	1/3	2.4*	7.3%	16
f-3	5.5	180	165	1/3	1.0	5.6%	52
f-4	9.5	230	210	1/3	1.1	7.4%	36
f-5	10.5	240	215	1/3	1.0	8.2%	28

* Sample f-2 data was off the scale probably due to the excess amount of Pb on the surface of the nanoparticles. The growth time was 5 min. each.

Ligand Exchange of PbTe QDs with 4-mercaptopyridine

A synthetic method used to prepare PbS QDs capped with 4-Mpy by our group[39] was modified for the synthesis of PbTe QDs capped with 4-Mpy. 1 mL of n-hexane solution of the as-synthesized PbTe QDs and 9 mL 0.01 M 4-Mpy methanol solution were transferred into a vial with a magnetic stirrer; the vial was wrapped with aluminium foil and stirred overnight. The solid samples were washed with 2 mL methanol 3 times and centrifuged. The samples were

redistributed in 10 mL methanol and sonicated for 30 min. The as-synthesized PbTe QDs capped with 4-Mpy were stored in methanol.

PbTe QDs stability test

For each PbTe QD to be tested, four types of TEM were used: (1) TEM sample made immediately after synthesis. (2) The same TEM sample stored on TEM copper grid at ambient environment for 130 days and measured again. (3) PbTe QDs sample stored in TCE solution at ambient environment for 130 days, and then new TEM sample was made and measured. (4) PbTe QDs solid sample stored in air for 130 days, and then new TEM sample was made using TCE as solvent and measured.

Sample characterization

Transmission electron microscope (TEM), high resolution transmission electron microscope (HRTEM), selected area x-ray diffraction (SAED), energy-dispersive x-ray spectroscopy (EDS), and powder x-ray diffraction (XRD) diffractometer were used to characterize the size, shape, crystal structure, and composition of PbTe QDs.

3.3.3 Results and Discussion

Synthesis and separation of PbTe QDs

Figure 3.29 lists the TEM images of PbTe QDs via the temperature controlled synthesis. Figure 3.30 shows the TEM images of the smallest sample f-1 of 2.6 nm with σ = 9.1% and the largest sample f-6 of 14.0 nm with σ = 8.7% synthesized. Table 3.12 includes the list of size and size distribution of PbTe QDs synthesized.

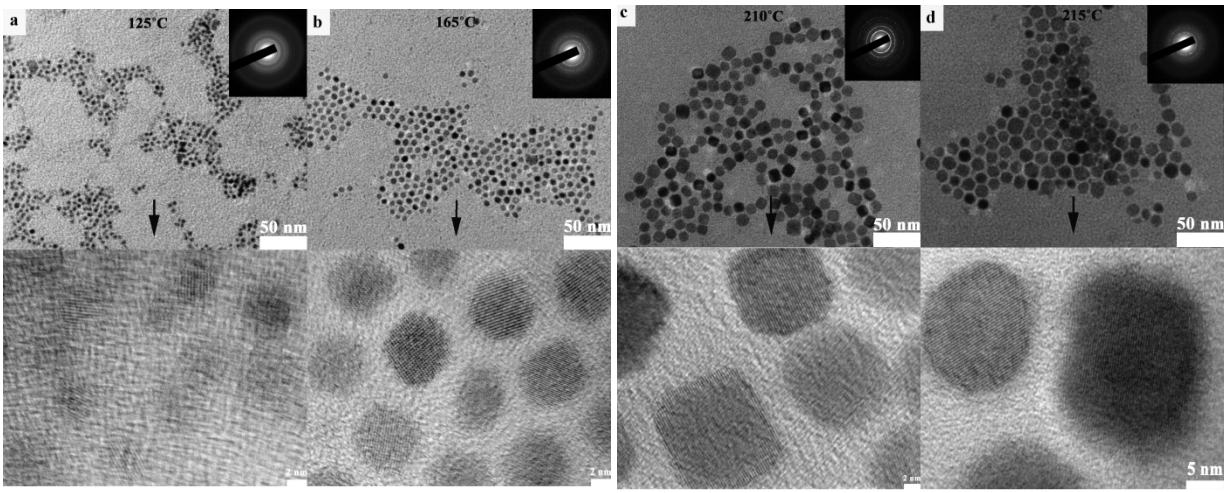

Figure 3.29 TEM, HRTEM images and SAED patterns of temperature-based synthesis of PbTe QDs. Figure 3.29a to Figure 3.29d corresponding to PbTe QDs samples f-2 of 3.3 nm with size distribution σ = 7.3%, f-3 of 5.5 nm with σ = 5.6%, f-4 of 9.5 nm with σ = 7.4%, and f-5 of 10.5 nm with σ = 8.2% at growth temperature of 125˚C, 165˚C, 210˚C, and 215˚C respectively. The insets at the top right show their SAED patterns. The HRTEM images at the bottom reveal that the PbTe QDs have high crystallinity.

The as-synthesized PbTe QDs have high crystalline quality. We have obtained all lattice fringe images from every PbTe QDs we synthesized. The size distribution of PbTe QDs (2.6 nm to 14.0 nm with a standard deviation of ~5.6-9.1%) is a little wider compared to our recent phosphine-free synthesis results of PbSe QDs (6.5 nm to 15.0 nm with a standard deviation of ~1.9-6.9%[18] using SeODE as Se precursor.[34] This is probably because the Te precursor to be injected was kept at room temperature, while the Se precursor to be injected was heated at an elevated temperature (125-160˚C). In the reaction mechanism study of sulfur-amine solutions, Ozin's group[19] demonstrated that heated sulfur-octylamine solution at 130˚C generated more H_2S, which combined with metal precursor to form metal sulfide. The reaction mechanism of

SeODE solution for the synthesis of PbSe is unclear. However, SeODE solution can generate active species such as H_2Se upon heating were both evidenced by our experiments and by Raston's group[34] investigation of SeODE solution. Although the reaction mechanism of our PbTe QDs synthesis method is complicated, our synthetic method offers an alternative way to tackle the fundamental reaction mechanism problems of the PbS, PbSe, and PbTe QDs synthesis using either acid--OA or base--OLA as capping ligand.

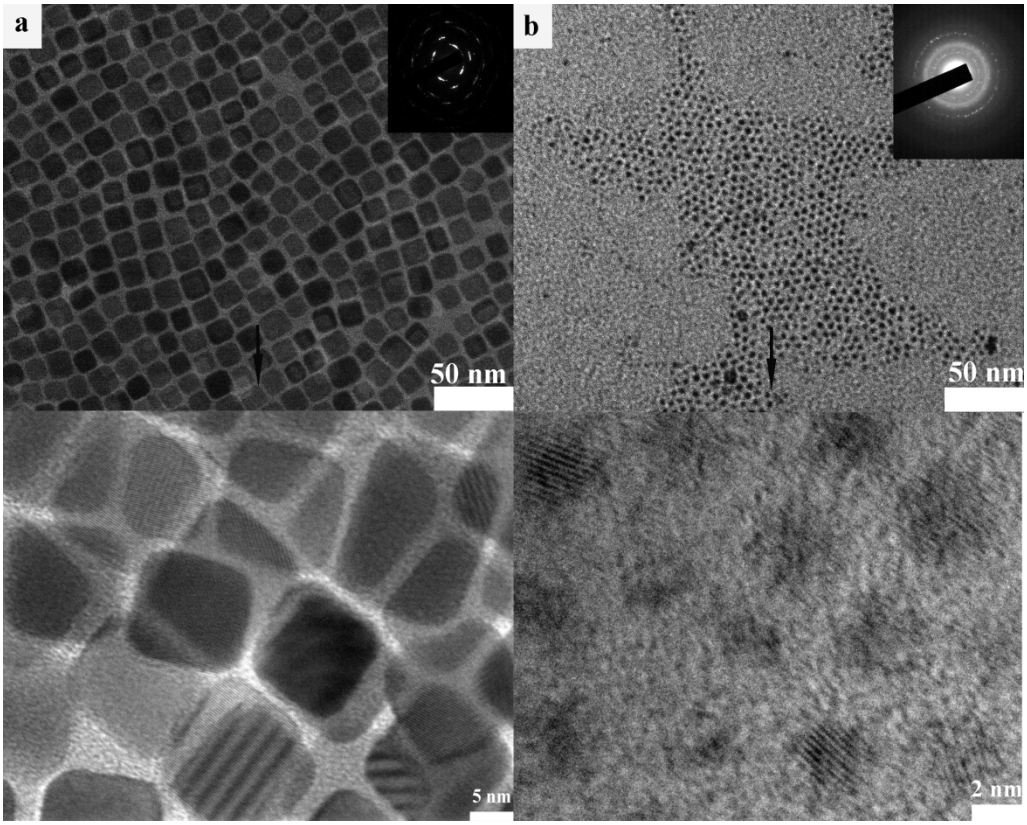

Figure 3.30 TEM and HRTEM images of the biggest and smallest PbTe QDs synthesized. Figure 3.30a, the biggest PbTe QDs (sample f-6) of 14.0 nm with size distribution σ = 8.7%. Figure 3.30b, the smallest PbTe QDs (sample f-1) of 2.6 nm with σ = 9.1%.

Table 3.12 PbTe QDs Synthesized by Hot-injection Method

Sample #	Average size (nm)	Size distribution (%)
f-1	2.6	9.1
f-2	3.3	7.3
f-3	5.5	5.6
f-4	9.5	7.4
f-5	10.5	8.2
f-6	14.0	8.7
f-8*	5.5	-
f-9*	9.5	-

*Capped with 4-Mpy.

For the separation and purification of the PbTe QDs, we found that, unlike the synthesis of PbSe QDs using either SeODE or SeOLA as the Se precursor, only one precipitation/centrifugation and extraction/centrifugation/suspension cycle was necessary in the post reaction process. Otherwise, the capping ligand OLA would be washed out (Figure 3.31).

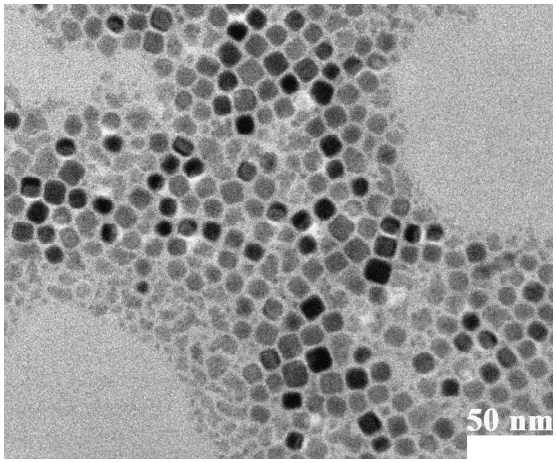

Figure 3.31 TEM image of PbTe QDs with excess washing. PbTe QDs purified two times lead to the loss of OLA ligand.

Temperature-based controlled synthesis of PbTe QDs

The TEM images of the obtained temperature-based controlled synthesis of PbTe QDs are shown in Figure 3.29, in which PbTe QDs show a relatively monodisperse distribution of sizes 3.3 nm with size distribution σ = 7.3% (sample f-2), 5.5 nm with σ = 5.6% (sample f-3), 9.5 nm with σ = 7.4% (sample f-4), and 10.5 nm with σ = 8.2% (sample f-5). The SAED patterns at the top right insets of the TEM images and the HRTEM images at the bottom in Fig. 1 confirmed the high crystallinity of the PbTe QDs. From Figure 3.29c of TEM image of sample f-4, we observed that the shape of the PbTe QDs began to change from spherical to cubic around the size of 9 to 10 nm. The TEM images showing large areas of the PbTe QDs synthesized can be seen in Figure 3.32. The temperature-based synthetic procedures developed here using only reaction temperature to control the size of PbTe QDs are powerful and practical tools for the size controlled monodisperse nanoparticle synthesis. The synthetic curve obtained in Figure 3.33 is a useful guideline for the synthesis of various sizes of PbTe QDs using the similar synthesis conditions. For example, to obtain PbTe QDs size of 8 nm, we can set the growth temperature at 180˚C and growth time for 5 min. To obtain PbTe QDs size smaller than 8 nm at that temperature, simply reduce growth time to 3 min. or 1 min. or 0.5 min., monodisperse PbTe QDs with size less than 8 nm will be produced. We found that the elemental analysis results from EDS (Table 3.13 to Table 3.16 and Figure 3.34) of samples f-2, f-3, f-4, and f-5 were identical: all had Pb and Te elements. All of them except sample f-2 had similar final Pb to Te ratio of 1:1. Sample f-2 data was off the scale probably due to the excess amount of Pb on the surface of the nanoparticles.

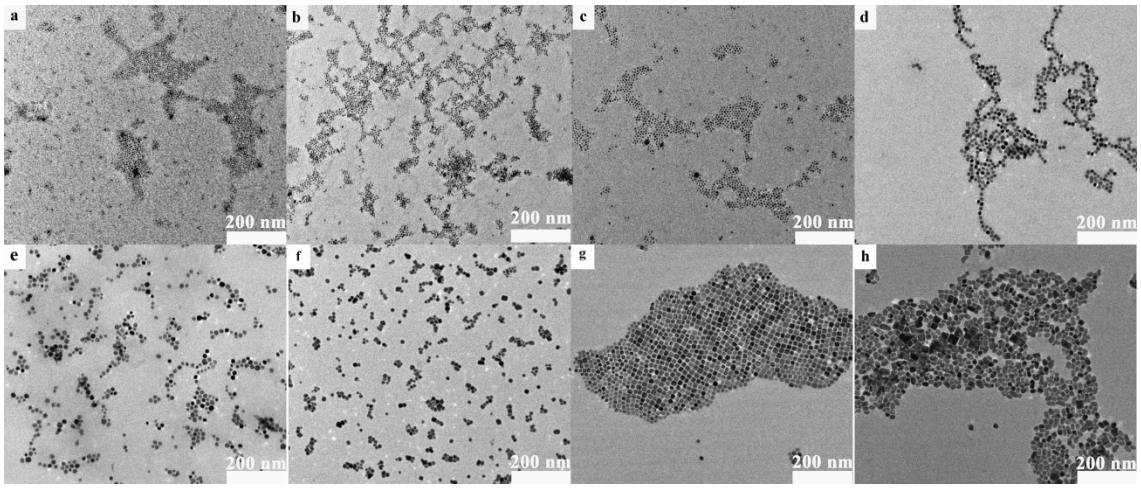

Figure 3.32 TEM images showing large areas of the hydrophobic PbTe QDs. Fig. 3.32a-3.32f corresponding to PbTe QDs sample f-1 to f-6. Figure 3.32g-h are samples of lead stearate based PbTe QDs.

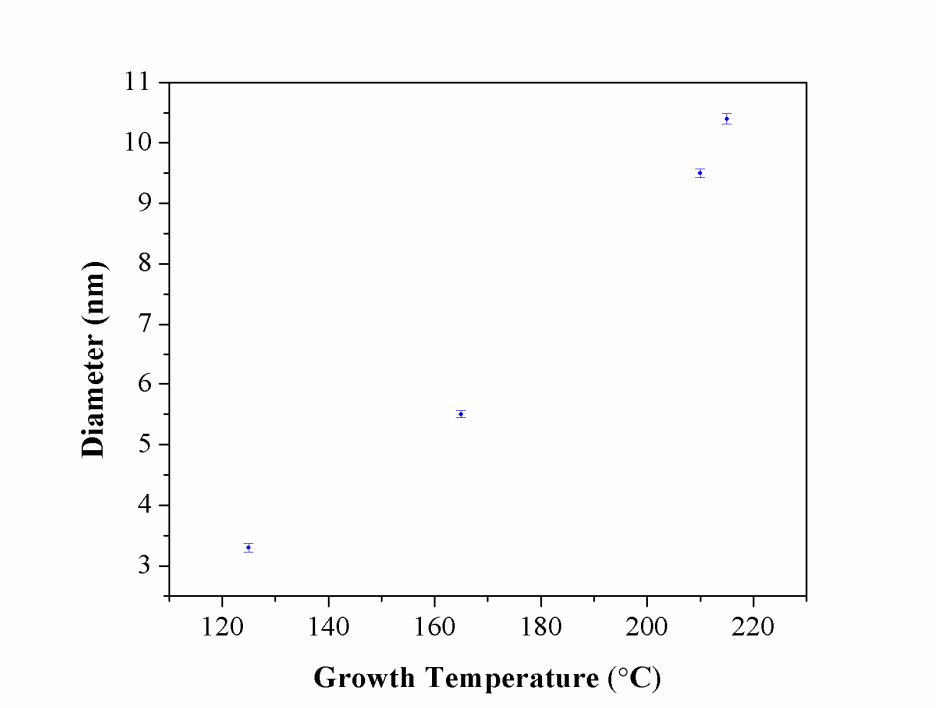

Figure 3.33 Temperature-based synthetic curve of PbTe QDs. When other conditions remain constant and the reaction growth time is at 5 min., narrowly distributed PbTe QDs were synthesized with various injection and growth temperatures.

Table 3.13 EDS Results of PbTe QDs sample f-2

Element	Weight %	Atomic %
TeL	20.2	29.2
PbL	79.8	70.8
Total	100.0	100.0

Table 3.14 EDS Results of PbTe QDs sample f-3

Element	Weight %	Atomic %
TeL	38.0	49.9
PbL	62.0	50.1
Total	100.0	100.0

Table 3.15 EDS Results of PbTe QDs sample f-4

Element	Weight %	Atomic %
TeL	35.0	46.7
PbL	65.0	53.3
Total	100.0	100.0

Table 3.16 EDS Results of PbTe QDs sample f-5

Element	Weight %	Atomic %
TeL	37.8	49.7
PbL	62.2	50.3
Total	100.0	100.0

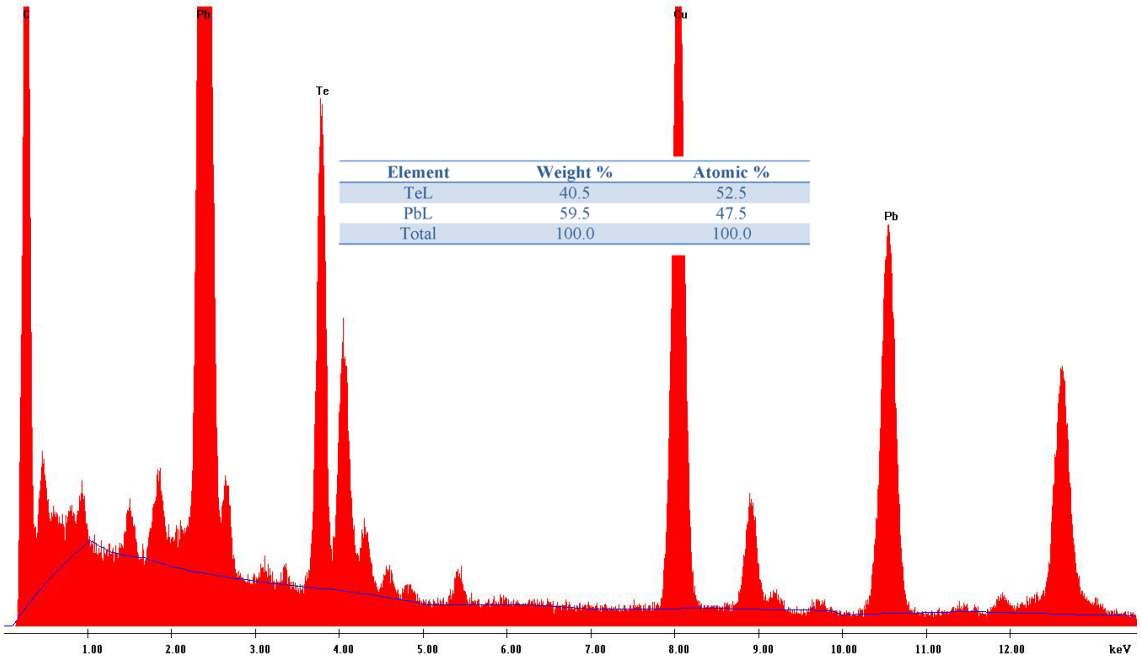

Element	Weight %	Atomic %
TeL	40.5	52.5
PbL	59.5	47.5
Total	100.0	100.0

Figure 3.34 EDS Result of PbTe QDs sample f-6.

Figure 3.35 is the HRTEM image of sample f-5 showing the lattice fringe of 3.2 ± 0.1 Å, which matches the JCPDS card file no. 38-1435 of 3.24 Å. Figure 3.36, the XRD and SAED data of sample f-5, shows that f-5 has an fcc structure with the *Fm3m* space group corresponding to JCPDS card file no. 38-1435. XRD pattern of the resulting PbTe QDs illustrated the values of the major peaks located in the range from 20° to 80° (2θ) corresponding to the characteristic diffraction of PbTe, verifying that only PbTe was present. The crystalline size was calculated by using the Scherrer equation from the line broadening of the (200) peak. It was 11.0 nm, which is also in consistent with TEM observation of the size of sample f-5 (10.5 nm). The HRTEM, SAED, XRD, and EDS data all pointed out that the as-synthesized PbTe QDs crystal structure and composition were PbTe. The TEM data revealed the shape of PbTe QDs was either spherical (< ~9-10 nm) or cubic (> ~9-10 nm).

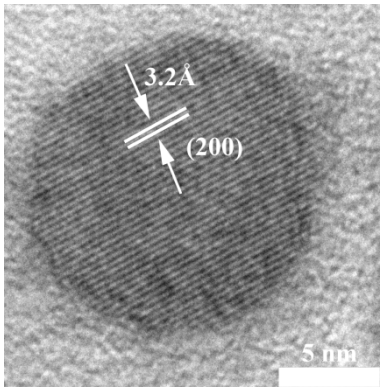

Figure 3.35 The HRTEM image of PbTe QDs sample f-5 of 10.5 nm with lattice fringe of 3.2Å ± 0.1 Å.

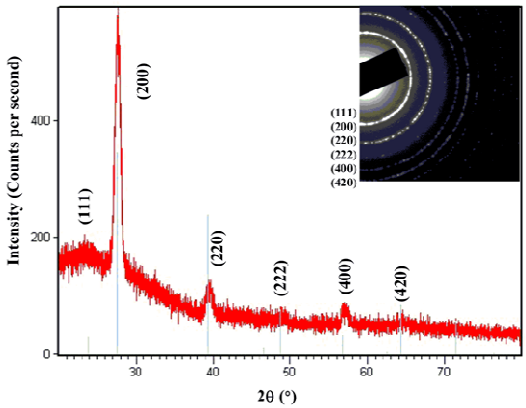

Figure 3.36 The XRD curve and SAED patterns of PbTe QDs sample f-5. The size of f-5 calculated from the full-width-half-maximum (FWHM) of the (220) peak of XRD using the Scherrer equation was 11.0 nm. The red plot is the actual XRD curve. It is in agreement with JCPDS card file no. 38-1435 (cubic phase PbTe). Inset in the top right shows electron diffractogram linked with the main diffraction rings of sample f-5.

Ligand exchange of PbTe QDs with 4-mercaptopyridine

The hydrophilic PbTe QDs f-8 and f-9 were the results of ligand exchange of PbTe QDs f-3 and f-4 using 4-Mpy to replace OLA. Both of their sizes remained unchanged. However, the

hydrophilic PbTe QDs connected more closely due to the hydrogen bond formation between 4-Mpy molecules (Figure 3.37). The hydrophilic PbTe QDs synthesis demonstrated a complete replacement of OLA ligand and formation of PbTe QDs network similar to Lu's result,[60] while Janssen's result[61] indicated a partial replacement of strong OA ligand using pyridine in the synthesis of PbSe QDs. Therefore, TOP was not a ligand for the synthesis of the hydrophobic PbTe QDs. Otherwise, there would be a partial replacement of TOP by 4-Mpy, generating a result similar to that of the Janssen group. The TEM images showing large areas of hydrophilic PbTe QDs synthesized were presented in Figure 3.38.

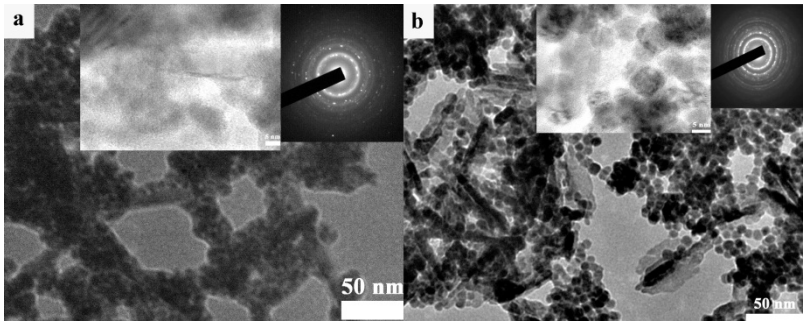

Figure 3.37 The TEM and HRTEM images and SAED patterns of the 4-Mpy capped hydrophilic PbTe QDs sample f-8 (5.5 nm) and f-9 (9.5 nm). Sample f-8 and f-9 were synthesized via ligand exchange between OLA and 4-Mpy. The PbTe QDs were networked together.

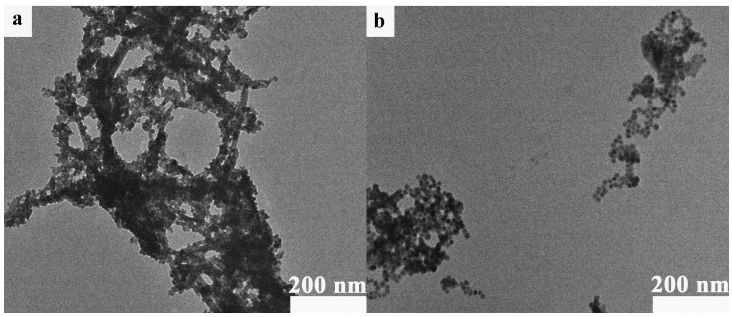

Figure 3.38 TEM images showing large areas of the hydrophilic PbTe QDs samples. Figure 3.38a-3.38b corresponding to PbTe QDs sample f-8-f-9.

PbTe QDs stability test

Table 3.17 and Figure 3.39 to Figure 3.40 show sample f-3 stability test results. Table 3.18 and Figure 3.41 list sample f-7 stability test results. Samples f-3 and f-7 were synthesized under the same conditions, but not at the same day with different batches of Pb and Te precursors. We found that except for the PbTe QD samples f-2 (3.3 nm), f-3 (5.5 nm), and f-7 (5.5 nm), all the sizes of the PbTe QDs samples stored as thin films on TEM copper grids measured 130 days later "swelling" compared to their original measured sizes, but without any significant shape and size distribution changes (sample f-6 is an example, its size became 14.9 nm instead of 14.0 nm. Refer to Figure 3.42 and Table 3.19.); all the sizes of PbTe QDs stored in TCE solution in air and measured 130 days later, also "swelling". However, both their shape and size distribution remain almost unchanged. PbTe QDs stored in solid form were not air-stable. For the stability test, we obtained different results compared to PbSe QDs synthesized using OA as capping agent. After PbSe QDs were stored for 390 h or longer, they shrank to smaller particles.[62-63] The "swelling" and "shrinking" differences between PbTe and PbSe QDs are probably due to the fact that long chain primary amine OLA is a good antioxidant. PbTe QDs samples f-2, f-3, and f-7 were stable both in TCE storage under ambient environment and stored as thin films on TEM copper grids, without size, shape, and size distribution changes. These air-stable small PbTe QDs may have potential to be used in quantum dots structured solar cell devices.

Table 3.17 Stability Test Results of PbTe QDs Sample f-3

Sample #	Sample measurement	Sample size (nm)	Sample distribution (%)
f-3a (f-3)	After synthesis	5.5	5.6
f-3b	Stored as thin films on TEM copper grid for 130 days	5.5	5.2
f-3c	Stored in TCE solution for 130 days	5.6	4.6

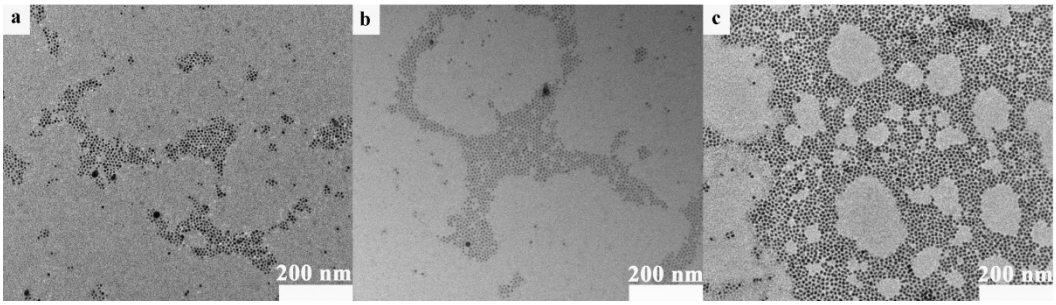

Figure 3.39 The TEM images of the PbTe QDs stability test of sample f-3. Figure 3.39a, f-3a of 5.5 nm with σ = 5.6%: samples measured after synthesis; Figure 3.39b, f-3b of 5.5 nm with σ = 5.2%: samples stored as thin films on TEM copper grid and measured after 130 days; Figure 3.39c, f-3c of 5.6 nm with σ = 4.6%: samples stored in TCE solution and measured after 130 days. No apparent changes observed for f-3 during this period.

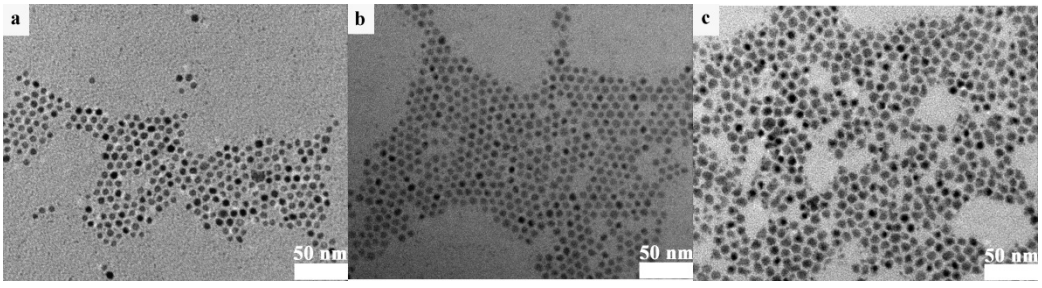

Figure 3.40 The TEM images of the PbTe QDs stability test of sample f-3 (Figure 3.40a-c) at a smaller scale bar of 50 nm compared to Figure 3.39 scale bar of (200 nm). Sample f-3a, f3-b, and f-3c have similar size.

Table 3.18 Stability Test Results of PbTe QDs Sample f-7

Sample #	Sample measurement	Sample size (nm)	Sample distribution (%)
f-7a (f-7)	After synthesis	5.5	5.7
f-7b	Stored as thin films on TEM copper grid for 130 days	5.6	5.0
f-7c	Stored in TCE solution for 130 days	5.5	5.2
f-7d	Stored in solid form for 130 days	decomposed	-

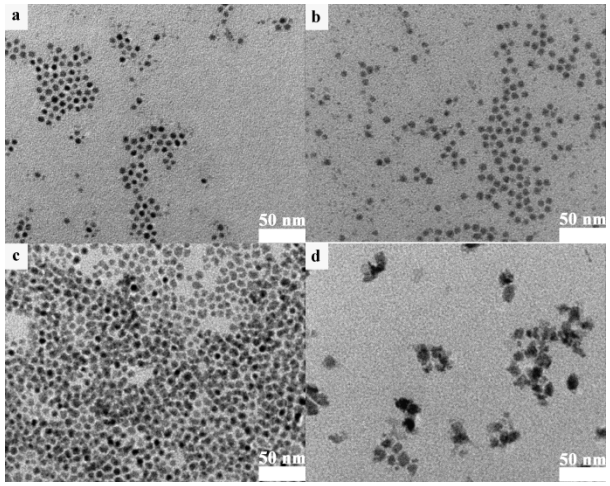

Figure 3.41 The TEM images of the PbTe QDs stability test of sample f-7. Figure 3.41a, f-7a of 5.5 nm with size distribution σ = 5.7%: samples measured after synthesis; Figure 3.41b, f-7b of 5.6 nm with σ = 5.0%: samples stored as thin films on TEM copper grid and measured after 130 days; Figure 3.41c, f-7c of 5.5 nm with σ = 5.2%: samples stored in TCE solution and measured after 130 days; Figure 3.41d, f-7d (decomposed): stored in solid form and measured after 130 days.

Table 3.19 Stability Test Results of PbTe QDs Sample f-6

Sample #	Sample measurement	Sample size (nm)	Sample distribution (%)
f-6a (f-6)	After synthesis	14.0	8.7
f-6b	Stored as thin films on TEM copper grid for 130 days	14.9	9.4

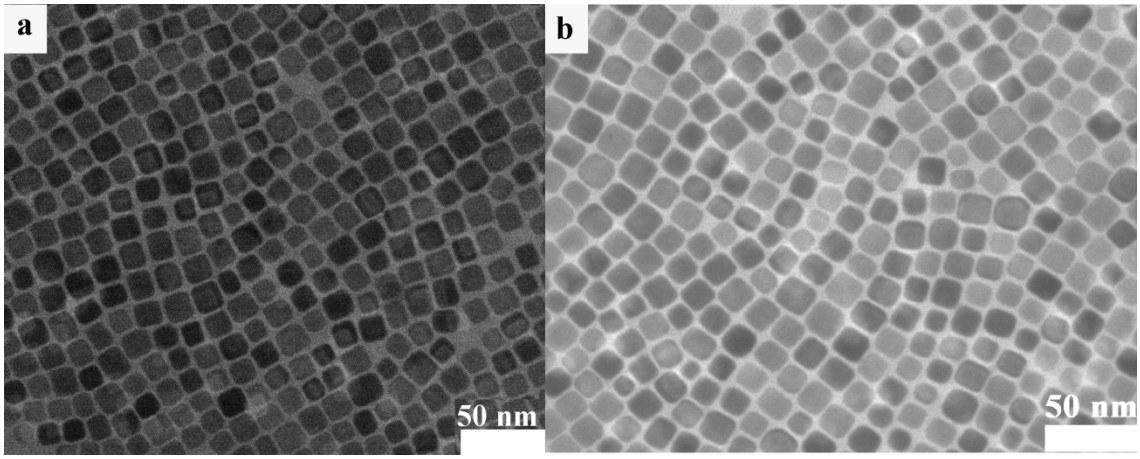

Figure 3.42 The TEM images of the PbTe QDs stability test of sample f-6. Figure 3.42a, f-6a of 14.0 nm with σ = 8.7%: samples measured after synthesis; Figure 3.42b, f-6b of 14.9 nm with σ = 9.4%: samples stored as thin films on TEM copper grid and measured after 130 days. The samples "swell" 6.4% in 130 days on TEM copper grid.

3.3.4 Conclusion

We have developed a modified, simple, hot-injection method to synthesize monodisperse PbTe QDs. We selected TOPTe as Te precursor, $PbCl_2$ as Pb metal source, and OLA as the capping ligand. The synthetic method used fewer reagents and reduced cost via simplified reaction and post reaction processes. The sizes of the PbTe QDs ranged from 2.6 nm to 14.0 nm with a standard deviation of ~5.6-9.1% (Table 3.20). Some small sizes of PbTe QDs synthesized

(3.3 and 5.5 nm) were air-stable. The temperature-based synthetic procedures developed by our group using only reaction temperature to control the size of nanoparticles are powerful and practical tools for the size controlled synthesis of other monodisperse nanoparticles. The synthetic results are reproducible with relatively high yield. This synthesis may be a potential candidate for industrial scale production.

Table 3.20 PbTe QDs Synthesized by Hot-injection Method

Sample #	Average size (nm)	Size distribution (%)	Synthetic Method
PbTe QD-1	2.6	9.1	Hot-injection
PbTe QD-2	3.3	7.3	Hot-injection
PbTe QD-3	5.5	5.6	Hot-injection
PbTe QD-4	9.5	7.4	Hot-injection
PbTe QD-5	10.5	8.2	Hot-injection
PbTe QD-6	14.0	8.7	Hot-injection
PbTe QD-7	5.5	5.7	Hot-injection

3.4 Controlled Synthesis of Se Nanoclusters and Se QDs

Selenium is one of very important semiconductor materials. Se QDs with size below 20 nm should have strong quantum confinement effects as we discussed in chapter 2.

Se QDs are mainly prepared by redox reaction in aqueous solution,[64-71] annealing at high temperature,[72-73] laser irradiation,[74] and embedding Se into host such as zeolites.[75-77] Most Se QDs reported are not monodisperse when the sizes are below 20 nm. These reports are lack of convincing evidence, such as TEM images, HRTEM images, XRD data, and size distribution data for Se QDs with size less than 20 nm though some Se QDs embedded in zeolites have small

size around 1-2 nm characterized by Raman spectroscopy. The lack of progress in the colloidal synthesis of single elemental QD is mainly due to some harsh synthetic conditions. It is common among single elemental QD synthesis. For example, the colloidal synthesis of monodisperse Ge QDs required severe reaction conditions.[78-80]

During the synthesis of PbSe QDs, we found a new solvent TDE to dissolve Se powder to obtain SeTDE solution as Se precursor. Two observations let us discover the simple solution precipitation or crystallization method for the synthesis of Se QDs with size less than 20 nm. One is that we obtained the TEM image of species from SeTDE solution as the result of curiosity; the other is we observed that some red powder remained in the reaction flask while dissolving the black t-Se power at high temperature. At that time I was very interested in this phenomenon and thought I could obtain nano Se from SeTDE though the topic was outside the scope of my research at that time. I had a very strong motivation to find out what happened in the SeTDE solution.

3.4.1 Introduction

My curiosity, strong motivation and persistence to obtain nano sized Se QDs really push me to success in the discovery, especially with the strong support of Prof. Lombardi.

It is well known that different size and shape of crystals can be grown from solution by controlling the nucleation and growth processes, such as adjusting the solubility, cooling rate, temperature, and time, etc.[81-82] There are many ways to synthesize nanoparticles. Most of them are complicated methods with multiple processes. Solution precipitation or crystallization is a simple method to growth crystals with different sizes, shapes, and crystal structures for bulk materials. By rapid cooling and crunching the liquids and supersaturated solution of some

compounds and metals, small crystals of micrometer size can be produced. For non-metals, to the best of our knowledge, there is no report of growing nanocrystals using this physical method till now because of the complicated processes of producing these kinds of nanomaterials.

We have developed a new, simple, and convenient method to synthesize Se nanoparticles. Elemental selenium nanoparticles with size less than 20 nm are successfully synthesized using a solution precipitation or crystallization method. It opens a new field for controlled synthesis of elemental, non-metal nanoparticles. By dissolving Se powder in liquid alkene or alkane solvents, which has higher boiling point than the melting point of t-Se, at elevated temperature to form a supersaturated solution, followed by the controlled rapid cooling, monodisperse Se QDs of 1 nm to 12.0 nm can be synthesized.

The solvents used here are TDE and ODE. Se QDs are prepared from either SeTDE or SeODE solution.

3.4.2 Experimental

Chemicals

Selenium (Se, 99.5%, powder, 200 mesh), 1-octadecene (ODE, 90%), acetone (99.9%), 1-tetradecene (TDE, 94%), tetradecane (TDA, 99%), cyclohexane (99.0%), and n-hexane (99+%) were purchased from ACROS Organic. Sulfur (S, 99.5-100.5%, powder) and carbon disulfide were from Fisher Chemical.

Synthesis of Se Nanoclusters and Se QDs

Synthesis of Se Nanoclusters

A typical synthesis of monodisperse Se nanoclusters is as follow. 0.917 g (11.61 mmol)

of Se black powder was loaded in a 50 mL round bottom flask, followed by adding 15.000 g (71.80 mmol, 19.35 mL) TDE. The mixture were heated and stirred rapidly to dissolve the Se powder. The mixture was refluxed for 2-3 hours. The red brown hot solution at 260°C was poured into a centrifuge tube immediately at a cooling rate of 0.35 K/s. The red precipitates then were centrifuged. After removing the excess solvent, 0.512 g of the red Se nanoclusterss were stored at room temperature for structure identification.

Synthesis of Se QDs

A typical synthesis of monodisperse Se QDs is as follow. 0.300 g (3.80 mmol) of Se black powder was loaded in a 50 mL round bottom flask, followed by adding 15.000 g (53.47 mmol, 19.01 mL) ODE. The mixture were heated and stirred rapidly to dissolve the Se powder. The mixture was refluxed for 2-3 hours. The red brown hot solution at 310°C was poured into a centrifuge tube immediately at a cooling rate of 0.91 K/s. The purple red precipitates then were centrifuged, followed by washing with n-hexane or cyclohexane or acetone to remove excess TDE and other impurities till the solution is almost colorless. After removing the excess solvent, 0.112 g of the purple red Se QDs were stored at room temperature for structure identification.

Synthesis of Bulk m-α-Se

A typical synthesis of bulk m-α-Se is as follow. 0.08 g (0.40 mmol) of Se black powder was loaded in a 50 mL round bottom flask, followed by adding 25 mL TDA. The mixture were heated and stirred rapidly to dissolve the Se powder. The mixture was refluxed for 2-3 hours. The light red hot solution at 260°C was poured into a centrifuge tube immediately. The small amount of red precipitates then were centrifuged, followed by washing with n-hexane and dried in air. The small amount of red Se crystals was re-dissolved in carbon disulfide for

recrystallization. The red crystal obtained from the recrystallization was stored in air for Raman measurement.

Sample characterization

Raman spectroscopy, ^{1}H and ^{13}C nuclear magnetic resonance spectroscopy (NMR), differential scanning calorimetry (DSC), mass spectrometry (MS), and gas chromatography and Mass Spectrometer (GC-MS) were used to monitor, analyze, and identify reactants, products, and Se nanoclusters and Se QDs synthesized. DSC curves were recorded for the investigation of phase transitions of Se QDs. UV-Vis-Near IR spectra were used to estimate the size of the Se nanoclusters. The crystal structures of Se QDs are determined by HRTEM, fast Fourier transformation of HRTEM (FFT), Raman spectroscopy, selected area x-ray diffraction (SAED), and XRD.

3.4.3 Results and Discussion

Two kinds of Se nanocrystals were produced from the precipitation of SeTDE solution. The synthesis turns micrometer trigonal t-Se_n (black) to nanometer m-α-Se_8 (red) and r-Se_6 (purple red). From microscale to nanoscale, for Se, it is just a simple journey, but for us, such a journey is not easy to be discovered and observed.

The synthetic results are listed in Table 3.21. These are the Se QDs, which have the crystal structure of m-α-Se_8 (red) we obtained that have TEM images taken. The r-Se_6 crystals without TEM images are not taken are not listed in the table. However, we will discuss their crystal structure and estimate their sizes. Part of the structure elucidation will be covered in chapter 5 for the Raman study.

Table 3.21 Se Nanoclusters and Se QDs Synthesized

Sample #	Average size (nm)	Size distribution (%)
Se QD-1	1.6	6.1
Se QD-2	4.3	6.0
Se QD-3	12.0	-

The crystal structure of Se nanoclusters sample Se QD-1 were confirmed by a combination of TEM (Figure 3.43), HRTEM (Figure 3.44), FFT of HREM (Figure 3.45), UV-Vis (Figure 3.46 and Figure 3.47), DSC (Figure 3.48), and Raman spectra (Figure 3.49).

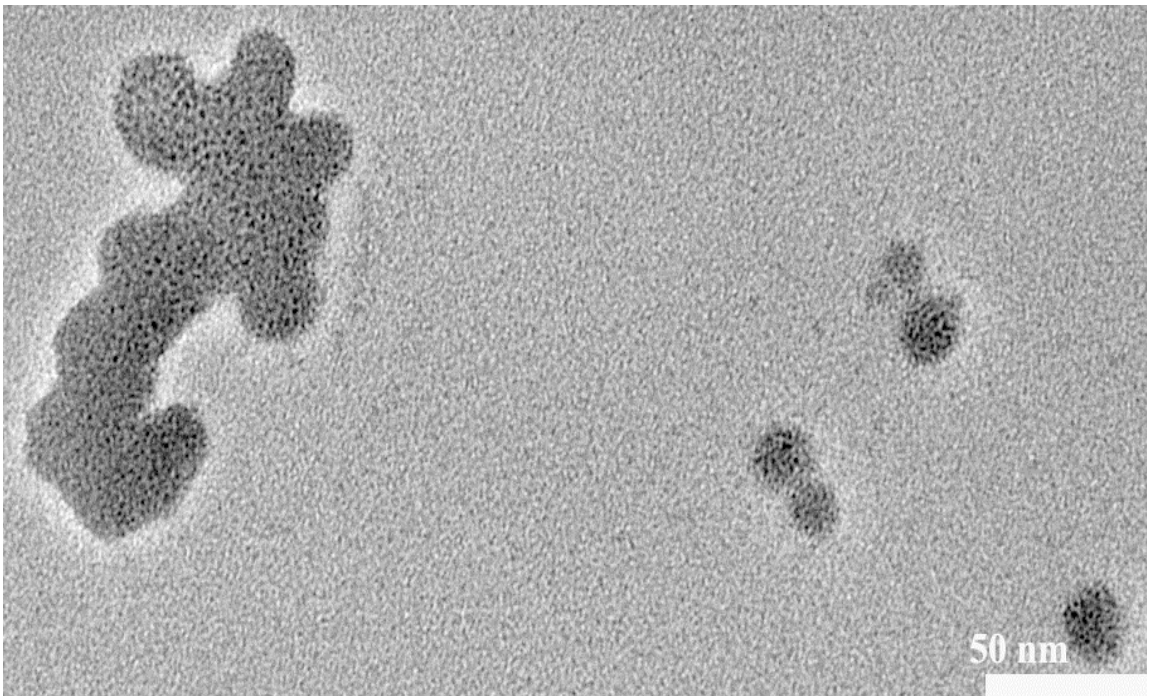

Figure 3.43 TEM image of Se nanoclusters sample Se QD-1. The average size of Se QD-1 is 1.6 nm with a size distribution of 6.1%.

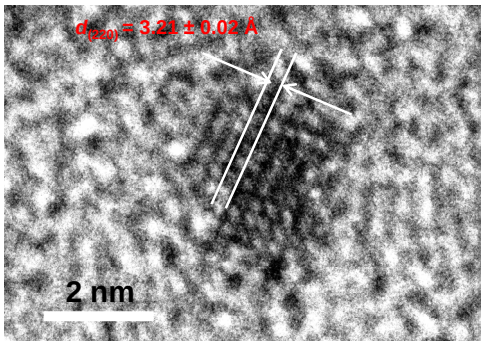

Figure 3.44 HRTEM image of Se nanoclusters sample Se QD-1. The lattice fringe of Se QD-1 measured is 3.21 ± 0.02 Å, which matches the bulk m-α-Se_8 data of ICDD, PDF Card 04-007-2085.

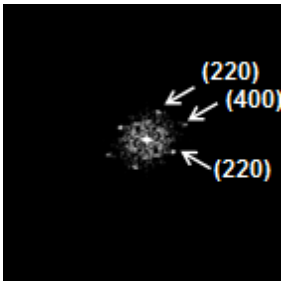

Figure 3.45 FFT of HRTEM image of sample SeQD-1. It clearly shows the (220) and (400) lattice planes of Se, matching the bulk m-α-Se_8 data of ICDD, PDF Card 04-007-2085.

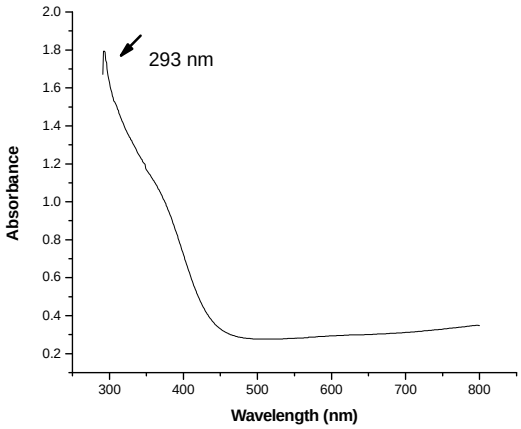

Figure 3.46 UV-Vis absorbance spectra of Se nanoclusters sample Se QD-1.

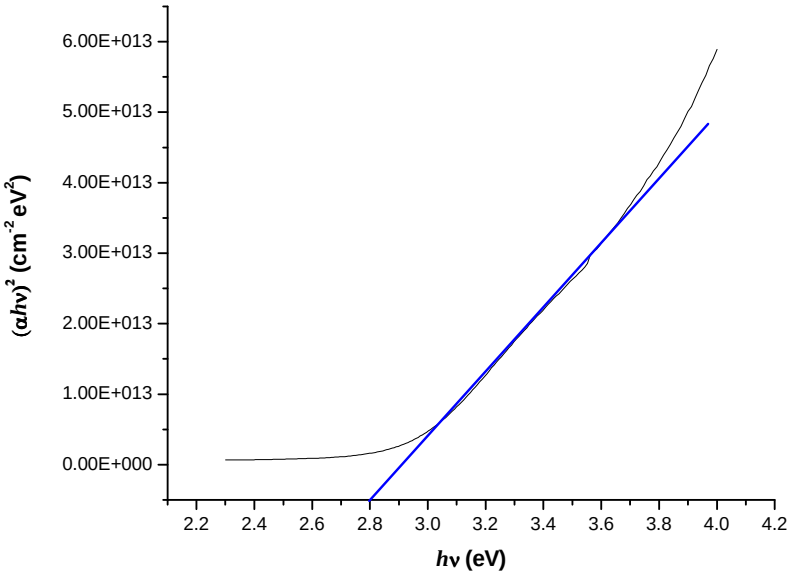

Figure 3.47 Tauc plots UV-Vis data from Figure 3.46. The band gap energy of Se QD-1 E_{QD} estimated from the intercepts at x axis is 2.80 eV.

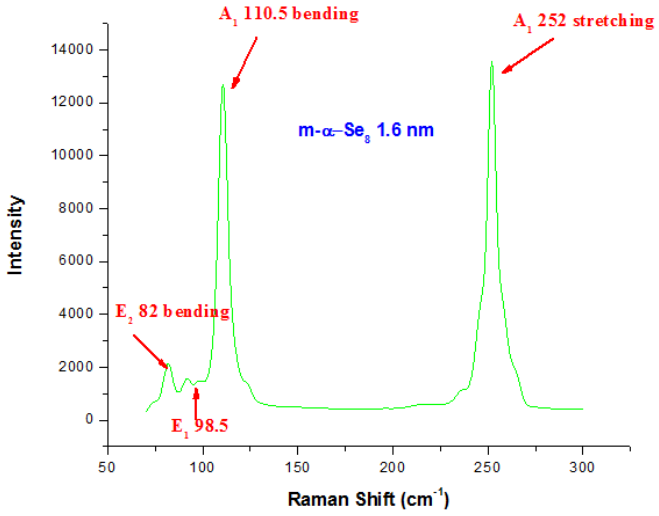

Figure 3.48 Raman spectrum of sample Se QD-1. The A_1 bending at 110.5 cm^{-1}, A_1 stretching at 252 cm^{-1}, E_1 at 98.5 cm^{-1}, and E_2 bending at 98.5 cm^{-1} prove it has m-α-Se_8 crystal structure.

The exciton Bohr radius of m-α-Se_8 is estimated using the equations below:

$$\boldsymbol{a_B} = \frac{\hbar^2 \boldsymbol{\varepsilon}}{\mu \boldsymbol{m_0 e^2}} = \mathbf{5.30} \times \mathbf{10^{-11}} \frac{\varepsilon}{\mu} \tag{5}$$

$$\boldsymbol{a_B} = \boldsymbol{a_e} + \boldsymbol{a_h} \tag{6}$$

$$\boldsymbol{a_e} = \mathbf{5.30} \times \mathbf{10^{-11}} \frac{\boldsymbol{\varepsilon}}{\boldsymbol{m_e^*}} \tag{7}$$

$$\boldsymbol{a_h} = \mathbf{5.30} \times \mathbf{10^{-11}} \frac{\boldsymbol{\varepsilon}}{\boldsymbol{m_h^*}} \tag{8}$$

where:

- a_B is the exciton Bohr radius in units of meter.
- a_e is radius of the electron in units of meter.
- a_h is radius of the hole in units of meter.
- m_0 is the mass of free electron.
- m_e is the effective mass of the electrons, which is $0.25m_0$[84-85].
- m_h is the effective mass of the holes, which is $1.35\text{-}2.7m_0$[86-87].
- ε is the dielectric constant of m-α-Se_8, which is 9.2.[88]

The exciton Bohr radius is estimated in the range from 2.13 nm to 2.31 nm based on the values of effective mass of holes of m-α-Se_8 we used. First, we take the experimental value from literature: $2.7m_0$ of t-Se as m_h for m-α-Se_8. Then, we calculate a_B of m-α-Se_8 by assuming the m_h of m-α-Se is $1.35m_0$ since there is no experimental data available for m_h of m-α-Se_8.

TEM image (Figure 3.43) of sample Se QD-1 demonstrates that the Se nanoclusters are monodisperse particles with a size of 1.6 nm and a size distribution of 6.1%. HRTEM image (Figure 3.44) of sample Se QD-1 and FFT of the HRTEM image reveal that he lattice fringe of Se QD-1 measured is 3.21 ± 0.02 Å, clearly showing the (220) and (400) lattice planes, which matches the crystal structure of bulk m-α-Se_8 data with ICDD, PDF Card 04-007-2085.

From the UV-Vis data of the absorbance spectra, the extinction coefficient α can be calculated using Equation 9 (refer to Equation 15 of chapter 2):

$$\alpha = B(h\nu - E_g)^n / h\nu \tag{9}$$

Extinction coefficient α can be calculated using Equation 10:[64]

$$\alpha = \frac{23000Ad}{M_w cl} \tag{10}$$

where:

- *A*: absorbance.
- *d*: 4.39 g/cm^3, density of m-Se.
- M_w: 78.96 g/mole, atomic mass of Se.
- *c*: 0.02 M, concentration of Se.
- *l*: 1 cm, length of the cuvette.

The band gap energy of Se QD-1 estimated from Figure-3.47 of Tauc plot $(\alpha h\nu)^2$ vs. $h\nu$ is 2.8 eV. Using Equation 11 (refer to Equation 16 of chapter 2), the radius of Se QD-1 is calculated as 0.25 nm. The diameter is 0.5 nm.

$$R = \left(\frac{\hbar^2 \pi^2}{2\mu(E_{QD} - E_g)}\right)^{1/2} \quad (11)$$

where:

- E_{QD} is 2.80 eV for Se QD-1.
- E_g is 2.53 eV
- m_e is the effective mass of the electrons, which is $0.25m_0$.
- m_h is the effective mass of the holes, which is $2.7m_0$.
- $\hbar$ is the reduced Planck's constant.
- R is the radius of Se QD-1.

The calculated diameter for Se QD-1 is 0.5 nm, while the diameter measured from TEM is 1.6 nm. The mismatch is due to several factors, such as the concentration of the Se solution is estimated, the E_g used, the m_h used, etc. Nevertheless, they are in the same range.

The Se QD-1 cannot be measured by XRD since its size is too small and beyond the measuring limit of the XRD used. Raman spectroscopy shows its strength in this case. The A_1 bending at 110.5 cm^{-1}, A_1 stretching at 252 cm^{-1}, E_1 at 98.5 cm^{-1}, and E_2 bending at 98.5 cm^{-1} (Figure 3.48) of sample Se QD-1 prove that the Se sample has m-α-Se_8 crystal structure.

The TEM image of sample Se QD-2 of 4.3 nm with a size distribution of 6.0% is shown in Figure 3.49. Figure 3.50 is the HRTEM image of Se QD-2, which also matches the crystal structure of bulk m-α-Se_8 data with ICDD, PDF Card 04-007-2085.

Figure 3.51 is the HRTEM image of Se QD-3. Figure 3.52 is the XRD result of Se QD-3, which matches the crystal structure of bulk m-α-Se_8 data with ICDD, PDF Card 04-007-2085.

The EDS result of Se QD-3 in Figure 3.53 demonstrates that the Se QD-3 consists of only Se element.

All of the measurements we used confirmed that the Se nanoclusters and Se QDs synthesized have the crystal sturcture of m-α-Se_8.

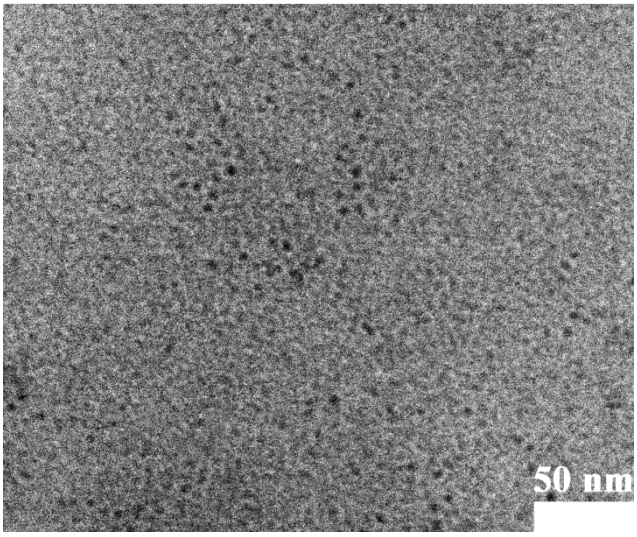

Figure 3.49 The TEM image of sample Se QD-2 of 4.3 nm with a size distribution of 6.0%.

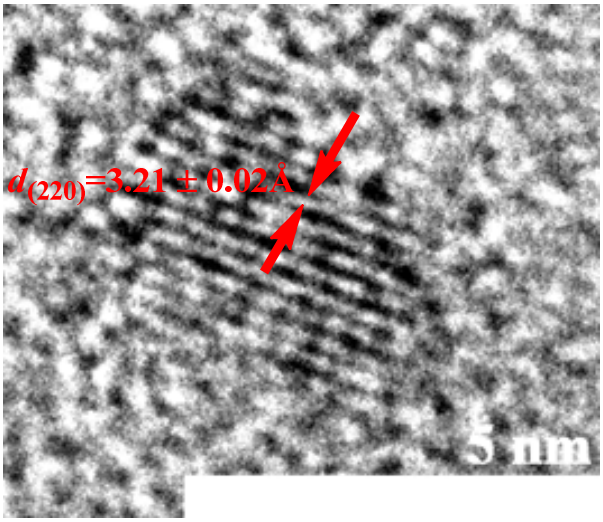

Figure 3.50 The HRTEM image of Se QD-2.

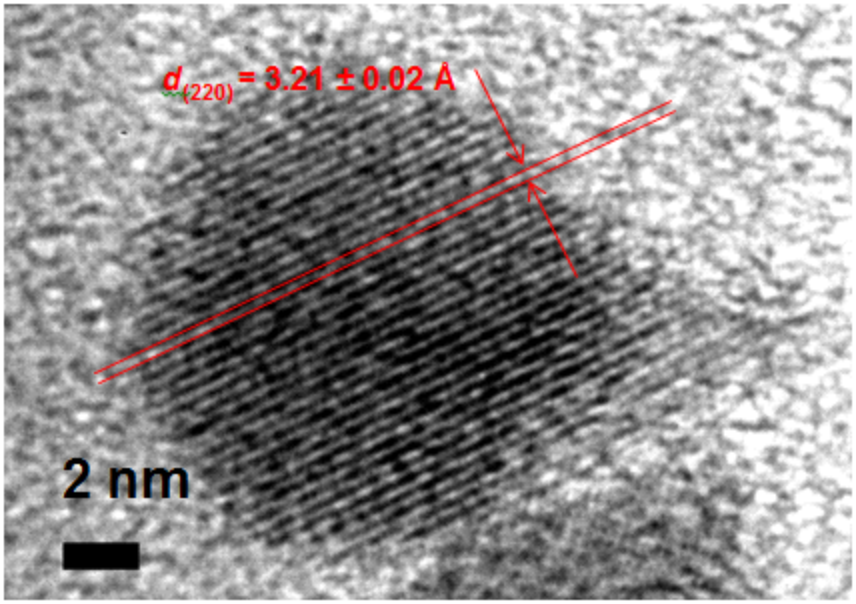

Figure 3.51 The HRTEM image of Se QD-3.

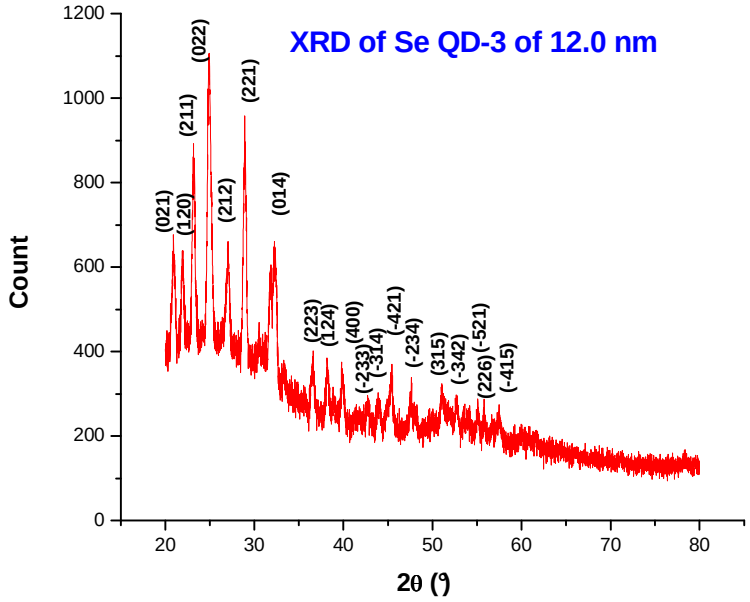

Figure 3.52 The XRD result of Se QD-3. It matches the bulk m-α-Se_8 data with ICDD, PDF Card 04-007-2085.

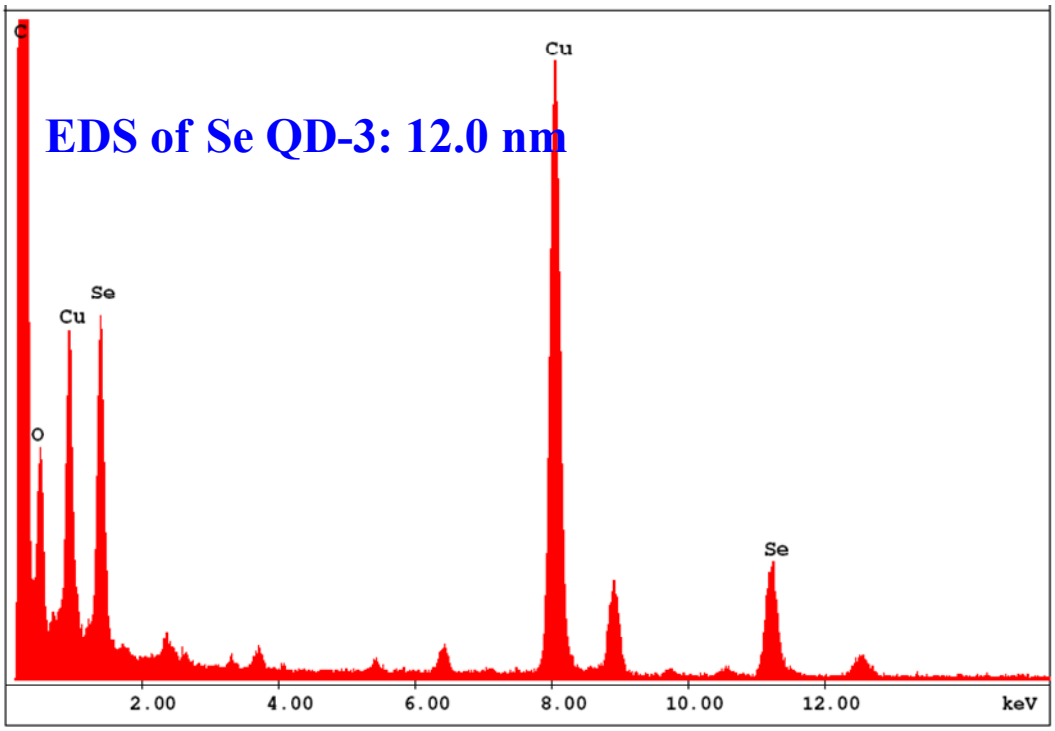

Figure 3.53 The EDS result of Se QD-3.

The phase transitions involved in the formation of m-α-Se_8 and r-Se_6 is illustrated in Figure 3.54. It is similar to Minaev's report of the liquid Se system phase transitions.[88-89] Contrary to the normal crystallization, the SeTDE solution still remains clear when it is cooled to room temperature slowly (naturally). This is probably due to the carbon-carbon double bond interactions with Se atoms or the formation of Se-C bond that make the Se soluble in TDE as section 3.3 described. The preliminary DSC result and some literature reports[89-90] support the finding. At 52°C, the weak capping ligand of alkene separated from Se; at 117°C, the m-α-Se_8 melted; at 124.5°C, it transfers to t-Se_n. It indicates that this simple solution precipitation is not a simple physical process. The process involves some chemical changes worth to be further investigated. The reason that we can obtain different size of monodisperse Se QDs is that the alkenes inside the SeTDE or SeODE solution are actually acted as capping ligands. They come out of the solution together with Se_8 to form Se QDs as Figure 3.56 indicated.

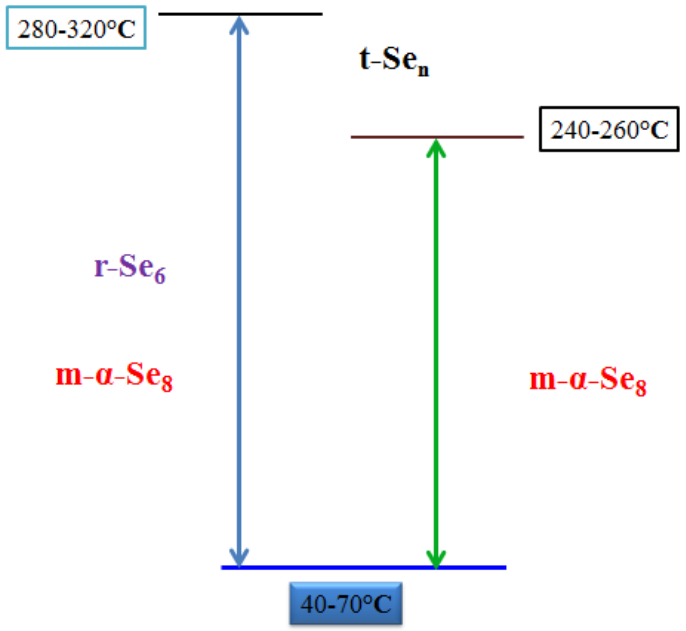

Figure 3.54 Solution Precipitation of Se Nanoclusters and Se QDs.

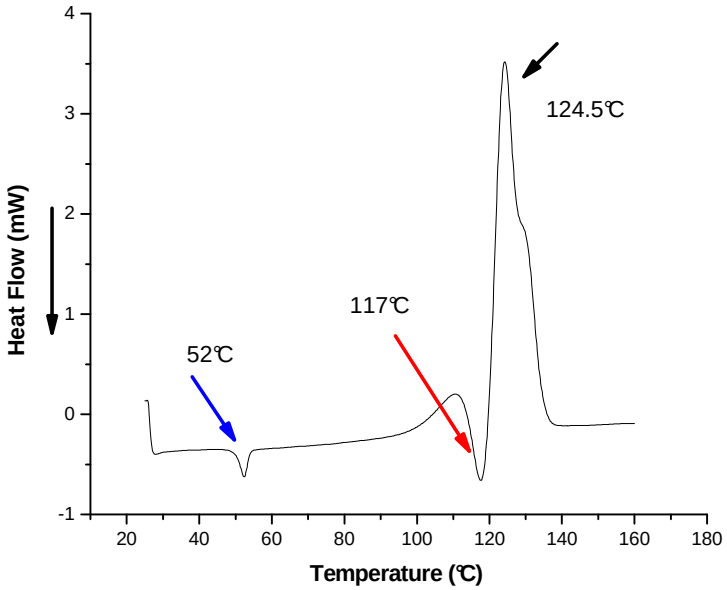

Figure 3.55 DSC scan of Se QD-3 at a rate of 10 K/min. The exothermic process at 52°C may represent the leaving of the weak capping ligand of alkene. The exothermic process at 117°C

indicates the melting of m-α-Se_8. The endotherm process at 124.5°C is the transfer of m-α-Se_8 to t-Se_n.

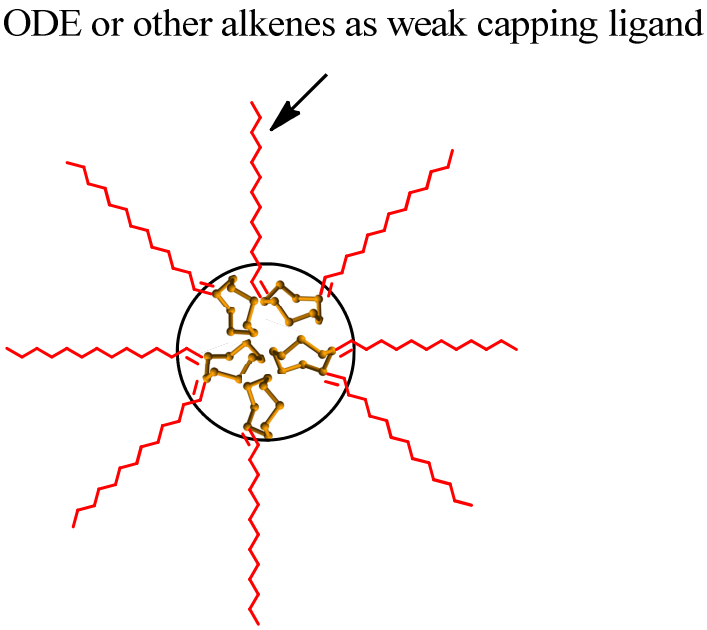

Figure 3.56 Weak alkene capping ligand of Se QDs.

Attempts to obtain S QDs using SODE or STDE, or STDA were all not successful. Perhaps the interactions between S_8 with the solvent SODE or STDE in the solution are much stronger than that of Se_8 with the solvent SODE or STDE. These lead to the S solubility increase significantly in SODE or STDE solution. Thus, the similar method used for preparing Se QDs cannot be extended to obtaining S QDs.

3.4.4 Conclusion

Monodisperse Se nanoclusters and Se QDs with size smaller than 20 nm were synthesized via the solution precipitation method. The crystals formation process is similar to the physical crystallization, but it also involves some complicated chemical changes. The optimal crystallization conditions were found. We have also confirmed that the Se QDs formed

is either m-α-Se_8 or r-Se_6 or their mixtures. The simple method can be easily scaled up for industrial production with a relative high yield. We propose that nanoparticles of non-metals can be produced via solution precipitation if there are solvents that have higher boiling point than the melting point of the non-metals and if they can form super-saturated solution at elevated temperature.

3.5 Controlled Synthesis of GO-QD Nanocomposites and Other QDs

STDE or SeTDE precursor solutions can be used as the universal precursor for the non-injection, one-pot synthesis of S-containing or Se-containing, binary and ternary QDs. They also make the non-injection, one-pot synthesis of 2D nanocomposites of graphene oxide or reduced graphene oxide with QD possible. We will explore the synthetic applications for producing energy-efficient nanomaterials using the new SeTDE precursor solution, $PbCl_2$-OLA, and OLA in this section.

3.5.1 Introduction

The energy-efficient materials consist of nanocomposites made of QDs with other materials have attracted enormous attentions recently.[91-93] However, the methods to produce the nanocomposites lag behind their applications. A typical example to synthesize nanocomposites is usually to obtain the individual components first, and then combined them together. It is similar to the hot-injection method to synthesize QD. We can simplify the synthetic process by using the newly discovered SeTDE precursor solution to obtain the nanocomposites in a single step. The following actual examples of synthetic applications of the new synthetic method reveal the power of the non-injection, one-pot synthetic method—its simplicity.

3.5.2. Experimental

Chemical

$PbCl_2$ (99-100%) was from J.T. Baker Chemical Company. Graphene oxide was from SinoCarbon (>95%). Methanol (absolute reagent, 99.8%, A.C.S.) was purchased from Spectrum Chemical. Tetrachloroethylene (TCE, 99%, extra pure), silver nitrate (99.0%), zinc chloride (>98%), manganese (II) chloride tetrahydrate (99%), selenium (Se, 99.5%, powder, 200 mesh), oleylamine (OLA, 80-90%), 1-tetradecene (TDE, 94%), and n-hexane (99+%) were purchased from ACROS Organic. All chemicals were used as received without further purification.

Synthesis of QD, GO-QD, and GO-Ag Nanocomposites

The following syntheses demonstrate the advantages of the non-injection, one-pot synthetic method. In a typical synthesis of the 6.4 nm GO-PbSeQD nanocomposites sample GO-PbSeQD-1, 0.094 g (0.34 mmol) $PbCl_2$, 3.39 g (10.14 mmol, 4.19 mL) OLA, 1.1 mL 0.6 M SeTDE solution, and 25 mg GO were introduced into a three-neck round-bottom flask at room temperature. The mixture was magnetically stirred and heated to 30℃ under vacuum for 15 min. Then, the vacuum was removed and the temperature of the mixture was further raised to 160℃ with a heating rate at about 20.1˚C/min. The temperature of the mixture was maintained at that level for 5 min. Then, the crude solution was cooled immediately in a water bath. The crude was centrifuged and washed with acetone. Next, 5 mL of TCE was added into the crude to extract the nanocomposites. After centrifuging, the as-synthesized GO-PbSeQD nanocomposites were stored in TCE.

Table 3.21 lists the amount of reagents used for the five different syntheses of QD, GO-QD nanocomposites, and GO-Ag nanocomposites, the reaction temperature, and the results of

these syntheses with sample size and size distribution. The reaction time is 5 min. for each of the synthesis. The heating rate is also the same for each of the synthesis at about 20.1˚C/min.

Table 3.21 QD, GO-QD, and GO-Ag Nanocomposites Synthesized

	Size (nm)	**σ** (%)	**$MnCl_2$·4 H_2O** (g)	**$PbCl_2$** (g)	**$ZnCl_2$** (g)	**OLA** (g)	**SeTDE** (mL)	**$AgNO_3$** (g)	**GO** (mg)	**Growth temp.** (°C)
MnSe QDs	5.6	8.0	0.065	-	-	3.39	1.1	-	-	160
ZnSe QDs	3.5	9.7	-	-	0.045	3.34	1.1	-	-	160
GO-PbSeQD-1	6.4	7.3	-	0.094	-	3.34	1.1	-	25	160
GO-PbSeQD-2	7.2	5.3	-	0.094	-	3,34	1.1	-	25	180
GO-Ag	27.6	12.5	-	-	-	4.29	1.1	0.090	25	160

Sample characterization

TEM and EDS are used to characterize the size, shape, and composition of the QD and nanocomposites synthesized.

3.5.3 Results and Discussion

The TEM images of the QD synthetic results are shown in Figure 3.57 and Figure 3.58. Figure 3.57a is TEM image of MnSe QDs of size 5.6 nm with a size distribution of 8.0%. Figure 3.57b is TEM image of ZnSe of 5.8 nm with a size distribution of 9.7%. It shows that SeTDE can be used as universal Se precursor for the synthesis of Se-containing QDs.

The EDS of $MnCl_2$ QDs in Figure 3.59 confirmed the components of the $MnCl_2$ are the same as its bulk material.

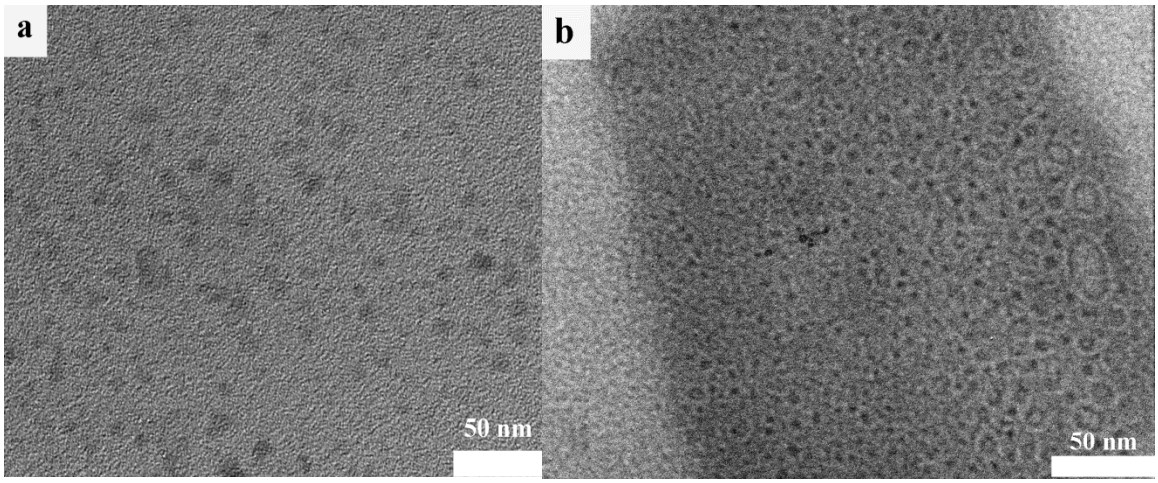

Figure 3.57 MnSe QDs and ZnSe QDs synthesized. Figure 3.57a, MnSe QDs of size 5.6 nm with a size distribution of 8.0%. Figure 3.57b, ZnSe of 5.8 nm with a size distribution of 9.7%.

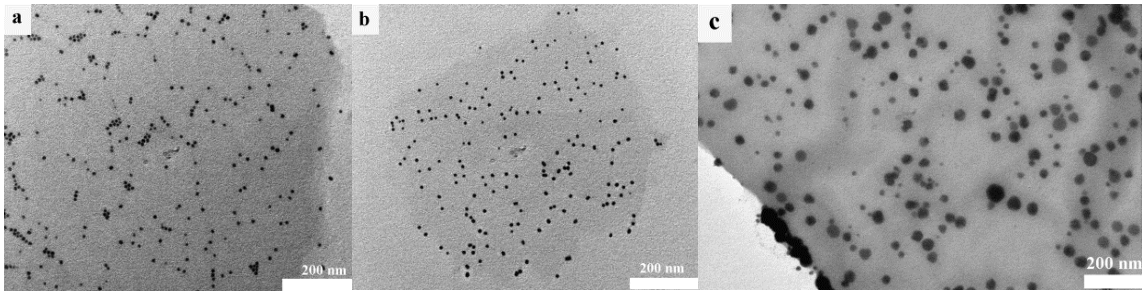

Figure 3.58 GO nanocomposites synthesized. Figure 3.58a, sample GO-PbSEQD-1 of size 6.4 nm with a size distribution of 7.3%. Figure 3.58b, sample GO-PbSEQD-2 of size 7.2 nm with a size distribution of 5.3%. Figure 3.58c, Go-Ag nanocomposites of size 27.6 nm with a size distribution of 12.5%.

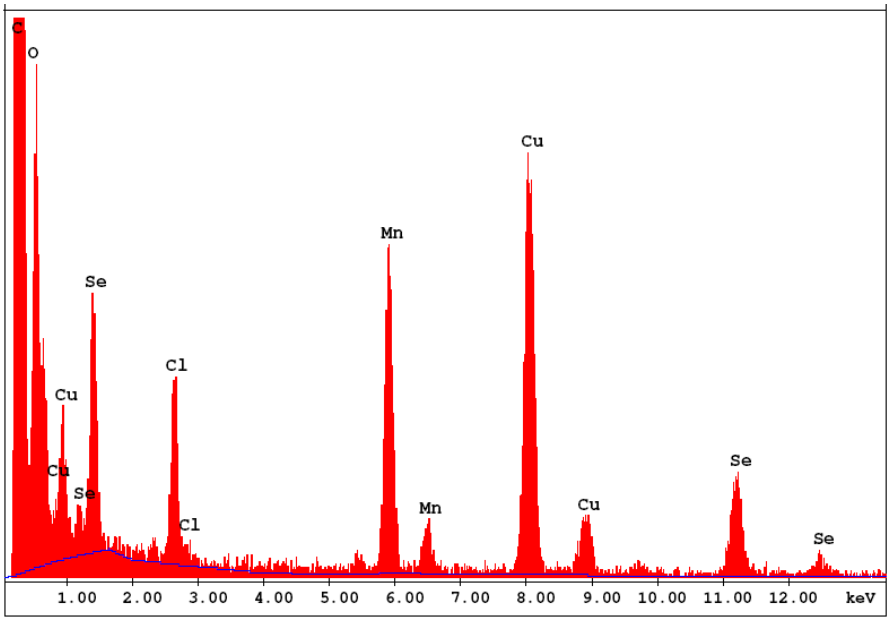

Figure 3.59 EDS result of $MnCl_2$ QDs.

The GO nanocomposites TEM results are displayed in Figure 3.58. The 2D GO-PbSeQD samples have monodisperse 0D PbSe QDs attached to it. The size of the PbSe QDs attached can be controlled by reaction temperature. At 160˚C, GO-PbSEQD-1 has a size of 6.4 nm with a size distribution of 7.3%; while at 160˚C, GO-PbSEQD-2 has a size of 7.2 nm with a size distribution of 5.3%. Here, we notice that the $PbCl_2$-OLA system is such a good synthetic system; it can be even used in the non-injection, one-pot synthesis of 0D contained nanocomposites. We predict that ternary or multi-chalgoen containing GO nanocomposites can be produced from STDE and SeTDE we developed. In the same time, multi-chalgoen containing QDs can also synthesized with the reagents and the synthetic systems we developed in this project. The GO-Ag nanocomposites are shown in Figure 3.57c though the Ag nanocrystals on the GO sheet have a relatively broad distribution of 12.5%. The new building blocks of the energy related nanomaterials using reagents and methods developed in this PhD research project may have great potential to be used as basic materials in solar cell applications. These new methods and

reagents provide alternative ways to synthesize energy-efficient materials that cannot be made before. It is obvious that nanocomposites including metal nanocrystals (Ag), binary QDs, and GO can be obtained using the non-injection, one-pot synthetic method.

3.5.4 Conclusion

The reagents, synthetic system, and synthetic methods developed by us are successfully used in the synthesis of other 0D QDs and 2D nanocomposites which are also monodisperse. It demonstrates the methods can be extended and are applicable to obtain other monodisperse nanomaterials.

We believe the techniques develop in this project will greatly enhance the development of new nanomaterials, especially in the fields of solar cell, semiconductor, and optoelectronic applications.

3.6 Chapter 3 Reference

(1) Shen, S.; Zhang, Y.; Peng, L.; Xu, B.; Du, Y.; Deng, M.; Xu, H.; Wang, Q. *Crystengcomm* **2011**, *13*, 4572.

(2) Yong, K.-T.; Sahoo, Y.; Swihart, M. T.; Prasad, P. N. *The Journal of Physical Chemistry C* **2007**, *111*, 2447.

(3) Ouyang, J.; Schuurmans, C.; Zhang, Y.; Nagelkerke, R.; Wu, X.; Kingston, D.; Wang, Z. Y.; Wilkinson, D.; Li, C.; Leek, D. M.; Tao, Y.; Yu, K. *ACS Appl Mater Interfaces* **2011**, *3*, 553.

(4) Wei, Y.; Yang, J.; Lin, A. W. H.; Ying, J. Y. *Chem Mater* **2010**, *22*, 5672.

(5) Joo, J.; Na, H. B.; Yu, T.; Yu, J. H.; Kim, Y. W.; Wu, F.; Zhang, J. Z.; Hyeon, T. *J Am Chem Soc* **2003**, *125*, 11100.

(6) Moreels, I.; Justo, Y.; De Geyter, B.; Haustraete, K.; Martins, J. C.; Hens, Z. *Acs Nano* **2011**, *5*, 2004.

(7) Shen, H.; Wang, H.; Li, X.; Niu, J. Z.; Wang, H.; Chen, X.; Li, L. S. *Dalton T* **2009**, 10534.

(8) Zhuang, Z.; Peng, Q.; Li, Y. *Chemical Society Reviews* **2011**, *40*, 5492.

(9) Kwon, S. G.; Hyeon, T. *Small* **2011**, *7*, 2685.

(10) de Mello Donegá, C.; Liljeroth, P.; Vanmaekelbergh, D. *Small* **2005**, *1*, 1152.

(11) Liu, T.-Y.; Li, M.; Ouyang, J.; Zaman, M. B.; Wang, R.; Wu, X.; Yeh, C.-S.; Lin, Q.; Yang, B.; Yu, K. *The Journal of Physical Chemistry C* **2009**, *113*, 2301.

(12) Jen-La Plante, I.; Zeid, T. W.; Yang, P.; Mokari, T. *J Mater Chem* **2010**, *20*, 6612.

(13) Zhuang, Z.; Lu, X.; Peng, Q.; Li, Y. *Chemistry – A European Journal* **2011**, *17*, 10445.

(14) Si, H.-Y.; Yuan, D.; Chen, J.-S.; Chow, G.-M. *RSC Advances* **2011**, *1*, 817.

(15) Li, Z.; Ji, Y.; Xie, R.; Grisham, S. Y.; Peng, X. *J Am Chem Soc* **2011**, *133*, 17248.

(16) Yordanov, G.; Yoshimura, H.; Dushkin, C. *Colloid & Polymer Science* **2008**, *286*, 813.

(17) Deng, Z.; Cao, L.; Tang, F.; Zou, B. *The Journal of Physical Chemistry B* **2005**, *109*, 16671.

(18) Pan, Y.; Lombardi, J. In *Nanotech 2011--NanoTech Conference & Expo 2011*; NSTI: Boston, USA, 2011; Vol. 1, p 303.

(19) Thomson, J. W.; Nagashima, K.; Macdonald, P. M.; Ozin, G. A. *J Am Chem Soc* **2011**, *133*, 5036.

(20) Koutselas, I.; Bampoulis, P.; Maratou, E.; Evagelinou, T.; Pagona, G.; Papavassiliou, G. C. *The Journal of Physical Chemistry C* **2011**, *115*, 8475.

(21) Wiewiorowski, T. K.; Touro, F. J. *The Journal of Physical Chemistry* **1966**, *70*, 234.

(22) Bateman, L.; Glazebrook, R. W.; Moore, C. G.; Porter, M.; Ross, G. W.; Saville, R. W. *Journal of the Chemical Society (Resumed)* **1958**, 2838.

(23) Meyer, B. *Chem Rev* **1976**, *76*, 367.

(24) Cademartiri, L.; Bertolotti, J.; Sapienza, R.; Wiersma, D. S.; von Freymann, G.; Ozin, G. A. *The Journal of Physical Chemistry B* **2005**, *110*, 671.

(25) Kothiyal, G. P.; Ghosh, B. *Prog Cryst Growth Ch* **1990**, *20*, 313.

(26) Wise, F. W. *Accounts Chem Res* **2000**, *33*, 773.

(27) Lide, D. R. *CRC Handbook of Chemistry and Physics*; 77th ed.; Boca Raton, 1996.

(28) Murray, C. B.; Norris, D. J.; Bawendi, M. G. *J Am Chem Soc* **1993**, *115*, 8706.

(29) Du, H.; Chen, C.; Krishnan, R.; Krauss, T. D.; Harbold, J. M.; Wise, F. W.; Thomas, G.; Silcox, J. *Nano Lett.* **2002**, *2*, 1321.

(30) Yu, W. W.; Falkner, J. C.; Shih, B. S.; Colvin, V. L. *Chem. Mater.* **2004**, *16*, 3318.

(31) Steckel, J. S.; Yen, B. K. H.; Oertel, D. C.; M. G. Bawendi *J. Am. Chem. Soc.* **2006**, *128*, 13032.

(32) Joo, J.; Pietryga, J. M.; McGuire, J. A.; Jeon, S.-H.; Williams, D. J.; Wang, H.-L.; Klimov, V. I. *J. Am. Chem. Soc.* **2009**, *131*, 10620.

(33) Li, H. B.; Chen, D.; Li, L. L.; Tang, F. Q.; Zhang, L.; Ren, J. *Crystengcomm* **2010**, *12*, 1127.

(34) Bullen, C.; van Embden, J.; Jasieniak, J.; Cosgriff, J. E.; Mulder, R. J.; Rizzardo, E.; Gu, M.; Raston, C. L. Chem Mater 2010, 22, 4135.

(35) Lokteva, Irina. (2010) Synthesis and Surface Characterization of Semiconductor Nanocrystals for Photovoltaic Application. (Doctoral Dissertation). Retrieved from Internet.

(36) Lardon, M. *J Am Chem Soc* **1970**, *92*, 5063.

(37) Dai, Q.; Zhang, Y.; Wang, Y.; Wang, Y.; Zou, B.; Yu, W. W.; Hu, M. Z. *The Journal of Physical Chemistry C* **2010**, *114*, 16160.

(38) Du, M.; Wang, Y.; Xu, J.; Yang, P.; Du, Y. *Colloid Journal* **2008**, *70*, 720.

(39) Fu, X. Q.; Pan, Y.; Wang, X.; Lombardi, J. R. *J Chem Phys* **2011**, *134*, 024707.

(40) Richter, A. P.; Lombardi, J. R.; Zhao, B. *J Phys Chem C* **2010**, *114*, 1610.

(41) Fonoberov, V. A.; Balandin, A. A. *Appl Phys Lett* **2004**, *85*, 5971.

(42) Dzhagan, V.; Lokteva, I.; Himcinschi, C.; Jin, X.; Kolny-Olesiak, J.; Zahn, D. R. *Nanoscale Research Letters* **2011**, *6*, 79.

(43) Arora, A. K.; Rajalakshmi, M.; Ravindran, T. R.; Sivasubramanian, V. *J Raman Spectrosc* **2007**, *38*, 604.

(44) Vanmaekelbergh, D.; Liljeroth, P. *Chemical Society Reviews* **2005**, *34*, 299.

(45) Vaqueiro, P.; Powell, A. V. *J Mater Chem* **2010**, *20*, 9577.

(46) Pei, Y.; LaLonde, A.; Iwanaga, S.; Snyder, G. J. *Energy & Environmental Science* **2011**, *Advance*.

(47) Zhang, G.; Finefrock, S.; Liang, D.; Yadav, G. G.; Yang, H.; Fang, H.; Wu, Y. *Nanoscale* **2011**, *Advance*.

(48) Baxter, J.; Bian, Z.; Chen, G.; Danielson, D.; Dresselhaus, M. S.; Fedorov, A. G.; Fisher, T. S.; Jones, C. W.; Maginn, E.; Kortshagen, U.; Manthiram, A.; Nozik, A.; Rolison, D. R.; Sands, T.; Shi, L.; Sholl, D.; Wu, Y. *Energy & Environmental Science* **2009**, *2*, 559.

(49) Sun, G.; Chang, F.; Soref, R. A. *Opt Express* **2010**, *18*, 3746.

(50) Antunez, P. D.; Buckley, J. J.; Brutchey, R. L. *Nanoscale* **2011.**

(51) Murphy, J. E.; Beard, M. C.; Norman, A. G.; Ahrenkiel, S. P.; Johnson, J. C.; Yu, P. R.; Micic, O. I.; Ellingson, R. J.; Nozik, A. J. *J Am Chem Soc* **2006**, *128*, 3241.

(52) Lu, W.; Fang, J.; Stokes, K. L.; Lin, J. *J Am Chem Soc* **2004**, *126*, 11798.

(53) Urban, J. J.; Talapin, D. V.; Shevchenko, E. V.; Murray, C. B. *J Am Chem Soc* **2006**, *128*, 3248.

(54) Mokari, T. L.; Zhang, M. J.; Yang, P. D. *J Am Chem Soc* **2007**, *129*, 9864.

(55) Zhang, J.; Kumbhar, A.; He, J. B.; Das, N. C.; Yang, K. K.; Wang, J. Q.; Wang, H.; Stokes, K. L.; Fang, J. Y. *J Am Chem Soc* **2008**, *130*, 15203.

(56) Ziqubu, N.; Ramasamy, K.; Rajasekhar, P. V. S. R.; Revaprasadu, N.; O'Brien, P. *Chem Mater* **2010**, *22*, 3817.

(57) Shen, H.; Wang, H.; Chen, X.; Niu, J. Z.; Xu, W.; Li, X. M.; Jiang, X.-D.; Du, Z.; Li, L. S. *Chem Mater* **2010**, *22*, 4756.

(58) Wang, Y.; Dai, Q.; Zou, B.; Yu, W. W.; Liu, B.; Zou, G. *Langmuir* **2010**, *26*, 19129.

(59) McDowell, M.; Wright, A. E.; Hammer, N. I. *Materials* **2010**, *3*, 614.

(60) Xiao, Q.; Weng, D.; Yang, Z.; Garay, J.; Zhang, M.; Lu, Y. *Nano Res.* **2010**, *3*, 685.

(61) Hanrath, T.; Veldman, D.; Choi, J. J.; Christova, C. G.; Wienk, M. M.; Janssen, R. A. *ACS Appl Mater Interfaces* **2009**, *1*, 244.

(62) Dai, Q.; Wang, Y.; Zhang, Y.; Li, X.; Li, R.; Zou, B.; Seo, J.; Liu, M.; Yu, W. W. *Langmuir* **2009**, *25*, 12320.

(63) Sykora, M.; Koposov, A. Y.; McGuire, J. A.; Schulze, R. K.; Tretiak, O.; Pietryga, J. M.; Klimov, V. I. *Acs Nano* **2010**, *4*, 2021.

(64) Johnson, J. A.; Saboungi, M.-L.; Thiyagarajan, P.; Csencsits, R.; Meisel, D. *The Journal of Physical Chemistry B* **1998**, *103*, 59.

(65) Dwivedi, C.; Shah, C. P.; Singh, K.; Kumar, M.; Bajaj, P. N. *Journal of Nanotechnology* **2011**, *2011*.

(66) Chen, Z.; Shen, Y.; Xie, A.; Zhu, J.; Wu, Z.; Huang, F. *Cryst Growth Des* **2009**, *9*, 1327.

(67) Stroyuk, A. L.; Raevskaya, A. E.; Kuchmiy, S. Y.; Dzhagan, V. M.; Zahn, D. R. T.; Schulze, S. *Colloids and Surfaces A: Physicochemical and Engineering Aspects* **2008**, *320*, 169.

(68) Mehta, S. K.; Chaudhary, S.; Kumar, S.; Bhasin, K. K.; Torigoe, K.; Sakai, H.; Abe, M. *Nanotechnology* **2008**, *19*.

(69) Gates, B.; Mayers, B.; Cattle, B.; Xia, Y. *Adv Funct Mater* **2002**, *12*, 219.

(70) Jeong, U.; Xia, Y. *Adv Mater* **2005**, *17*, 102.

(71) Zhang, Y.; Wang, J.; Zhang, L. *Langmuir* **2010**, *26*, 17617.

(72) Ueda, A.; Wu, M.; Aga, R.; Meldrum, A.; White, C. W.; Collins, W. E.; Mu, R. *Surface and Coatings Technology* **2007**, *201*, 8542.

(73) Raevskaya, A. E.; Stroyuk, A. L.; Kuchmiy, S. Y.; Dzhagan, V. M.; Zahn, D. R. T.; Schulze, S. *Solid State Commun* **2008**, *145*, 288.

(74) Singh, S. C.; Mishra, S. K.; Srivastava, R. K.; Gopal, R. *The Journal of Physical Chemistry C* **2010**, *114*, 17374.

(75) Goldbach, A.; Saboungi, M.-L. *Accounts Chem Res* **2005**, *38*, 705.

(76) Goldbach, A.; Iton, L. E.; Saboungi, M.-L. *Chem Phys Lett* **1997**, *281*, 69.

(77) Goldbach, A.; Iton, L. E.; Grimsditch, M.; Saboungi, M.-L. *Chem Mater* **2004**, *16*, 5107.

(78) Lee, D. C.; Pietryga, J. M.; Robel, I.; Werder, D. J.; Schaller, R. D.; Klimov, V. I. *J Am Chem Soc* **2009**, *131*, 3436.

(79) Warner, J. H.; Tilley, R. D. *Nanotechnology* **2006**, *17*, 3745.

(80) Codoluto, S. C.; Baumgardner, W. J.; Hanrath, T. *Crystengcomm* **2010**, *12*, 2903.

(81) Leubner, I. H. *Precision crystallization : theory and practice of controlling crystal size*; CRC Press/Taylor & Francis: Boca Raton, 2010.

(82) Glicksman, M. E. *Principles of solidification : an introduction to modern casting and crystal growth concepts*; Springer Verlag: New York, 2011.

(83) A. Feltz, A. *Amorphous and Vitreous Non-organic Solids*; "Mir" Publ.: Moscow, 1986.

(84) Huber, C. A.; Huber, T. E. *J Appl Phys* **1988**, *64*, 6588.

(85) Tutihasi, S.; Chen, I. *Physical Review* **1967**, *158*, 623.

(86) Tutihasi, S.; Chen, I. *Solid State Commun* **1967**, *5*, 255.

(87) Gobrecht, H.; Tausend, A. *Proceedings of the International Conference on the Physics of Semiconductors, p.1189;* Academic Press Inc.: New York, 1965.

(88) Caywood, John. (1969). *Optical and Electric Properties of a-Selenium*. (Doctoral Dissertation). Retrieved from Internet.

(89) Minaev, S. ; Timoshenkov, S. P.; Kalugin, V. V. *J. Optoelectron. Adv. Mater.* **2005**, *7(4)*, 1717.

(90) Minaev, V. S. *J Optoelectron Adv M* **2001**, *3*, 233.

(91) Prezhdo, O. V.; Kamat, P. V.; Schatz, G. C. *The Journal of Physical Chemistry C* **2011**, *115*, 3195.

(92) Kamat, P. V. *The Journal of Physical Chemistry Letters* **2010**, *1*, 520.

(93) Kamat, P. V. *The Journal of Physical Chemistry Letters* **2011**, *2*, 242.

Chapter 4 Surface Enhanced Raman Spectroscopy of PbS QDs

4.1 Introduction

Considerable interest has been found in examining the size dependence of semiconductor quantum dots (QDs).[1,2] When the radius of a spherically shaped semiconductor particle is reduced to that of the semiconductor Bohr radius or less, the valence and conduction bands are known to split into narrower bands due to quantum confinement effects. These bands are shown to mimic those of still smaller atoms. The energies of the resulting levels are known to be strongly size dependent. When a molecule is adsorbed on the surface of a QD, there is the possibility of charge-transfer transitions between the molecule and semiconductor, and it is expected that the spectroscopic location of these transitions will also be size dependent. Indeed a size dependent charge-transfer transition has been identified for 4-mercaptopyridine (4-Mpy) and 4-mercaptobenzoic acid (4-Mba) on ZnO QDs.[3] The charge-transfer nature of this transition was later confirmed using Ag-assisted *p*-aminothiophenol on ZnO QDs.[4] In all three cases, the size at which resonance was observed was about 28 nm, and was attributed to a likely surface-bound exciton-acceptor complex near the QD surface.[5] The size at which this resonance was observed, however, is far larger than that of the exciton Bohr radius, which in ZnO is less than 2 nm, so that quantum confinement effects are probably not involved. It would be of considerable interest to examine size dependent charge-transfer resonances in the vicinity of the Bohr radius. However, in ZnO the difficulties of controlling the QD size for small particles preclude a careful size dependent study. We therefore have turned our attention to lead sulfide (PbS), which has a much larger exciton Bohr radius (18 nm),[6] with a considerably smaller bandgap (0.41 eV) as well. We are thus easily able to synthesize QDs in this range, with relatively monodisperse distributions.

In this way, we are able to explore the effect of increasing quantum confinement on charge-transfer in these systems.

In a recent work, electron injection from colloidal PbS nanoparticles to TiO_2 nanoparticles has been observed as a function of particle size.[7] In a similar system, charge-transfer between PbS and TiO_2-nanobelts was measured.[8] Size dependent optical properties on PbS QDs have also been examined.[9] They found that smaller QDs display more efficient charge-transfer in that system. Size dependent optical nonlinearities in PbS QDs have been shown to be associated with photoexcited free carriers.[10] In this study we examine the charge-transfer resonance between 4-Mpy and size selected PbS QDs in the diameter range of 5.0–10.2 nm. The Raman spectrum of the molecule is followed, and lines are chosen, which are markers for charge-transfer. The degree of charge-transfer is then obtained as a function of particle size as well as excitation wavelength.

4.2 Experimental

Chemicals

$PbCl_2$ (99.999%) and oleylamine (OLA, 80%–90%) were purchased from Sigma-Aldrich. Methanol and hexanes were purchased from Fisher Scientific. The other chemicals were all analytical grade without further purification.

Sample preparation

The PbS QDs synthesis is based on the previously reported hot injection methods.[9, 11, 12] One (1.0) mmol $PbCl_2$ and 5 mL OLA were introduced to a three neck round-bottom flask at

room temperature. The mixture was magnetically stirred and heated to 100°C under vacuum for 60 min. to form a special Pb-OLA complex. Then, the mixture was kept under nitrogen at 100°C for another 5 min. A solution of 0.67 mmol sulfur in 2.5 mL OLA (preheated at 80°C under vacuum for 30 min.) was quickly injected into the above Pb-OLA complex solution. The resulting mixture was rapidly heated to 210°C and aged at that temperature for 5 min. Cold hexanes were added to the solution to quench the reaction, and then the solution was centrifuged to remove excess $PbCl_2$. The supernatant was transferred to another centrifuge tube. Minimum amount of methanol was added to precipitate PbS QDs. The resulting precipitate was redispersed in hexanes. Various sizes of the PbS QDs were obtained by carrying various batches of the synthesis at a variety of growth time of 10, 20, 40, 60, and 120 min., respectively.

The samples for Raman measurement were prepared as follows: 5 mL of the above PbS dispersion was introduced to an Erlenmeyer flask, and then 5 mL of 4-Mpy (0.1 M) methanol solution was added. The mixture was stirred for 12 h at room temperature to change the capping ligand of PbS QDs from OLA to 4-Mpy. Then the mixture was centrifuged and rinsed once more with distilled water. The purified PbS QDs capped with 4-Mpy were redispersed into 20 mL methanol solution. 10 μL of the above PbS-4-Mpy dispersion was dropped onto a silicon wafer. It was spread into a circle of about 2 cm in diameter. After solvent evaporation, Raman measurements were taken on these samples.

Instruments

X-ray diffraction (XRD) patterns of the resulting PbS particles were recorded on a Bruker D8 Advanced X-ray diffractometer using Cu Kα radiation (λ = 0.1542 nm). The morphologies of samples were observed by transmission electron microscope (TEM, JEM-2100) and scanning

electron microscope (LEO-1550, 5 kV) equipped with an energy dispersive X-ray spectrometer (EDS). The Raman spectra of 4-Mpy on PbS QDs were investigated at the excitation wavelengths of 488.0 nm and 514.5 nm, obtained from an Ar+ laser (Spectra Physics), at 632.8 nm, obtained from a He/Ne laser (Melles Griot), and at 785 nm, obtained from a diode laser. To ensure the obtained spectra were comparable, the settings, including the lasers power and exposure time, were all the same. The silicon line at 520 nm was used to calibrate the observed wavenumbers, and the background was subtracted from the Raman spectrum for the intensity measurements.

4.3 Results and Discussion

XRD pattern of the resulting PbS QDs is illustrated in Figure 4.1. 2θ values of the major peaks located in the range from 20° to 80° correspond to the characteristic diffraction of PbS,[12, 13] verifying the presence of PbS only. The TEM image of the obtained PbS QDs (8.2 nm) is shown in Figure 4.2, in which PbS QDs show a relatively monodisperse distribution with an average diameter of 8.2±1.0 nm. The insert shows the fast Fourier transform image of PbS QDs, confirming the crystallinity of PbS particles. The sizes and TEM images of other five sized PbS QDs can be seen in Table 4.1 and Figure 4.3. The sizes and size distributions (standard deviation) of the PbS QDs were measured from TEM images using *i*TEM 5.1 of Olympus Soft Imaging Solutions GmbH. A minimum of 120 QDs were counted on each image to obtain the average diameter of the PbS QDs.

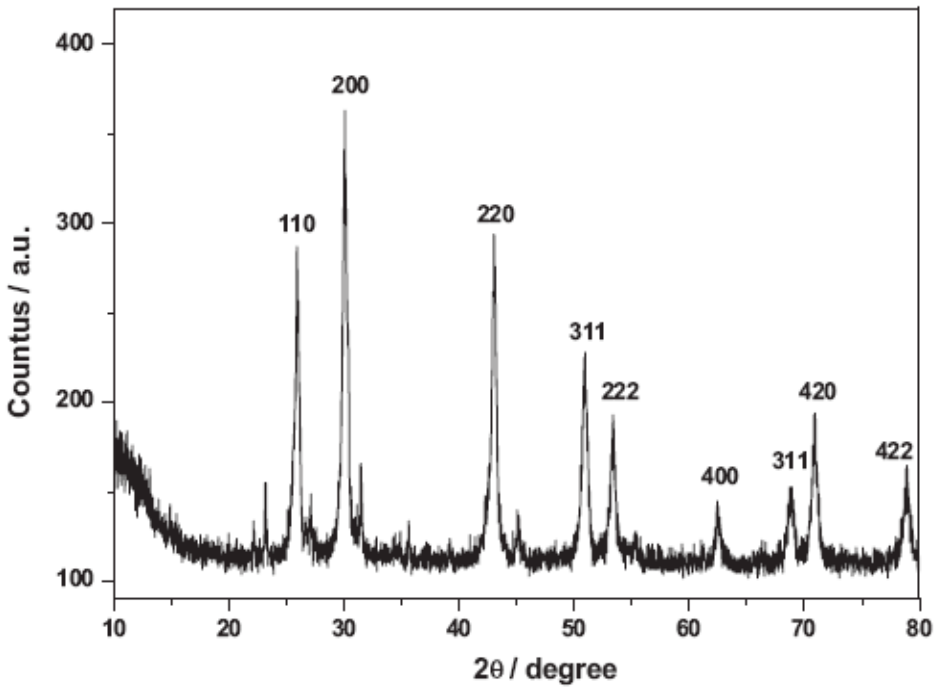

Figure 4.1 XRD of the resulting PbS QDs.

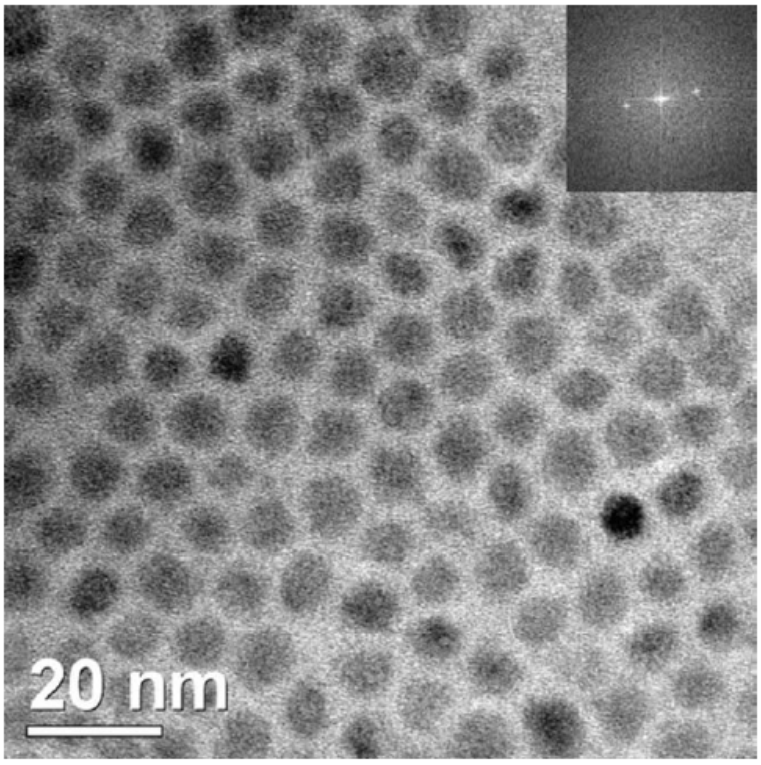

Figure 4.2 TEM image of PbS QDs sample d. Average size is 8.2 nm.

Table 4.1 Average Sizes of PbS QDs Synthesized

Sample	Average size (nm)	Growth Time (min.)
(a)	5.0±0.5	5
(b)	6.1±0.6	10
(c)	7.3±0.8	20
(d)	8.2±1.0	40
(e)	8.9±0.9	60
(f)	10.2±1.2	120

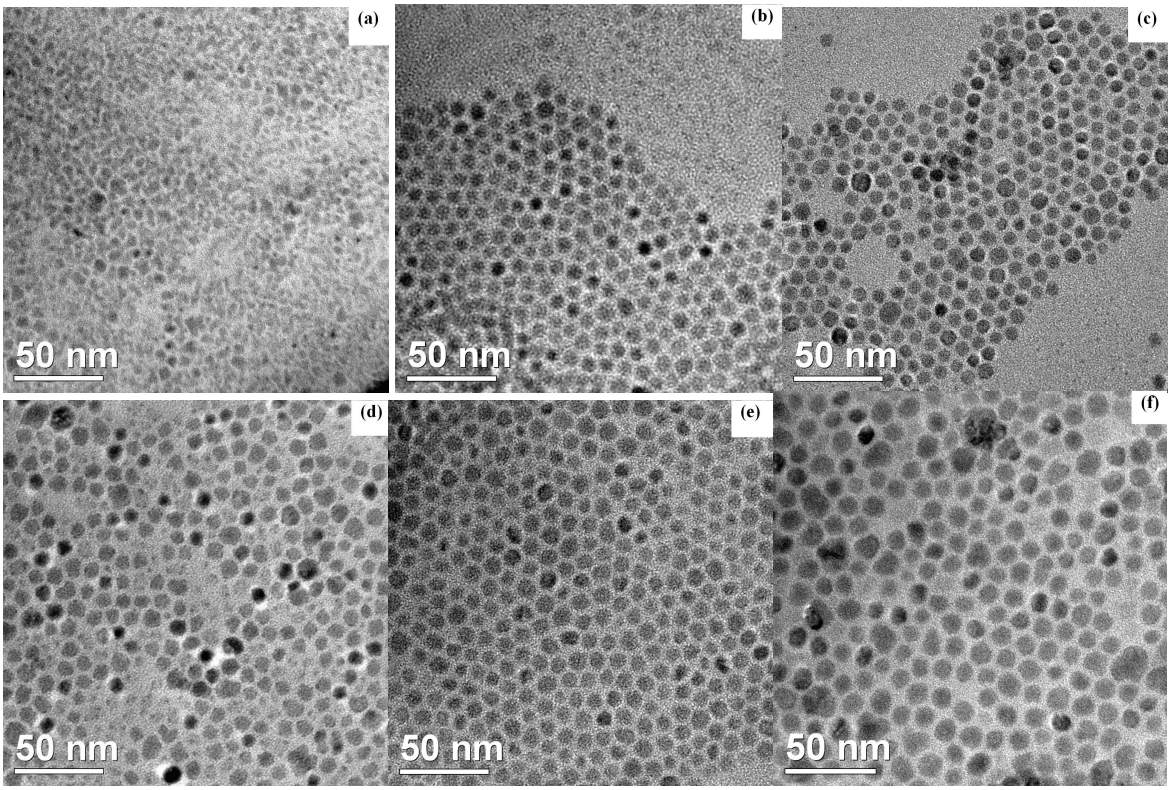

Figure 4.3 TEM images and sizes (Figure 4.3a-4.3f) of PbS QDs: (a) 5.0 ± 0.5 nm, (b) 6.1 ± 0.6 nm, (c) 7.3 ± 0.8 nm (d) 8.2 ± 1.0 nm (e) 8.9 ± 0.9 nm (f) 10.2 ± 1.2 nm.

In Figure 4.4 we display a comparison of the Raman spectrum of 4-Mpy powder with that of 4-Mpy adsorbed on the PbS QDs (8.9 nm diameter). It is clear that the Raman signals of 4-Mpy adsorbed on PbS QDs is considerably different and considerably enhanced compared to that of 4-Mpy powder, since the observed enhanced Raman signal is from a monolayer of 4-Mpy on PbS surfaces.[14-16] In Table 4.2 we list the wavenumber measurements of the observed lines as well as those from previous work.[17-21] It can be seen that the spectrum of 4-Mpy on the QDs resembles that of the powder spectrum, with some shifts in frequency, but more importantly, severe differences in relative intensity. This is similar to surface-enhanced Raman spectroscopy (SERS), which is normally carried out on a metal surface. For comparison in Table 4.2, we list the observed SERS spectrum of 4-Mpy on a Ag electrode at −0.8 V (versus SCE). In Figure 4.4, the most serious differences are the large enhancement of the lines at 1278 and 1586 cm^{-1}, which are considerably weaker in the powder spectrum. Other notable enhancements are observed at 780 and 682 cm^{-1}, which are also quite weak in the powder spectrum. The first two lines are, in fact, the most intense in the spectrum of 4-Mpy on the PbS surface while the latter two are at least comparable in intensity to the other lines of the spectrum. Referring to the assignments of the bands it can be seen that the first two lines are assigned to b_2 symmetry, while the latter two are of b_1 symmetry. Many of the totally symmetric a_1 modes are seen to be either suppressed or reduced in relative intensity on the PbS surface. These observations are characteristic of surface enhancement, and are taken to be signs of strong charge-transfer contributions to the enhancement factor.[22]

Table 4.2 Spectral lines and assignments of 4-Mpy observed bands

Assignment[a]	Symmetry[a]	Wang, Rothberg[a]	Powder[b]	SERS −0.8V[c]	PbS 514.5 nm[b]
					1645
8a	a_1	1620	1615	1605	1623
8b	b_2	1580	1587	1576	1586
					1499
19a	a_1	1470	1467	1463	1464
14	b_2		1396	1373	
3	b_2	1287–1318	1291		1278
ip-NH def		1250			1232
9	a_1	1220		1213	1216
9 NH^+	a_1	1206	1197	1195	
12 C=S	a_1	1099	1107	1096	1107
18	a_1	1030–1050	1041	1051	1037
1	a_1	1013	989		1009
4	b_1	760	785		780
6	a_1	720	721	713	
11 C–H oop	b_1	700			682

[a] Columns 1–3 are the assignments of Wang and Rothberg[14] obtained by analogy with the benzene spectrum. They are also consistent with those of benzene thiol[20]

[b] Columns 4 and 6 are from this work (see Figure 4.4).

[c] Column 5 is the SERS on Ag electrode from Chao[17] *et al.*

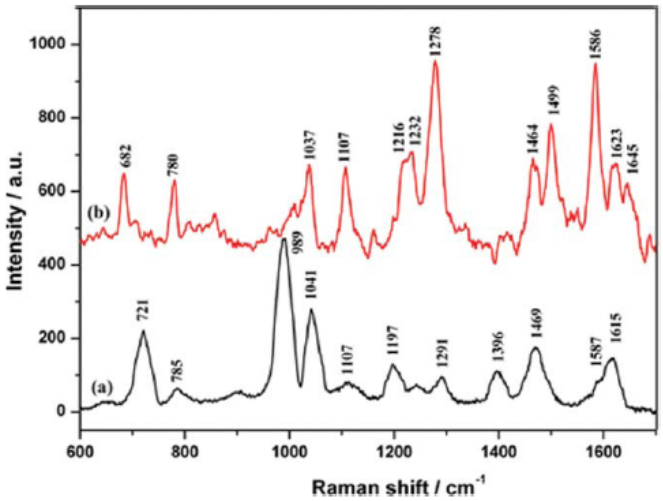

Figure 4.4 (a) Comparison of the Raman spectrum of 4-Mpy powder (b) with that of 4-Mpy adsorbed on a 8.9 nm PbS QD. Excitation is at 514.5 nm.

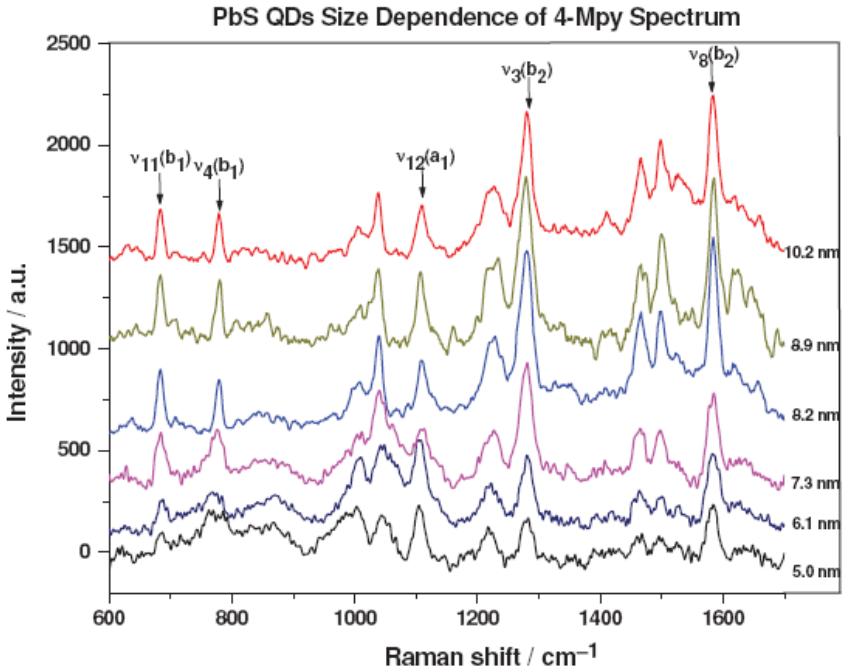

Figure 4.5 Raman spectra of 4-Mpy on PbS QDs of sizes from 5.0 to 10.2 nm.

In Figure 4.5 we show the Raman spectra of 4-Mpy on PbS QDs of various sizes between 5.0 and 10.2 nm in diameter. The arrows mark the normal modes at 682 (ν11, b_1), 780 (ν4, b_1), 1107 (ν12, a_1), 1278 (ν3, b_2) and 1586 cm^{-1} (ν8, b_2), which will be used for analysis. Note that as the particle diameter grows, the Raman intensity increases, until a maximum is reached at 8.9 nm, then decreases (the baselines of each spectrum are offset to increase clarity). We are primarily interested in measuring the degree of charge-transfer in each spectrum. For that we require the ratio (R) of intensity of a non-totally symmetric line either the b_1 or b_2 lines to that of a totally symmetric line a_1. We choose totally symmetric lines (a_1) as a reference since they are not sensitive to charge-transfer effect. They derive most of their intensity from Franck–Condon factors (the Albrecht A-Term), while the non-totally symmetric lines are derived from vibronic coupling (B-Terms) which are highly sensitive to charge-transfer contributions to the

enhancement.[19] Use of the ratio also has the advantage of making our measure of charge-transfer independent of other effects on the total enhancement factor. The degree of charge-transfer, [4, 18] (p_{CT}) is then defined as:

$$p_{CT} = \frac{R}{1+R} \tag{1}$$

When R is zero, there is presumably no charge-transfer ($p_{CT} = 0$), while for large R, the degree of charge-transfer approaches 1. In Figure 4.6 we show the results of determination of the degree of charge-transfer as a function of quantum dot size, using the ratios of intensities of the four non-totally symmetric lines (ν11, ν4, ν3, ν8) to the totally symmetric line (ν12). Note that the p_{CT} goes through a resonance at the particle size around 8.2 nm.

We have chosen the ν12 (a_1) line as a reference because it is fairly intense and relatively isolated from interference with nearby lines. The other totally symmetric (a_1) possibilities are the ν9 line, which is strongly overlapped by the NH in-plane deformation, while the ν18 line at 1037 cm^{-1} or the ν19a line at 1464 cm^{-1} are similarly overlapped. Nevertheless we tried to subtract out the nearby lines and obtained cruder results, which also showed resonances at approximately the same particle size (8.2 nm), but the results were not deemed sufficiently reliable to present.

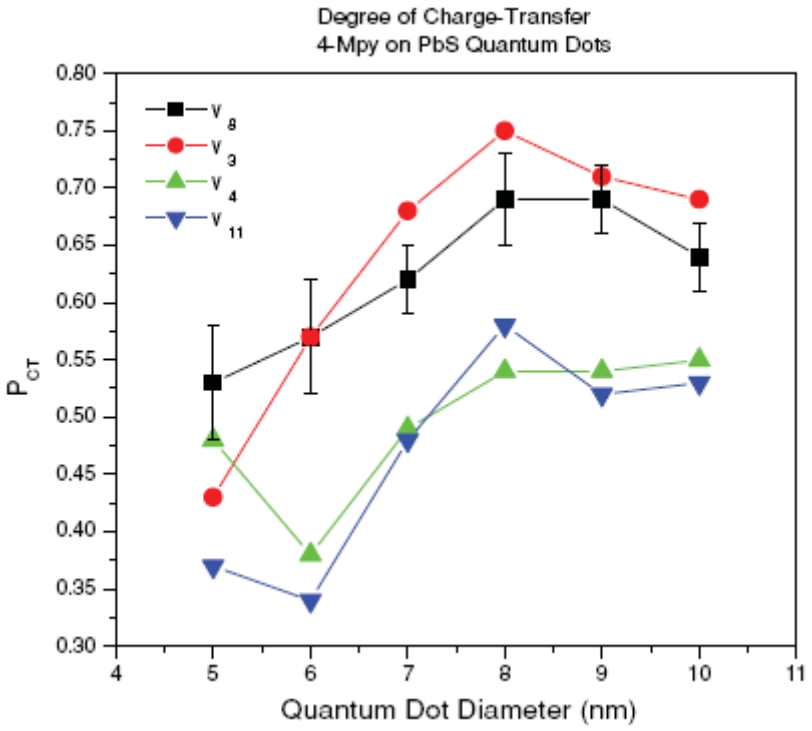

Figure 4.6 Degree of charge-transfer (p_{CT}) as a function of PbS QDs diameter. The black and red points are for ratios of the b_2 lines (ν8 and ν3) while the green and blue points are for the b_1 lines (ν4 and ν11).

Using the particle size at which resonance occurs (8.2 nm), we have also obtained the excitation profiles of 4-Mpy using several laser lines at 488, 514.5, 632.8, and 785 nm (see Figure 4.7). Plots of the excitation profiles are illustrated in Figure 4.7 (b_1 lines) and (b_2 lines) in the right hand inset. With so few points a pattern is difficult to discern, except to note that the charge-transfer resonances are most likely centered around 525 nm. This is confirmed by fitting the profiles to a Gaussian curve using energy as the abscissa.

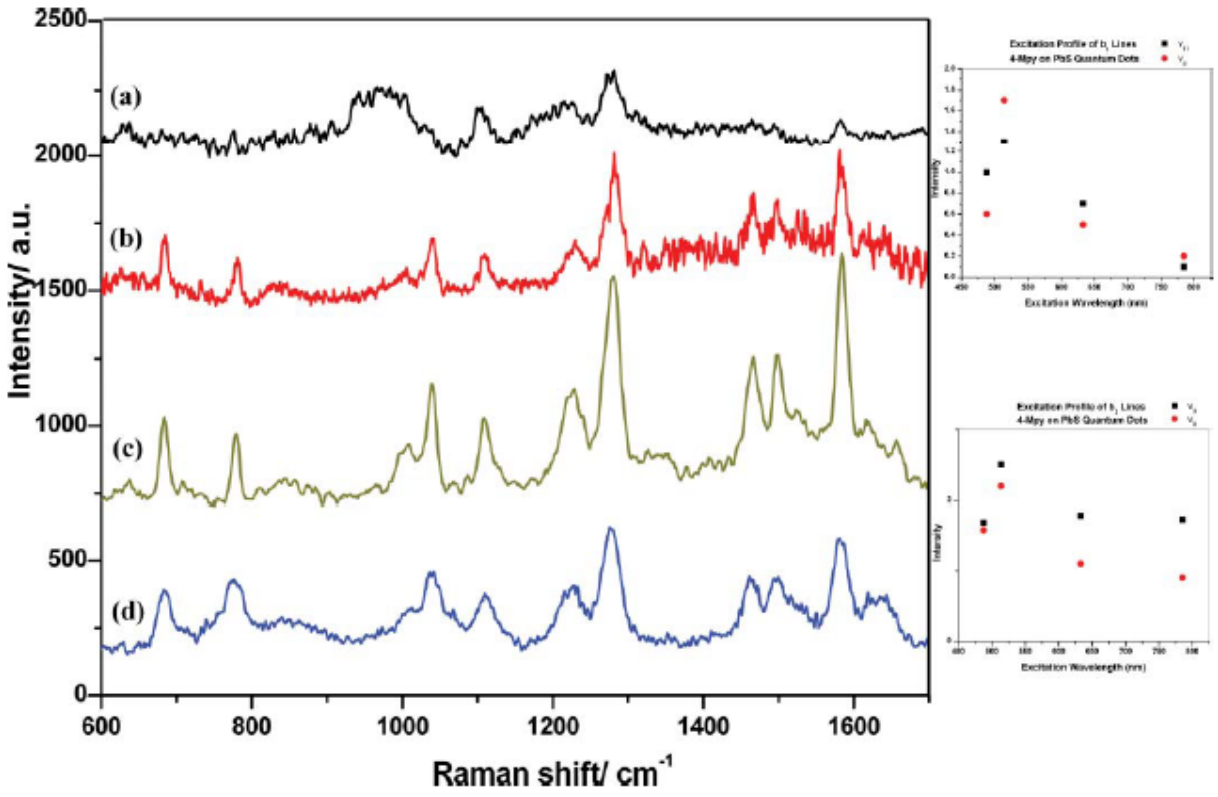

Figure 4.7 Raman spectra of 4-Mpy on 8.2 nm PbS QDs at various excitation wavelengths: (a) 785 nm, (b) 632.8 nm, (c) 514.5 nm, and (d) 488 nm. On the right are excitation profiles of the non-totally symmetric lines of 4-Mpy on PbS QDs: (a) is for b_1 modes, while (b) is for b_2 modes.

These results indicate that charge-transfer transitions exist between PbS QDs and 4-Mpy molecules adsorbed on the surface. By scanning the particle size and measuring degree of charge-transfer, we have shown that a maximum occurs at ~8.2 nm. Further, by scanning the excitation wavelength for the 8.2 nm particle, we obtain a maximum in the intensity of the b_1 and b_2 lines at approximately 525 nm. In order to further analyze our results, we use the functional form of the bandgap of PbS QDs as a function of particle size determined by Moreels *et al.*[9] They show that the energies can be fit to the form:

$$E_0 = 0.41 + \frac{1}{0.0252d^2 + 0.283d} \quad (2)$$

Where d is the particle diameter. We have plotted this in Figure 4.8 for particles in the range d = 2–15 nm. We have also included in the graph both the ionization potential (IP) and electron affinity (EA) of 4-Mpy, as well as the photon energies of the 488 and 514.5 nm laser lines. Note that in the range of particle sizes used in this experiment, we should expect charge-transfer from the valence band of the QDs to unfilled levels of the molecule at approximately 2.41 eV (514.5 nm). This is close to our observed resonance in excitation energy. It is also close to the size-dependent resonance observed at around 8.2 nm.

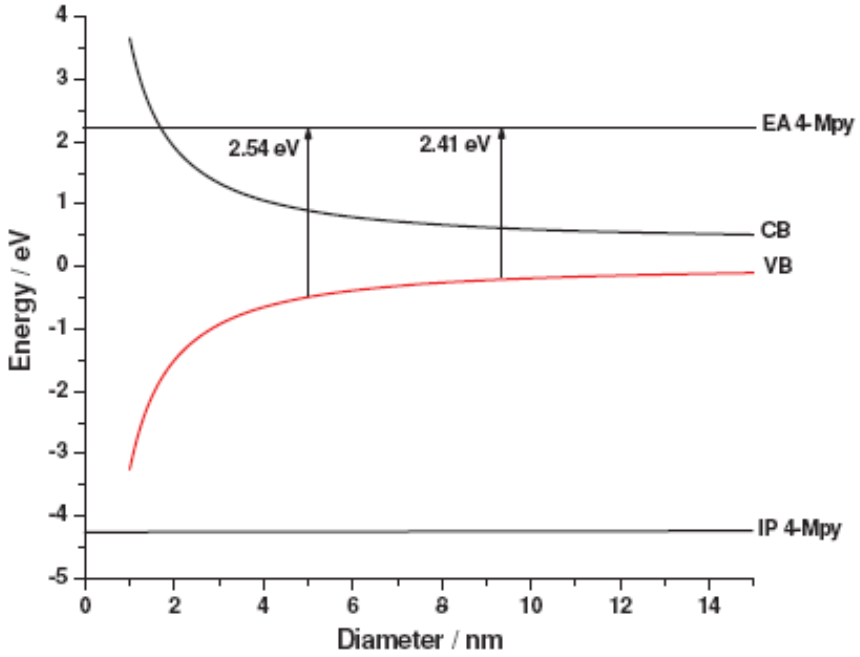

Figure 4.8 Size dependence of conduction and valence bands for PbS QDs. Also shown are the electron affinity (EA) and ionization potential (IP) of 4-Mpy, as well as the energy of the 488 nm

(2.54 eV) and 514.5 nm (2.41 eV) laser lines. The bulk bandgap of PbS is 0.42 eV. The zero of energy is at the bulk conduction band (-4.6 eV from vacuum).

4.4 Conclusion

PbS QDs SERS study demonstrates that the charge-transfer resonance accounts for the enhancement. By measuring the degree of charge-transfer, we not only validate the size dependence of PbS QDs quantum confinement effect, which has a maximum of degree of charge-transfer at ~8.2 nm, but also show the wavelength dependence of PbS QDs quantum confinement effect, which generates maximum intensity at 525 nm with PbS QDs of 8.2 nm. The quantum confinement effects of PbS QDs are both size dependence and wave length dependence where charge-transfer plays an important role for the enhancement.

4.5 Chapter 4 Reference

(1) Brus, L. *The Journal of Physical Chemistry* **1986**, *90*, 2555.

(2) Klein, M. C.; Hache, F.; Ricard, D.; Flytzanis, C. *Phys Rev B* **1990**, *42*, 11123.

(3) Sun, Z.; Zhao, B.; Lombardi, J. R. *Appl Phys Lett* **2007**, *91*, 221106.

(4) Richter, A. P.; Lombardi, J. R.; Zhao, B. *J Phys Chem C* **2010**, *114*, 1610.

(5) Fonoberov, V. A.; Balandin, A. A. *Appl Phys Lett* **2004**, *85*, 5971.

(6) Machol, J. L.; Wise, F. W.; Patel, R. C.; Tanner, D. B. *Phys Rev B* **1993**, *48*, 2819.

(7) Hyun, B.-R.; Zhong, Y.-W.; Bartnik, A. C.; Sun, L.; Abruña, H. D.; Wise, F. W.; Goodreau, J. D.; Matthews, J. R.; Leslie, T. M.; Borrelli, N. F. *Acs Nano* **2008**, *2*, 2206.

(8) Wang, D.; Zhao, H.; Wu, N.; El Khakani, M. A.; Ma, D. *The Journal of Physical Chemistry Letters* **2010**, *1*, 1030.

(9) Moreels, I.; Lambert, K.; Smeets, D.; De Muynck, D.; Nollet, T.; Martins, J. C.; Vanhaecke, F.; Vantomme, A.; Delerue, C.; Allan, G.; Hens, Z. *Acs Nano* **2009**, *3*, 3023.

(10) Neo, M. S.; Venkatram, N.; Li, G. S.; Chin, W. S.; Wei, J. *The Journal of Physical Chemistry C* **2009**, *113*, 19055.

(11) Joo, J.; Na, H. B.; Yu, T.; Yu, J. H.; Kim, Y. W.; Wu, F.; Zhang, J. Z.; Hyeon, T. *J Am Chem Soc* **2003**, *125*, 11100.

(12) Cademartiri, L.; Bertolotti, J.; Sapienza, R.; Wiersma, D. S.; von Freymann, G.; Ozin, G. A. *The Journal of Physical Chemistry B* **2005**, *110*, 671.

(13) Wang, S.; Pan, A.; Yin, H.; He, Y.; Lei, Y.; Xu, Z.; Zou, B. *Mater Lett* **2006**, *60*, 1242.

(14) Song, W.; Wang, Y.; Hu, H.; Zhao, B. *J Raman Spectrosc* **2007**, *38*, 1320.

(15) Wang, Y.; Sun, Z.; Hu, H.; Jing, S.; Zhao, B.; Xu, W.; Zhao, C.; Lombardi, J. R. *J Raman Spectrosc* **2007**, *38*, 34.

(16) Fu, X.; Bei, F.; Wang, X.; Yang, X.; Lu, L. *J Raman Spectrosc* **2009**, *40*, 1290.

(17) Wang, Z.; Rothberg, L. J. *The Journal of Physical Chemistry B* **2005**, *109*, 3387.

(18) Chao, Y.; Zhou, Q.; Li, Y.; Yan, Y.; Wu, Y.; Zheng, J. *The Journal of Physical Chemistry C* **2007**, *111*, 16990.

(19) Lim, J. S.; Choi, H.; Lim, I. S.; Park, S. B.; Lee, Y. S.; Kim, S. K. *The Journal of Physical Chemistry A* **2009**, *113*, 10410.

(20) Baldwin, J. A.; Vlc□ková, B.; Andrews, M. P.; Butler, I. S. *Langmuir* **1997**, *13*, 3744.

(21) Hu, J.; Zhao, B.; Xu, W.; Li, B.; Fan, Y. *Spectrochimica Acta Part A: Molecular and Biomolecular Spectroscopy* **2002**, *58*, 2827.

(22) Lombardi, J. R.; Birke, R. L. *The Journal of Physical Chemistry C* **2008**, *112*, 5605.

Chapter 5 Raman Spectroscopy of Se Nanoclusters and Se QDs

5.1 Introduction

The size of the Se nanoclusters synthesized in chapter 3 is very small. It is just too close to the boundary of amorphous and crystalline Se and makes the characterization difficult because selenium is very sensitive to photo and thermal stimulation and undertake rapid phase transitions.[1-2] Among the characterization methods for Se QDs, XRD may be the best tool because during the measurement there is almost no energy transferred to the samples. However, the size of the Se nanoclusters we synthesized is beyond the measurement of the XRD instrument. HRTEM and TEM measurements may induce phase transitions of Se. For example, it is very difficult to snap a high quality HRTEM image of Se nanoclusters using HRTEM. The strong electron beams at high voltage "burn" the Se very frequently in a short time. HRTEM is possible to prompt the transformation of amorphous Se (a-Se) to crystalline Se under such a high energy. To clarify these uncertainties for the structure elucidation of Se nanoclusters, we need to find an alternative characterization method. Raman spectroscopy is that alternative. It uses a non-destructive approach. Besides, each forms of Se have Raman spectra with distinguished absorbance peaks.

Photo-induced Se structure changes were reported by Roy's group[1] in 1998. They observed the ring to chain conversion of a-Se using the 488 nm excitation wavelength. Lukács group[3] recently observed the photo-induced structural changes, which are reversible after relaxation, in a-Se using the 785 nm excitation wavelength. Tallman group also reported the photo-crystallization of a-Se, which is an irreversible process, using the excitation 633 nm wavelength.[4-5] Our study of the Se nanoclusters and Se QDs synthesized reveals that crystalline

m-α-Se_8 also undergo the laser stimulated, photo-induced reversible structure changes at certain energy level under the laser illumination of the 785 nm excitation wavelength; while these Se QDs carry out the irreversible changes under the laser illumination of either the 488 nm or the 633 nm excitation wavelength. The reversible phase transformation of Se nanoclusters first observed by us may bring new applications for Se QDs. Se QDs may be used as storage media since the reversible phase changes mimic the on and off storage process of the memory card of the computer devices.

5.2 Experimental

Chemicals

Selenium (Se, 99.5%, powder, 200 mesh, t-Se), 1-octadecene (ODE, 90%), acetone (99.9%), 1-tetradecene (TDE, 94%), and n-hexane (99+%) were purchased from ACROS Organic. Se nanoclusters (m-α-Se_8), Se QDs (m-α-Se_8 and r-Se_6), and bulk m-Se were synthesized by us. All chemicals were used as received without further purification.

Instrument

Raman spectra were measured using a Bruker Senterra Raman microscope equipped with excitation wavelength of 488 nm, 633 nm, and 785 nm, a 1,200 l/mm holographic grating, a CCD detector, and adjustable laser power.

Sample preparation and measurement

The Raman samples were prepared by placing Se nanoclusters or Se QDs, or bulk t-Se, or bulk m-Se on top of a silicon wafer. Sample images were taken using the 50 X objective of the microscope. The sample Raman spectra were recorded using different excitation wavelength at varies energy levels with a variety of exposure and accumulation times.

5.3 Results and Discussion

The irreversible changes of Se nanoclusters: Se_8-Se_n, using the 633 nm excitation wavelength as laser source, are shown in Figure 5.1. The laser illumination cycle performed is as follow: the sample got a 5 s exposure with two accumulations (10 s total exposure), then 1 min. relaxation (no laser illumination on the sample). The laser always shines on the same spot of the sample. The left side image of Figure 5.1 is the image of the sample before laser illumination. The "burnt", black image (after the third laser illumination), right side of Figure 5.1 indicates that the Se crystals are changed from ring (Se_8) to chain structure (Se_n). They support the Raman spectra results shown in Figure 5.2. The top left of Figure 5.2 displays the sample spectrum after the first laser illumination, showing the typical E_1 bending of Se_8 ring at 252 cm^{-1} (only Se_8 rings exist). The top right of Figure 5.2 shows the sample spectrum after the 3rd laser illumination. The photo-induced irreversible ring to chain changes occurred. The typical A_1 stretching[6] of t-Se (Se_n chain) at 233 cm^{-1} is observed while at the same time the typical E_1 bending of Se_8 ring at 252 cm^{-1} (ring) is still presented. The bottom left of Figure 5.2 presents the sample spectrum after the 17th laser illumination. The intensity of the A_1 stretching mode of Se_n at 233 cm^{-1} become stronger while the intensity of the E_1 bending of Se_8 ring at 252 cm^{-1} become weaker. Their intensities are almost at the same level. More rings are transferred to chains. The bottom right of Figure 5.2 represents the sample spectrum after the 30th laser illumination. The intensity of the A_1 stretching mode of Se_n chain at 233 cm^{-1} continues to increase while the intensity of the E_1 bending of Se_8 ring at 252 cm^{-1} remains decreasing. Their intensities reverse order. There is more Se_8 transfer to Se_n. After 210th laser illumination (Figure 5.3), most of Se_8 become Se_n. It is known that the m-Se to t-Se phase transformation is an irreversible process. Additional Raman measurements observe no increase of the intensity of

peak at 252 cm^{-1}, only decrease. This confirms the photo-induced, irreversible m-α-Se_8 to t-Se phase transition. The laser illumination at 488 nm wavelength also induces the same irreversible phase transition.

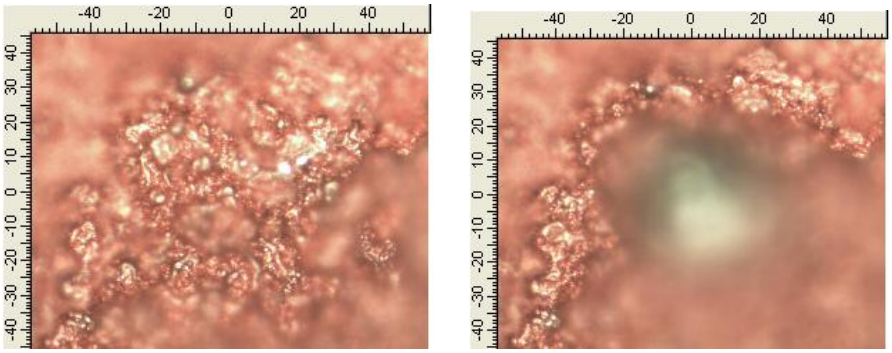

Figure 5.1 Images of Se nanoclusters irreversible phase transition at the excitation wavelength of 633 nm. The left image is taken after the first illumination. The "burnt", black image of the right side of Figure 5.1 indicates that the Se particles are changed from Se_8 ring to Se_n chain.

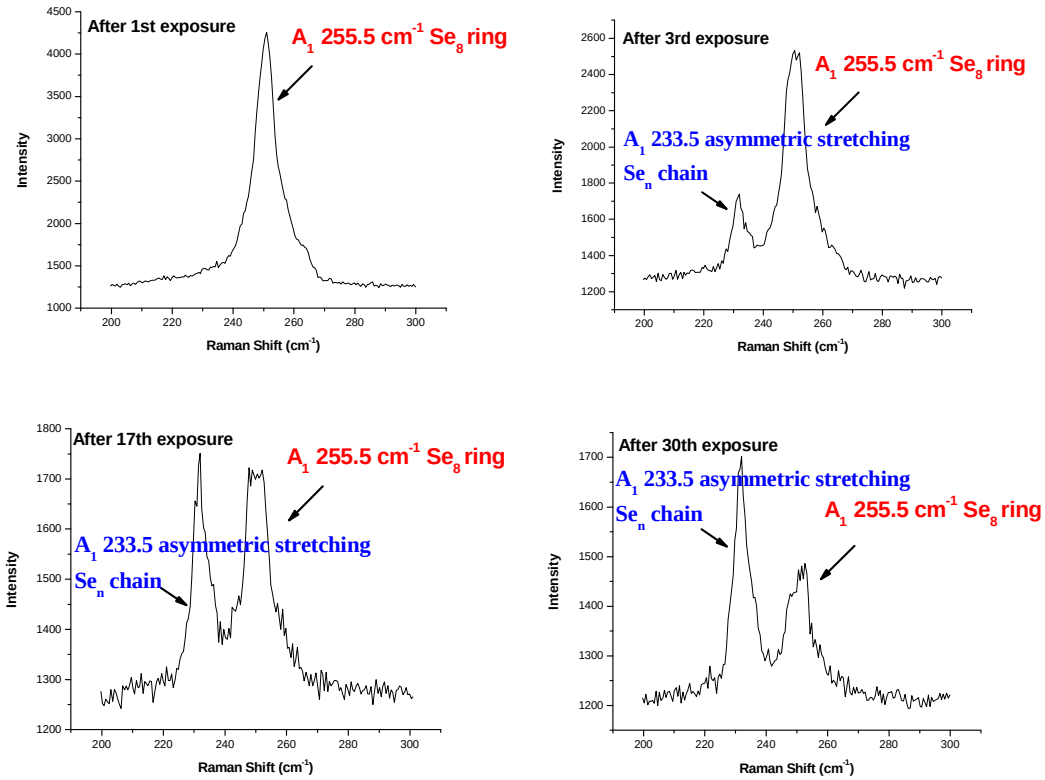

Figure 5.2 Irreversible transformations of Se nanoclusters from Se_8 to Se_n.

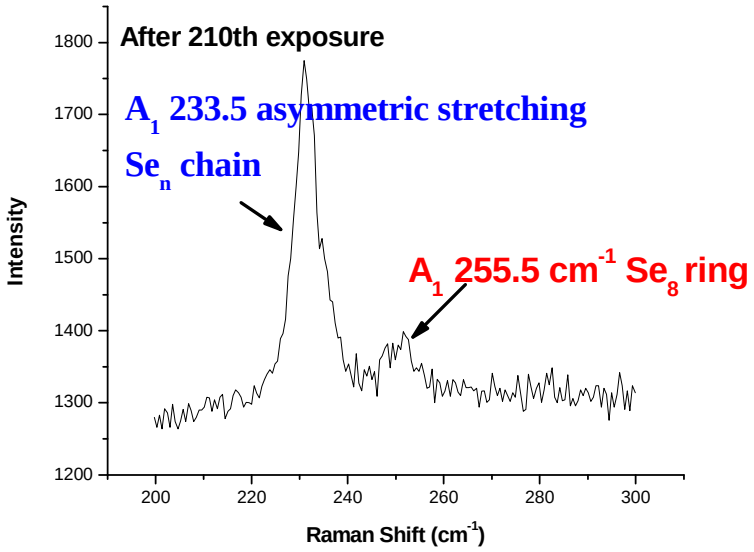

Figure 5.3 Se nanoclusters ring to chain phase transition. After long laser illumination, almost all Se nanoclusters become Se_n.

The reversible changes of Se nanoclusters Se_8-Se_n-Se_8, using the 785 nm excitation wavelength as laser source, are shown in Figure 5.4. The laser illumination cycle performed is as follow: the sample got a 1 s exposure with five accumulations (5 s total exposure), then 5 min. relaxation (no laser illumination on the sample). The laser always shines on the same spot of the sample. The left image is taken after first laser illumination. The right image is taken after the 30th laser illumination. It shows a slightly "burning" effect indicating that the Se particles are changed from Se_8 to Se_n. Figure 5.5 illustrated the whole process of the reversible phase transition: Se_8-Se_n-Se_8 under the laser illumination at the excitation wavelength of 785 nm. After the first laser illumination, Raman spectrum indicated that only ring structure (the typical ring E_1 bending of Se_8 ring at 252 cm^{-1}) existed in the Se nanoclusters (bottom spectrum of Figure 5.4). After the 35th laser illumination, Raman spectrum revealed that both ring (the

typical ring E_1 bending of Se_8 ring at 252 cm^{-1}) and (the typical chain A_1 stretching mode of Se_n at 233 cm^{-1}) structures were co-existed (middle spectrum of Figure 5.4) (Se_8-Se_n transition occurred). After the 65th laser illumination, only rings left (the typical chain A_1 stretching mode of t-Se at 233 cm^{-1}disappeared) (Se_n-Se_8 transition occurred).

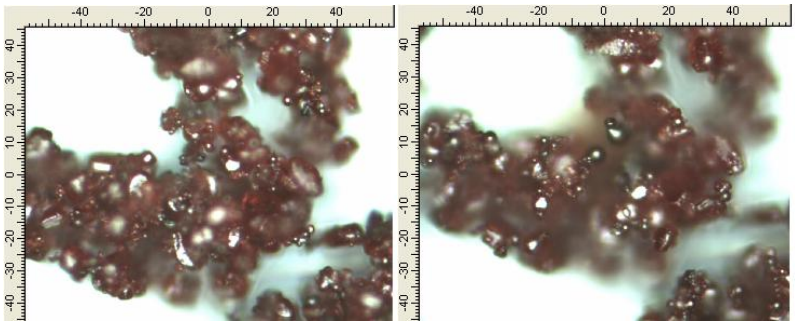

Figure 5.4 Reversible ring to chain changes of Se nanoclusters at the excitation wavelength of 785 nm. The left image is taken after first laser illumination. The right image is taken after the 30th laser illumination. It shows a slightly "burning" effect indicating that the Se particles are changed from ring (Se_8) to chain structure (Se_n).

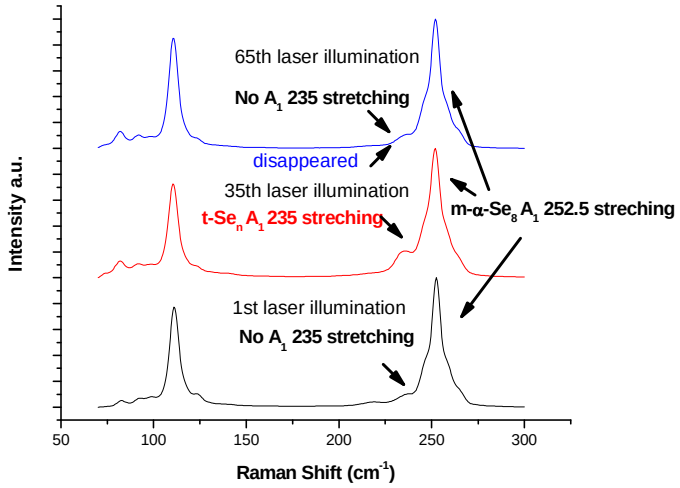

Figure 5.5 Reversible changes: Se nanoclusters phase transition of Se_8-Se_n-Se_8 under the laser illumination at the excitation wavelength of 785 nm. After the first laser illumination, Raman

spectrum indicated that only ring structure (typical ring E_1 bending of Se_8 ring at 252 cm^{-1}) existed in the Se nanoclusters (bottom spectrum). After the 35th laser illumination, Raman spectrum revealed that both ring (the typical ring E_1 bending of Se_8 ring at 252 cm^{-1}) and (the typical chain A_1 stretching mode of t-Se at 233 cm^{-1}) structures were co-existed (middle spectrum). After the 65th laser illumination, only rings left (the typical chain A_1 stretching mode of t-Se at 233 cm^{-1}disappeared).

The normal laser power used for the 633 nm excitation wavelength is 0.2 mW. Only 0.093 mW reach the sample. The normal laser power used for the 785 nm excitation wavelength is 10 mW. Only 2.3 mW reach the sample.

The reversible phase transition may be due to the partial departure of the weak alkene capping ligand and temporary break of the Se-Se bond of Se_8 ring to form Se_n chain as Lukács[5] indicated. After relaxation, the broken Se-Se reformed with the interactions of the weak capping ligand to generate the Se_8 ring again. Further investigations are necessary for better understanding the mechanism of the photo-induced reversible phase transition.

The Raman modes and results (including assigned peaks) of Se QDs (r-Se_6), Se QDs (m-α-Se_8), Se nanoclusters (m-α-Se_8), bulk m-Se, and bulk t-Se (Se_n) were shown in Figure 5.6. Raman peak positions of Se_6, Se_8, and the literature values are listed in both Table 5.1 and Table 5.2.

From the experimental results, we find that all these different Se crystal structures can be identified using Raman spectroscopy. It demonstrates that Raman spectroscopy is indeed a powerful tool for Se structure elucidation.

Table 5.1 Raman Modes of Se_6.[6-8]

Mode Symmetry	E_g	A_{1g}	E_g	A_{1g}
Calculated Se_6 (D_{3d}) (cm^{-1})	112	136	280	276
Se_6 QDs (cm^{-1})	**110**	**131**	**-**	**251**
Experimental in Bulk (cm^{-1})	102	129	221	247
Experimental in Zeloite (cm^{-1})	104, 108	135, 137	274, 274	274, 274

Table 5.2 Raman Modes of Se_8.[6, 8-11]

Mode Symmetry	E_2	E_2	A_1	E_3	A_1	E_3	E_2	E_1
Calculated Se_8 (D_{4d})	33	80	110	121	271	290	287	273
Se_8 QDs	**-**	**82**	**110.5**	**-**	**252**		**-**	
Bulk (Monoclinic)	50	84	114	128	249	239	254	254
Bulk Monoclinic	**-**	**79**	**110.5**	**124**	**255.5**		**246**	
Rb-YSe	31	79	109	130	259		272	
Sr-YSe	30	75	107	122				

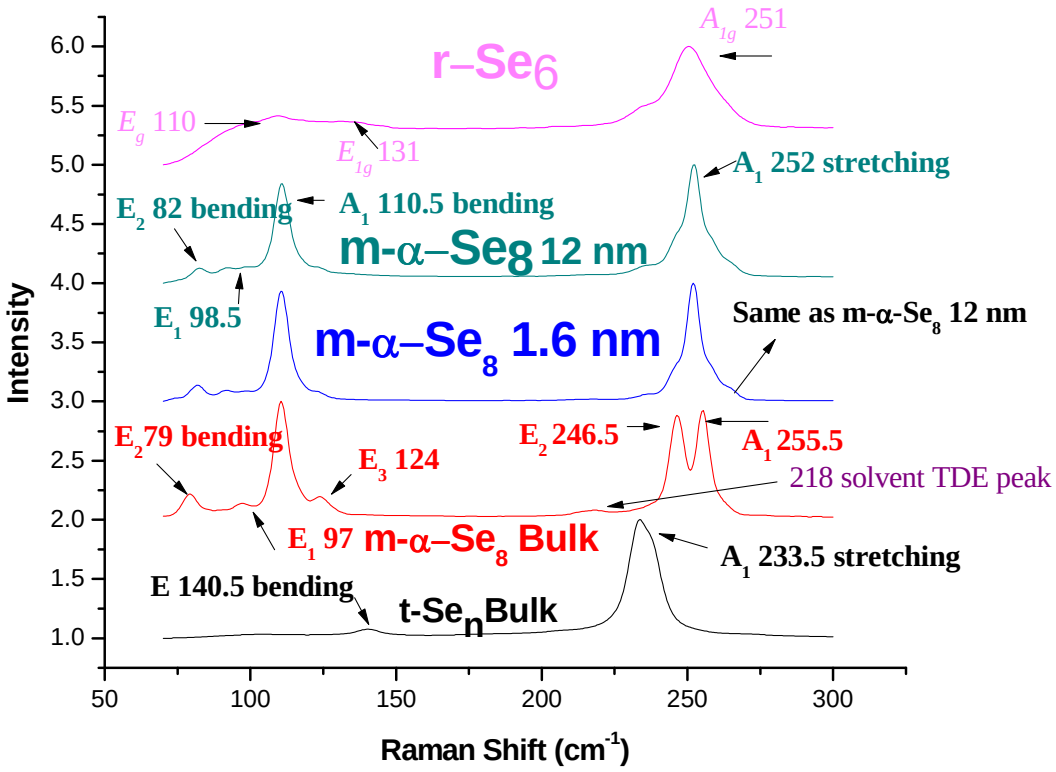

Figure 5.6 Raman spectra of Se. From top to bottom: Se QDs (r-Se_6), Se QDs (m-α-Se_8, 12 nm), Se QDs (m-α-Se_8, 1.6 nm), m-Se bulk (m-α-Se_8 bulk), and t-Se bulk (t-Se_n bulk).

5.4 Conclusion

We observed the reversible Se_8-Se_n-Se_8 phase transitions of Se nanoclusters using excitation wavelength 785 nm as laser illumination source at the power of 2.3 mM. We also revealed that using higher energy excitation wavelength; Se nanoclusters always proceed with an irreversible phase transition of Se_8-Se_n. Raman spectroscopy is a powerful tool for the structure elucidation of Se with different structures.

5.5 Chapter 5 Reference

(1) Roy, A.; Kolobov, A.V.; Oyanagi, H.; Tanaka, K. *Philosophical Magazine B* **2005**, *78 (1)*, 87-94.

(2) Kolobov, A.V. (Ed.): *Photo-Induced Metastability in Amorphous Semiconductors*; Wiley-VCH: Weinheim, 2003.

(3) Lukacs, R.; Veres, M.; Shimakawa, K.; Kugler, S. *J Appl Phys* **2010**, *107*, 073517.

(4) Tallman, R.; Weinstein, B.; Reznik, A.; Kubota, M.; Tanioka, K.; Rowlands, J. *J Non-Cryst Solids* **2008**, *354*, 4577.

(5) Tallman, R. E.; Reznik, A.; Weinstein, B. A.; Baranovskii, S. D.; Rowlands, J. A. *Appl Phys Lett* **2008**, *93*, 212103.

(6) Kohara, S.; Goldbach, A.; Koura, N.; Saboungi, M. L.; Curtiss, L. A. *Chem Phys Lett* **1998**, *287*, 282.

(7) Goldbach, A.; Iton, L. E.; Saboungi, M.-L. *Chem Phys Lett* **1997**, *281*, 69.

(8) Goldbach, A.; Saboungi, M.-L. *Accounts Chem Res* **2005**, *38*, 705.

(9) Chen, Z.; Shen, Y.; Xie, A.; Zhu, J.; Wu, Z.; Huang, F. *Cryst Growth Des* **2009**, *9*, 1327.

(10) Minaev, V. S. *J Optoelectron Adv M* **2001**, *3*, 233.

(11) Emeleus, H. J. *Advances in Inorganic Chemistry & Radiochemistry, Volume 28*, Academic Press: London, 1984.

Chapter 6 Conclusions

6.1 Summary

This research project addresses several important fields of semiconductor quantum dots, including: synthesis and characterization, synthetic application, Raman, and SERS studies of semiconductor quantum dots (Figure 6.1 is the summary of the achievement).

For the synthesis and characterization, we have successfully synthesized four kinds of monodisperse QDs: PbS, PbSe, PbTe, and Se QDs with the following major achievement:

(1) Homogeneous nucleation for the formation of nanocrystals can occur at low temperature and does not need high temperature to overcome a high energy barrier. We have obtained monodisperse PbS QDs at the nucleation and growth temperature of 45°C.

(2) Monodisperse single elemental Se QDs can be produced by simple solution crystallization from TDE (1-tetradecene) or ODE (1-octadecene).

(3) TDE is a better non-coordinating solvent compare to ODE. STDE and SeTDE are stable reagents with long storage time. They can be used as universal precursors for S-containing and Se-containing QDs.

(4) Monodisperse QDs synthesis can be carried out at low temperature and relatively short reaction time using the simple, non-injection, one-pot synthetic method.

(5) $PbCl_2$-OLA is a universal system for the synthesis of Pb-chaclogenide QDs.

For the synthetic application, energy-efficient nanocomposites and other QDs were obtained with the newly developed non-injection, one-pot method, SeTDE precursor, and $PbCl_2$-OLA system. They are MnSe QDs, ZnSe QDs, GO-PbSe QDs nanocomposites, and GO-Ag nanocomposites.

For the Raman study, we observed the reversible Se_8-Se_n-Se_8 phase transitions of Se nanoclusters using excitation wavelength 785 nm as laser illumination source at the power of 2.3 mM. We also revealed that using higher energy excitation wavelength; Se nanoclusters always proceed with an irreversible phase transition of Se_8-Se_n. In addition, we used Raman spectroscopy to determine the crystal structure of the 1.6 nm Se nanoclusters we synthesized, which cannot be characterized by X-ray diffractometer.

For SERS study, we found both size and wavelength dependent quantum confinement effects (QCEs) of PbS QDs absorbed with 4-Mpy.

6.2 Future Studies

We will focus on the following four areas as Figure 6.2 shown:

(1) Continue the SERS studies of PbSe, PbTe, and Se QDs.

(2) Synthesize other S-containing and Se-containing semiconductor QDs, nanocomposites, and energy-efficient materials using the STDE and SeTDE precursor.

(3) Study the properties of GO-QD nanocomposites and GO-Ag nanocomposites for their potential applications in the solar cell field.

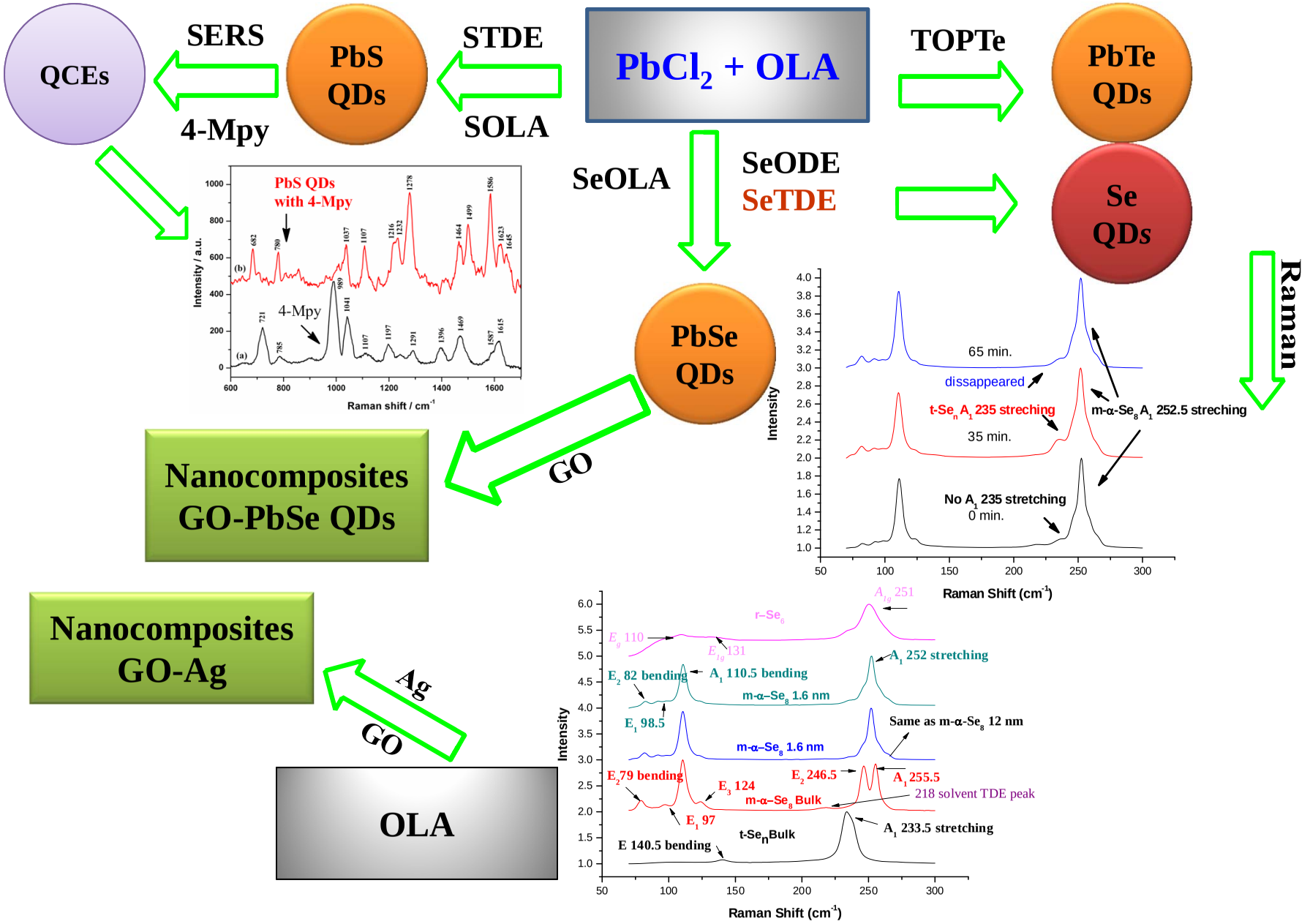

Figure 6.1 Summary of the achievement.

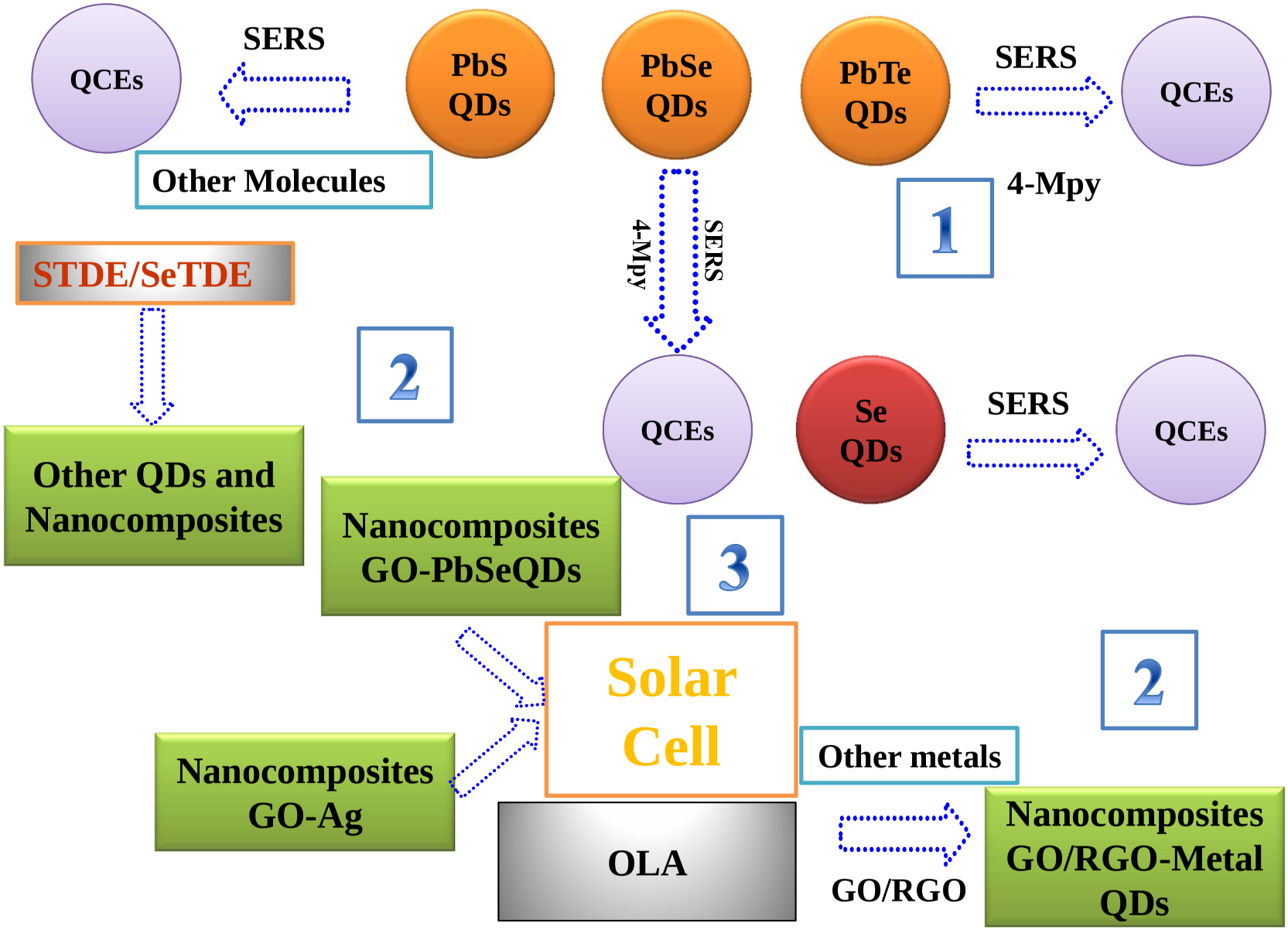

Figure 6.2 Future studies.

Bibliography

Chapter 1 Reference

(1) Brus, L. E. *The Journal of Chemical Physics* **1984**, *80*, 4403.

(2) Bawendi, M. G.; Steigerwald, M. L.; Brus, L. E. *Annual Review of Physical Chemistry* **1990**, *41*, 477.

(3) Alivisatos, A. P. *The Journal of Physical Chemistry* **1996**, *100*, 13226.

(4) Wang, L.-J.; Cao, G.; Tu, T.; Li, H.-O.; Zhou, C.; Hao, X.-J.; Su, Z.; Guo, G.-C.; Jiang, H.-W.; Guo, G.-P. *Appl Phys Lett* **2010**, *97*, 262113.

(5) Coe-Sullivan, S. *Nat Photon* **2009**, *3*, 315.

(6) Wolf, S. A.; Awschalom, D. D.; Buhrman, R. A.; Daughton, J. M.; von Molnár, S.; Roukes, M. L.; Chtchelkanova, A. Y.; Treger, D. M. *Science (New York, N.Y.)* **2001**, *294*, 1488.

(7) Nozik, A. J.; Beard, M. C.; Luther, J. M.; Law, M.; Ellingson, R. J.; Johnson, J. C. *Chem Rev* **2010**, *110*, 6873.

(8) Beard, M. C. *The Journal of Physical Chemistry Letters* **2011**, *2*, 1282.

(9) Hetsch, F.; Xu, X.; Wang, H.; Kershaw, S. V.; Rogach, A. L. *The Journal of Physical Chemistry Letters* **2011**, *2*, 1879.

(10) Donega, C. d. M. *Chemical Society Reviews* **2011**, *40*, 1512.

(11) Carbone, L.; Cozzoli, P. D. *Nano Today* **2010**, *5*, 449.

(12) Evans, C. M.; Evans, M. E.; Krauss, T. D. *J Am Chem Soc* **2010**, *132*, 10973.

(13) Sun, Z.; Zhao, B.; Lombardi, J. R. *Appl Phys Lett* **2007**, *91*, 221106.

(14) Richter, A. P.; Lombardi, J. R.; Zhao, B. *J Phys Chem C* **2010**, *114*, 1610.

(15) Fonoberov, V. A.; Balandin, A. A. *Appl Phys Lett* **2004**, *85*, 5971.

(16) Murray, C. B.; Norris, D. J.; Bawendi, M. G. *J Am Chem Soc* **1993**, *115*, 8706.

(17) De Mello Donegá, C.; Liljeroth, P.; Vanmaekelbergh, D. *Small* **2005**, *1*, 1152.

(18) Moreels, I.; Justo, Y.; De Geyter, B.; Haustraete, K.; Martins, J. C.; Hens, Z. *Acs Nano* **2011**, *5*, 2004.

(19) Murray, C. B.; Sun, S.; Gaschler, W.; Doyle, H.; Betley, T. A.; Kagan, C. R. *IBM J. Res. Dev.* **2001**, *45*.

(20) Li, H. B.; Chen, D.; Li, L. L.; Tang, F. Q.; Zhang, L.; Ren, J. *Crystengcomm* **2010**, *12*, 1127.

(21) Lu, W.; Fang, J.; Stokes, K. L.; Lin, J. *J Am Chem Soc* **2004**, *126*, 11798.

(22) Urban, J. J.; Talapin, D. V.; Shevchenko, E. V.; Murray, C. B. *J Am Chem Soc* **2006**, *128*

Chapter 2 Reference

(1) Alivisatos, A. P. *Science* **1996**, *271*, 933.

(2) Yoffe, A. D. *Advances in Physics* **2001**, *50*, 1.

(3) Donega, C. d. M. *Chemical Society Reviews* **2011**, *40*, 1512.

(4) Smith, A.; Nie, S. *Accounts Chem Res* **2010**, *43*, 190.

(5) Bera, D.; Qian, L.; Tseng, T.-K.; Holloway, P. H. *Materials* **2010**, *3*, 2260.

(6) Rogach, A. L. *Semiconductor nanocrystal quantum dots : synthesis, assembly, spectroscopy, and applications*; Springer: Wien ; New York, 2008.

(7) Sattler, K. D. *Handbook of nanophysics. Nanoparticles and quantum dots*; Taylor & Francis: Boca Raton, 2011.

(8) Sattler, K. D. *Handbook of nanophysics. Nanoelectronics and nanophotonics*; CRC Press/Taylor & Francis: Boca Raton, 2011.

(9) Sattler, K. D. *Handbook of nanophysics. Principles and methods*; Taylor & Francis: Boca Raton, Fla., 2011.

(10) Sattler, K. D. *Handbook of nanophysics. Nanotubes and nanowires*; Taylor & Francis: Boca Raton, Fla., 2011.

(11) Sattler, K. D. *Handbook of nanophysics. Functional nanomaterials*; Taylor & Francis: Boca Raton, 2011.

(12) Sattler, K. D. *Handbook of nanophysics. Clusters and fullerenes*; Taylor & Francis: Boca Raton, Fla., 2011.

(13) Yu, P. *Fundamentals of semiconductors : physics and materials properties*; 4th ed.; Springer: New York, 2010.

(14) Lamberti, C. *Characterization of semiconductor heterostructures and nanostructures*; 1st ed.; Elsevier: Amsterdam, Netherlands ; Boston Mass., 2008.

(15) Birke, R. L.; Znamenskiy, V.; Lombardi, J. R. *The Journal of Chemical Physics* **2010**, *132*, 214707.

(16) Richter, A. P.; Lombardi, J. R.; Zhao, B. *J Phys Chem C* **2010**, *114*, 1610.

(17) Ma, S.; Livingstone, R.; Zhao, B.; Lombardi, J. R. *The Journal of Physical Chemistry Letters* **2011**, *2*, 671.

(18) Livingstone, R.; Zhou, X.; Tamargo, M. C.; Lombardi, J. R.; Quagliano, L. G.; Jean-Mary, F. *The Journal of Physical Chemistry C* **2010**, *114*, 17460.

(19) Brus, L. E. *The Journal of Chemical Physics* **1984**, *80*, 4403.

(20) Kayanuma, Y. *Phys Rev B* **1988**, *38*, 9797.

(21) Wong, E. M.; Bonevich, J. E.; Searson, P. C. *The Journal of Physical Chemistry B* **1998**, *102*, 7770.

(22) Cherkasov, Y. A. *Russian Physics Journal* **1976**, *19*, 203.

(23) Dedigamuwa, Gayan S. (2010) *Fabrication and characterization of surfactant-free PbSe quantum dot films and PbSe-polymer hybrid structures*. (Doctoral Dissertation). Retrieved from Scholar Commons Citation.

(24) Huber, C. A.; Huber, T. E. *J Appl Phys* **1988**, *64*, 6588.

(25) Tutihasi, S.; Chen, I. *Solid State Commun* **1967**, *5*, 255.

(26) Tutihasi, S.; Chen, I. *Physical Review* **1967**, *158*, 623.

(27) Bouroushian, M. *Electrochemistry of metal chalcogenides*; 1st.ed. ed.; Springer: New York, 2009.

(28) Devillanova, Francesco A. Handbook of Chalcogen Chemistry: New Perspectives in Sulfur, Selenium and Tellurium. Cambridge: RSC Publishing, 2007.

(29) Lide, D. R. *CRC Handbook of Chemistry and Physics*; 77th ed.; Boca Raton, 1996.

(30) Wise, F. W. *Accounts Chem Res* **2000**, *33*, 773.

(31) Kothiyal, G. P.; Ghosh, B. *Prog Cryst Growth Ch* **1990**, *20*, 313.

(32) Medintz, I. L.; Uyeda, H. T.; Goldman, E. R.; Mattoussi, H. *Nat Mater* **2005**, *4*, 435.

(33) Popescu, A. Mihai *Non-Crystalline Chalcogenides*; Kluwer Academic Publishers: New York, 2002.

(34) Chen, Z.; Shen, Y.; Xie, A.; Zhu, J.; Wu, Z.; Huang, F. *Cryst Growth Des* **2009**, *9*, 1327.

(35) Mehta, S. K.; Chaudhary, S.; Kumar, S.; Bhasin, K. K.; Torigoe, K.; Sakai, H.; Abe, M. *Nanotechnology* **2008**, *19*.

(36) Zhang, Y.; Wang, J.; Zhang, L. *Langmuir* **2010**, *26*, 17617.

(37) Sarin, Love. (2010) *Nano-Selenium: Novel Formulations for Biological and Environmental Applications*. (Doctoral Dissertation). Retrieved from Internet.

(38) Singh, S. C.; Mishra, S. K.; Srivastava, R. K.; Gopal, R. *The Journal of Physical Chemistry C* **2010**, *114*, 17374.

(39) Johnson, J. A.; Saboungi, M.-L.; Thiyagarajan, P.; Csencsits, R.; Meisel, D. *The Journal of Physical Chemistry B* **1998**, *103*, 59.

(40) Lee, D. C.; Pietryga, J. M.; Robel, I.; Werder, D. J.; Schaller, R. D.; Klimov, V. I. *J Am Chem Soc* **2009**, *131*, 3436.

(41) Warner, J. H.; Tilley, R. D. *Nanotechnology* **2006**, *17*, 3745.

(42) Codoluto, S. C.; Baumgardner, W. J.; Hanrath, T. *Crystengcomm* **2010**, *12*, 2903.

(43) Taylor, B. R.; Kauzlarich, S. M.; Delgado, G. R.; Lee, H. W. H. *Chem Mater* **1999**, *11*, 2493.

(44) Prabakar, S.; Shiohara, A.; Hanada, S.; Fujioka, K.; Yamamoto, K.; Tilley, R. D. *Chem Mater* **2009**, *22*, 482.

(45) Gates, B.; Mayers, B.; Cattle, B.; Xia, Y. *Adv Funct Mater* **2002**, *12*, 219.

(46) Goldbach, A.; Saboungi, M.-L. *Accounts Chem Res* **2005**, *38*, 705.

(47) Stroyuk, A. L.; Raevskaya, A. E.; Kuchmiy, S. Y.; Dzhagan, V. M.; Zahn, D. R. T.; Schulze, S. *Colloids and Surfaces A: Physicochemical and Engineering Aspects* **2008**, *320*, 169.

(48) Caywood, John. (1969). *Optical and Electric Properties of a-Selenium*. (Doctoral Dissertation). Retrieved from Internet.

(49) Huang, X.; Yin, Z.; Wu, S.; Qi, X.; He, Q.; Zhang, Q.; Yan, Q.; Boey, F.; Zhang, H. *Small* **2011**, *7*, 1876.

(50) Stankovich, S.; Dikin, D. A.; Dommett, G. H. B.; Kohlhaas, K. M.; Zimney, E. J.; Stach, E. A.; Piner, R. D.; Nguyen, S. T.; Ruoff, R. S. *Nature* **2006**, *442*, 282.

(51) Prezhdo, O. V.; Kamat, P. V.; Schatz, G. C. *The Journal of Physical Chemistry C* **2011**, *115*, 3195.

(52) Gong, Ru J. *Graphene - Synthesis, Characterization, Properties and Applications*. Rijeka: InTech, 2011.

(53) Kamat, P. V. *The Journal of Physical Chemistry Letters* **2010**, *1*, 520.

(54) Kamat, P. V. *The Journal of Physical Chemistry Letters* **2011**, *2*, 242.

(55) Bai, S.; Shen, X. *RSC Advances* **2012**, *2*, 64.

(56) LaMer, V. K.; Dinegar, R. H. *J Am Chem Soc* **1950**, *72*, 4847.

(57) Kwon, S. G.; Hyeon, T. *Small* **2011**, *7*, 2685.

(58) de Mello Donegá, C.; Liljeroth, P.; Vanmaekelbergh, D. *Small* **2005**, *1*, 1152.

(59) Murray, C. B.; Norris, D. J.; Bawendi, M. G. *J Am Chem Soc* **1993**, *115*, 8706.

(60) Yang, Y. A.; Wu, H.; Williams, K. R.; Cao, Y. C. *Angewandte Chemie International Edition* **2005**, *44*, 6712.

(61) Cao, Y. C.; Wang, J. *J Am Chem Soc* **2004**, *126*, 14336.

(62) McDowell, M.; Wright, A. E.; Hammer, N. I. *Materials* **2010**, *3*, 614.

(63) Jasieniak, J.; Bullen, C.; van Embden, J.; Mulvaney, P. *The Journal of Physical Chemistry B* **2005**, *109*, 20665.

(64) Pan, Y.; Lombardi, J. In *Nanotech 2011--NanoTech Conference & Expo 2011*; NSTI: Boston, USA, 2011; Vol. 1, p 303.

(65) Li, N.; Zhang, X.; Chen, S.; Hou, X.; Liu, Y.; Zhai, X. *Materials Science and Engineering: B* **2011**, *176*, 688.

(66) Li, Z.; Ji, Y.; Xie, R.; Grisham, S. Y.; Peng, X. *J Am Chem Soc* **2011**, *133*, 17248.

(67) Ouyang, J.; Schuurmans, C.; Zhang, Y.; Nagelkerke, R.; Wu, X.; Kingston, D.; Wang, Z. Y.; Wilkinson, D.; Li, C.; Leek, D. M.; Tao, Y.; Yu, K. *ACS Appl Mater Interfaces* **2011**, *3*, 553.

(68) Lokteva, Irina. (2010) *Synthesis and Surface Characterization of Semiconductor Nanocrystals for Photovoltaic Application*. (Doctoral Dissertation). Retrieved from Internet.

(69) Bullen, C.; van Embden, J.; Jasieniak, J.; Cosgriff, J. E.; Mulder, R. J.; Rizzardo, E.; Gu, M.; Raston, C. L. *Chem Mater* **2010**, *22*, 4135.

(70) Leubner, I. H. *Precision crystallization : theory and practice of controlling crystal size*; CRC Press/Taylor & Francis: Boca Raton, 2010.

(71) Moreels, Iwan. (2009) *Colloidal Semiconductor Nanocrystals: From Synthesis to Photonic Applications*. (Doctoral Dissertation). Retrieved from Internet.

(72) Moreels, I.; Lambert, K.; Smeets, D.; De Muynck, D.; Nollet, T.; Martins, J. C.; Vanhaecke, F.; Vantomme, A.; Delerue, C.; Allan, G.; Hens, Z. *Acs Nano* **2009**, *3*, 3023.

(73) Moreels, I.; Lambert, K.; De Muynck, D.; Vanhaecke, F.; Poelman, D.; Martins, J. C.; Allan, G.; Hens, Z. *Chem Mater* **2007**, *19*, 6101.

(74) Urban, J. J.; Talapin, D. V.; Shevchenko, E. V.; Murray, C. B. *J Am Chem Soc* **2006**, *128*, 3248.

(75) Patterson, A. L. *Physical Review* **1939**, *56*, 978.

(76) Holzwarth, U.; Gibson, N. *Nat Nanotechnol* **2011**, *6*, 534.

(77) Manifacier, J. C.; De Murcia, M.; Fillard, J. P.; Vicario, E. *Thin Solid Films* **1977**, *41*, 127.

(78) Mills, G.; Li, Z.; Meisel, D. *The Journal of Physical Chemistry* **1988**, *92*, 822.

(79) Sun, Z.; Zhao, B.; Lombardi, J. R. *Appl Phys Lett* **2007**, *91*, 221106.

(80) Wang, D.; Zhao, H.; Wu, N.; El Khakani, M. A.; Ma, D. *The Journal of Physical Chemistry Letters* **2010**, *1*, 1030.

Chapter 3 Reference

(1) Shen, S.; Zhang, Y.; Peng, L.; Xu, B.; Du, Y.; Deng, M.; Xu, H.; Wang, Q. *Crystengcomm* **2011**, *13*, 4572.

(2) Yong, K.-T.; Sahoo, Y.; Swihart, M. T.; Prasad, P. N. *The Journal of Physical Chemistry C* **2007**, *111*, 2447.

(3) Ouyang, J.; Schuurmans, C.; Zhang, Y.; Nagelkerke, R.; Wu, X.; Kingston, D.; Wang, Z. Y.; Wilkinson, D.; Li, C.; Leek, D. M.; Tao, Y.; Yu, K. *ACS Appl Mater Interfaces* **2011**, *3*, 553.

(4) Wei, Y.; Yang, J.; Lin, A. W. H.; Ying, J. Y. *Chem Mater* **2010**, *22*, 5672.

(5) Joo, J.; Na, H. B.; Yu, T.; Yu, J. H.; Kim, Y. W.; Wu, F.; Zhang, J. Z.; Hyeon, T. *J Am Chem Soc* **2003**, *125*, 11100.

(6) Moreels, I.; Justo, Y.; De Geyter, B.; Haustraete, K.; Martins, J. C.; Hens, Z. *Acs Nano* **2011**, *5*, 2004.

(7) Shen, H.; Wang, H.; Li, X.; Niu, J. Z.; Wang, H.; Chen, X.; Li, L. S. *Dalton T* **2009**, 10534.
(8) Zhuang, Z.; Peng, Q.; Li, Y. *Chemical Society Reviews* **2011**, *40*, 5492.
(9) Kwon, S. G.; Hyeon, T. *Small* **2011**, *7*, 2685.
(10) de Mello Donegá, C.; Liljeroth, P.; Vanmaekelbergh, D. *Small* **2005**, *1*, 1152.
(11) Liu, T.-Y.; Li, M.; Ouyang, J.; Zaman, M. B.; Wang, R.; Wu, X.; Yeh, C.-S.; Lin, Q.; Yang, B.; Yu, K. *The Journal of Physical Chemistry C* **2009**, *113*, 2301.
(12) Jen-La Plante, I.; Zeid, T. W.; Yang, P.; Mokari, T. *J Mater Chem* **2010**, *20*, 6612.
(13) Zhuang, Z.; Lu, X.; Peng, Q.; Li, Y. *Chemistry – A European Journal* **2011**, *17*, 10445.
(14) Si, H.-Y.; Yuan, D.; Chen, J.-S.; Chow, G.-M. *RSC Advances* **2011**, *1*, 817.
(15) Li, Z.; Ji, Y.; Xie, R.; Grisham, S. Y.; Peng, X. *J Am Chem Soc* **2011**, *133*, 17248.
(16) Yordanov, G.; Yoshimura, H.; Dushkin, C. *Colloid & Polymer Science* **2008**, *286*, 813.
(17) Deng, Z.; Cao, L.; Tang, F.; Zou, B. *The Journal of Physical Chemistry B* **2005**, *109*, 16671.
(18) Pan, Y.; Lombardi, J. In *Nanotech 2011--NanoTech Conference & Expo 2011*; NSTI: Boston, USA, 2011; Vol. 1, p 303.
(19) Thomson, J. W.; Nagashima, K.; Macdonald, P. M.; Ozin, G. A. *J Am Chem Soc* **2011**, *133*, 5036.
(20) Koutselas, I.; Bampoulis, P.; Maratou, E.; Evagelinou, T.; Pagona, G.; Papavassiliou, G. C. *The Journal of Physical Chemistry C* **2011**, *115*, 8475.
(21) Wiewiorowski, T. K.; Touro, F. J. *The Journal of Physical Chemistry* **1966**, *70*, 234.
(22) Bateman, L.; Glazebrook, R. W.; Moore, C. G.; Porter, M.; Ross, G. W.; Saville, R. W. *Journal of the Chemical Society (Resumed)* **1958**, 2838.
(23) Meyer, B. *Chem Rev* **1976**, *76*, 367.
(24) Cademartiri, L.; Bertolotti, J.; Sapienza, R.; Wiersma, D. S.; von Freymann, G.; Ozin, G. A. *The Journal of Physical Chemistry B* **2005**, *110*, 671.
(25) Kothiyal, G. P.; Ghosh, B. *Prog Cryst Growth Ch* **1990**, *20*, 313.
(26) Wise, F. W. *Accounts Chem Res* **2000**, *33*, 773.
(27) Lide, D. R. *CRC Handbook of Chemistry and Physics*; 77th ed.; Boca Raton, 1996.
(28) Murray, C. B.; Norris, D. J.; Bawendi, M. G. *J Am Chem Soc* **1993**, *115*, 8706.

(29) Du, H.; Chen, C.; Krishnan, R.; Krauss, T. D.; Harbold, J. M.; Wise, F. W.; Thomas, G.; Silcox, J. *Nano Lett.* **2002**, *2*, 1321.

(30) Yu, W. W.; Falkner, J. C.; Shih, B. S.; Colvin, V. L. *Chem. Mater.* **2004**, *16*, 3318.

(31) Steckel, J. S.; Yen, B. K. H.; Oertel, D. C.; M. G. Bawendi *J. Am. Chem. Soc.* **2006**, *128*, 13032.

(32) Joo, J.; Pietryga, J. M.; McGuire, J. A.; Jeon, S.-H.; Williams, D. J.; Wang, H.-L.; Klimov, V. I. *J. Am. Chem. Soc.* **2009**, *131*, 10620.

(33) Li, H. B.; Chen, D.; Li, L. L.; Tang, F. Q.; Zhang, L.; Ren, J. *Crystengcomm* **2010**, *12*, 1127.

(34) Bullen, C.; van Embden, J.; Jasieniak, J.; Cosgriff, J. E.; Mulder, R. J.; Rizzardo, E.; Gu, M.; Raston, C. L. Chem Mater 2010, 22, 4135.

(35) Lokteva, Irina. (2010) Synthesis and Surface Characterization of Semiconductor Nanocrystals for Photovoltaic Application. (Doctoral Dissertation). Retrieved from Internet.

(36) Lardon, M. *J Am Chem Soc* **1970**, *92*, 5063.

(37) Dai, Q.; Zhang, Y.; Wang, Y.; Wang, Y.; Zou, B.; Yu, W. W.; Hu, M. Z. *The Journal of Physical Chemistry C* **2010**, *114*, 16160.

(38) Du, M.; Wang, Y.; Xu, J.; Yang, P.; Du, Y. *Colloid Journal* **2008**, *70*, 720.

(39) Fu, X. Q.; Pan, Y.; Wang, X.; Lombardi, J. R. *J Chem Phys* **2011**, *134*, 024707.

(40) Richter, A. P.; Lombardi, J. R.; Zhao, B. *J Phys Chem C* **2010**, *114*, 1610.

(41) Fonoberov, V. A.; Balandin, A. A. *Appl Phys Lett* **2004**, *85*, 5971.

(42) Dzhagan, V.; Lokteva, I.; Himcinschi, C.; Jin, X.; Kolny-Olesiak, J.; Zahn, D. R. *Nanoscale Research Letters* **2011**, *6*, 79.

(43) Arora, A. K.; Rajalakshmi, M.; Ravindran, T. R.; Sivasubramanian, V. *J Raman Spectrosc* **2007**, *38*, 604.

(44) Vanmaekelbergh, D.; Liljeroth, P. *Chemical Society Reviews* **2005**, *34*, 299.

(45) Vaqueiro, P.; Powell, A. V. *J Mater Chem* **2010**, *20*, 9577.

(46) Pei, Y.; LaLonde, A.; Iwanaga, S.; Snyder, G. J. *Energy & Environmental Science* **2011**, *Advance*.

(47) Zhang, G.; Finefrock, S.; Liang, D.; Yadav, G. G.; Yang, H.; Fang, H.; Wu, Y. *Nanoscale* **2011**, *Advance*.

(48) Baxter, J.; Bian, Z.; Chen, G.; Danielson, D.; Dresselhaus, M. S.; Fedorov, A. G.; Fisher, T. S.; Jones, C. W.; Maginn, E.; Kortshagen, U.; Manthiram, A.; Nozik, A.; Rolison, D. R.; Sands, T.; Shi, L.; Sholl, D.; Wu, Y. *Energy & Environmental Science* **2009**, *2*, 559.

(49) Sun, G.; Chang, F.; Soref, R. A. *Opt Express* **2010**, *18*, 3746.

(50) Antunez, P. D.; Buckley, J. J.; Brutchey, R. L. *Nanoscale* **2011.**

(51) Murphy, J. E.; Beard, M. C.; Norman, A. G.; Ahrenkiel, S. P.; Johnson, J. C.; Yu, P. R.; Micic, O. I.; Ellingson, R. J.; Nozik, A. J. *J Am Chem Soc* **2006**, *128*, 3241.

(52) Lu, W.; Fang, J.; Stokes, K. L.; Lin, J. *J Am Chem Soc* **2004**, *126*, 11798.

(53) Urban, J. J.; Talapin, D. V.; Shevchenko, E. V.; Murray, C. B. *J Am Chem Soc* **2006**, *128*, 3248.

(54) Mokari, T. L.; Zhang, M. J.; Yang, P. D. *J Am Chem Soc* **2007**, *129*, 9864.

(55) Zhang, J.; Kumbhar, A.; He, J. B.; Das, N. C.; Yang, K. K.; Wang, J. Q.; Wang, H.; Stokes, K. L.; Fang, J. Y. *J Am Chem Soc* **2008**, *130*, 15203.

(56) Ziqubu, N.; Ramasamy, K.; Rajasekhar, P. V. S. R.; Revaprasadu, N.; O'Brien, P. *Chem Mater* **2010**, *22*, 3817.

(57) Shen, H.; Wang, H.; Chen, X.; Niu, J. Z.; Xu, W.; Li, X. M.; Jiang, X.-D.; Du, Z.; Li, L. S. *Chem Mater* **2010**, *22*, 4756.

(58) Wang, Y.; Dai, Q.; Zou, B.; Yu, W. W.; Liu, B.; Zou, G. *Langmuir* **2010**, *26*, 19129.

(59) McDowell, M.; Wright, A. E.; Hammer, N. I. *Materials* **2010**, *3*, 614.

(60) Xiao, Q.; Weng, D.; Yang, Z.; Garay, J.; Zhang, M.; Lu, Y. *Nano Res.* **2010**, *3*, 685.

(61) Hanrath, T.; Veldman, D.; Choi, J. J.; Christova, C. G.; Wienk, M. M.; Janssen, R. A. *ACS Appl Mater Interfaces* **2009**, *1*, 244.

(62) Dai, Q.; Wang, Y.; Zhang, Y.; Li, X.; Li, R.; Zou, B.; Seo, J.; Liu, M.; Yu, W. W. *Langmuir* **2009**, *25*, 12320.

(63) Sykora, M.; Koposov, A. Y.; McGuire, J. A.; Schulze, R. K.; Tretiak, O.; Pietryga, J. M.; Klimov, V. I. *Acs Nano* **2010**, *4*, 2021.

(64) Johnson, J. A.; Saboungi, M.-L.; Thiyagarajan, P.; Csencsits, R.; Meisel, D. *The Journal of Physical Chemistry B* **1998**, *103*, 59.

(65) Dwivedi, C.; Shah, C. P.; Singh, K.; Kumar, M.; Bajaj, P. N. *Journal of Nanotechnology* **2011**, *2011*.

(66) Chen, Z.; Shen, Y.; Xie, A.; Zhu, J.; Wu, Z.; Huang, F. *Cryst Growth Des* **2009**, *9*, 1327.

(67) Stroyuk, A. L.; Raevskaya, A. E.; Kuchmiy, S. Y.; Dzhagan, V. M.; Zahn, D. R. T.; Schulze, S. *Colloids and Surfaces A: Physicochemical and Engineering Aspects* **2008**, *320*, 169.

(68) Mehta, S. K.; Chaudhary, S.; Kumar, S.; Bhasin, K. K.; Torigoe, K.; Sakai, H.; Abe, M. *Nanotechnology* **2008**, *19*.

(69) Gates, B.; Mayers, B.; Cattle, B.; Xia, Y. *Adv Funct Mater* **2002**, *12*, 219.

(70) Jeong, U.; Xia, Y. *Adv Mater* **2005**, *17*, 102.

(71) Zhang, Y.; Wang, J.; Zhang, L. *Langmuir* **2010**, *26*, 17617.

(72) Ueda, A.; Wu, M.; Aga, R.; Meldrum, A.; White, C. W.; Collins, W. E.; Mu, R. *Surface and Coatings Technology* **2007**, *201*, 8542.

(73) Raevskaya, A. E.; Stroyuk, A. L.; Kuchmiy, S. Y.; Dzhagan, V. M.; Zahn, D. R. T.; Schulze, S. *Solid State Commun* **2008**, *145*, 288.

(74) Singh, S. C.; Mishra, S. K.; Srivastava, R. K.; Gopal, R. *The Journal of Physical Chemistry C* **2010**, *114*, 17374.

(75) Goldbach, A.; Saboungi, M.-L. *Accounts Chem Res* **2005**, *38*, 705.

(76) Goldbach, A.; Iton, L. E.; Saboungi, M.-L. *Chem Phys Lett* **1997**, *281*, 69.

(77) Goldbach, A.; Iton, L. E.; Grimsditch, M.; Saboungi, M.-L. Chem Mater 2004, 16, 5107.

(78) Lee, D. C.; Pietryga, J. M.; Robel, I.; Werder, D. J.; Schaller, R. D.; Klimov, V. I. *J Am Chem Soc* **2009**, *131*, 3436.

(79) Warner, J. H.; Tilley, R. D. *Nanotechnology* **2006**, *17*, 3745.

(80) Codoluto, S. C.; Baumgardner, W. J.; Hanrath, T. *Crystengcomm* **2010**, *12*, 2903.

(81) Leubner, I. H. *Precision crystallization : theory and practice of controlling crystal size*; CRC Press/Taylor & Francis: Boca Raton, 2010.

(82) Glicksman, M. E. *Principles of solidification : an introduction to modern casting and crystal growth concepts*; Springer Verlag: New York, 2011.

(83) A. Feltz, A. *Amorphous and Vitreous Non-organic Solids*; “Mir” Publ.: Moscow, 1986.

(84) Huber, C. A.; Huber, T. E. *J Appl Phys* **1988**, *64*, 6588.

(85) Tutihasi, S.; Chen, I. *Physical Review* **1967**, *158*, 623.

(86) Tutihasi, S.; Chen, I. *Solid State Commun* **1967**, *5*, 255.

(87) Gobrecht, H.; Tausend, A. *Proceedings of the International Conference on the Physics of Semiconductors, p.1189;* Academic Press Inc.: New York, 1965.

(88) Caywood, John. (1969). *Optical and Electric Properties of a-Selenium*. (Doctoral Dissertation). Retrieved from Internet.

(89) Minaev, S. ; Timoshenkov, S. P.; Kalugin, V. V. *J. Optoelectron. Adv. Mater.* **2005**, *7(4)*, 1717.

(90) Minaev, V. S. *J Optoelectron Adv M* **2001**, *3*, 233.

(91) Prezhdo, O. V.; Kamat, P. V.; Schatz, G. C. *The Journal of Physical Chemistry C* **2011**, *115*, 3195.

(92) Kamat, P. V. *The Journal of Physical Chemistry Letters* **2010,** *1*, 520.

(93) Kamat, P. V. *The Journal of Physical Chemistry Letters* **2011**, *2*, 242.

Chapter 4 Reference

(1) Brus, L. *The Journal of Physical Chemistry* **1986**, *90*, 2555.

(2) Klein, M. C.; Hache, F.; Ricard, D.; Flytzanis, C. *Phys Rev B* **1990**, *42*, 11123.

(3) Sun, Z.; Zhao, B.; Lombardi, J. R. *Appl Phys Lett* **2007**, *91*, 221106.

(4) Richter, A. P.; Lombardi, J. R.; Zhao, B. *J Phys Chem C* **2010**, *114*, 1610.

(5) Fonoberov, V. A.; Balandin, A. A. *Appl Phys Lett* **2004**, *85*, 5971.

(6) Machol, J. L.; Wise, F. W.; Patel, R. C.; Tanner, D. B. *Phys Rev B* **1993**, *48*, 2819.

(7) Hyun, B.-R.; Zhong, Y.-W.; Bartnik, A. C.; Sun, L.; Abruña, H. D.; Wise, F. W.; Goodreau, J. D.; Matthews, J. R.; Leslie, T. M.; Borrelli, N. F. *Acs Nano* **2008**, *2*, 2206.

(8) Wang, D.; Zhao, H.; Wu, N.; El Khakani, M. A.; Ma, D. *The Journal of Physical Chemistry Letters* **2010**, *1*, 1030.

(9) Moreels, I.; Lambert, K.; Smeets, D.; De Muynck, D.; Nollet, T.; Martins, J. C.; Vanhaecke, F.; Vantomme, A.; Delerue, C.; Allan, G.; Hens, Z. *Acs Nano* **2009**, *3*, 3023.

(10) Neo, M. S.; Venkatram, N.; Li, G. S.; Chin, W. S.; Wei, J. *The Journal of Physical Chemistry C* **2009**, *113*, 19055.

(11) Joo, J.; Na, H. B.; Yu, T.; Yu, J. H.; Kim, Y. W.; Wu, F.; Zhang, J. Z.; Hyeon, T. *J Am Chem Soc* **2003**, *125*, 11100.

(12) Cademartiri, L.; Bertolotti, J.; Sapienza, R.; Wiersma, D. S.; von Freymann, G.; Ozin, G. A. *The Journal of Physical Chemistry B* **2005**, *110*, 671.

(13) Wang, S.; Pan, A.; Yin, H.; He, Y.; Lei, Y.; Xu, Z.; Zou, B. *Mater Lett* **2006**, *60*, 1242.

(14) Song, W.; Wang, Y.; Hu, H.; Zhao, B. *J Raman Spectrosc* **2007**, *38*, 1320.

(15) Wang, Y.; Sun, Z.; Hu, H.; Jing, S.; Zhao, B.; Xu, W.; Zhao, C.; Lombardi, J. R. *J Raman Spectrosc* **2007**, *38*, 34.

(16) Fu, X.; Bei, F.; Wang, X.; Yang, X.; Lu, L. *J Raman Spectrosc* **2009**, *40*, 1290.

(17) Wang, Z.; Rothberg, L. J. *The Journal of Physical Chemistry B* **2005**, *109*, 3387.

(18) Chao, Y.; Zhou, Q.; Li, Y.; Yan, Y.; Wu, Y.; Zheng, J. *The Journal of Physical Chemistry C* **2007**, *111*, 16990.

(19) Lim, J. S.; Choi, H.; Lim, I. S.; Park, S. B.; Lee, Y. S.; Kim, S. K. *The Journal of Physical Chemistry A* **2009**, *113*, 10410.

(20) Baldwin, J. A.; Vlčková, B.; Andrews, M. P.; Butler, I. S. *Langmuir* **1997**, *13*, 3744.

(21) Hu, J.; Zhao, B.; Xu, W.; Li, B.; Fan, Y. *Spectrochimica Acta Part A: Molecular and Biomolecular Spectroscopy* **2002**, *58*, 2827.

(22) Lombardi, J. R.; Birke, R. L. *The Journal of Physical Chemistry C* **2008**, *112*, 5605.

Chapter 5 Reference

(1) Roy, A.; Kolobov, A.V.; Oyanagi, H.; Tanaka, K. *Philosophical Magazine B* **2005**, *78 (1)*, 87-94.

(2) Kolobov, A.V. (Ed.): *Photo-Induced Metastability in Amorphous Semiconductors*; Wiley-VCH: Weinheim, 2003.

(3) Lukacs, R.; Veres, M.; Shimakawa, K.; Kugler, S. *J Appl Phys* **2010**, *107*, 073517.

(4) Tallman, R.; Weinstein, B.; Reznik, A.; Kubota, M.; Tanioka, K.; Rowlands, J. *J Non-Cryst Solids* **2008**, *354*, 4577.

(5) Tallman, R. E.; Reznik, A.; Weinstein, B. A.; Baranovskii, S. D.; Rowlands, J. A. *Appl Phys Lett* **2008**, *93*, 212103.

(6) Kohara, S.; Goldbach, A.; Koura, N.; Saboungi, M. L.; Curtiss, L. A. *Chem Phys Lett* **1998**, *287*, 282.

(7) Goldbach, A.; Iton, L. E.; Saboungi, M.-L. *Chem Phys Lett* **1997**, *281*, 69.

(8) Goldbach, A.; Saboungi, M.-L. *Accounts Chem Res* **2005**, *38*, 705.

(9) Chen, Z.; Shen, Y.; Xie, A.; Zhu, J.; Wu, Z.; Huang, F. *Cryst Growth Des* **2009**, *9*, 1327.

(10) Minaev, V. S. *J Optoelectron Adv M* **2001**, *3*, 233.

(11) Emeleus, H. J. *Advances in Inorganic Chemistry & Radiochemistry, Volume 28*, Academic Press: London, 1984.